2013

Wireless Signal Networks: A Proof of Concept for Subsurface Characterization and A System Design with Reconfigurable Radio

Suk-Un Yoon
Lehigh University

Wireless Signal Networks: A Proof of Concept for Subsurface Characterization and A System Design with Reconfigurable Radio

by

Suk-Un Yoon

A Dissertation
Presented to the Graduate and Research Committee
of Lehigh University
in Candidacy for the Degree of
Doctor of Philosophy
in
Computer Engineering

Lehigh University
January 2013

Approved and recommended for acceptance as a dissertation in partial fulfillment of the requirements for the degree of Doctor of Philosophy.

Date

Liang Cheng, Dissertation Advisor

Accepted Date

Committee Members

Henry Baird

Sibel Pamukcu

Eugene Perevalov

Parvathinathan Venkitasubramaniam

Dedication

To my wife and my family.

Acknowledgements

I would like to thank many people who have helped me to complete this dissertation at Lehigh University. I would like to give my special gratitude to my wife, Se Eun Kim for her support, understanding, patience, sacrifices, and love.

I would like to express the deepest appreciation to my advisor, Dr. Liang Cheng for his advice, guidance, and support throughout this dissertation. Above all and the most needed, he provided me unflinching encouragement and support on both an academic and a personal level. Without his guidance and persistent help this dissertation would not have been possible. I wish also thank my committee members, Dr. Henry Baird, Dr. Sibel Pamukcu, Dr. Eugene Perevalov, and Dr. Parvathinathan Venkitasubramaniam for their invaluable guidance and suggestions. It was my great honor and pleasure to work with Dr. Sibel Pamukcu on a NSF project which is the basis for the dissertation researches.

The faculty, staff, and students at Lehigh University are the most dedicated and generous people that I have ever met and I feel honored to have worked with them. I would also like to express my gratitude to Lehigh University Korean students, Ehsan Ghazanfari, Zi Wang, Xu Li, Lisa Frye, Zhongliang Liang, and Professor Xiaotong Zhang with whom I have enjoyed numerous fruitful discussions and spent memorable times.

Contents

List of Tables

List of Figures

Abstract

Subsurface monitoring has been accomplished through traditional techniques including direct soil sampling, probing and soundings, and using geophysical mapping tools. Although these techniques have been successfully implemented to characterize the global state of geo-media in an interested site, there are challenges associated with these techniques including difficulties in providing real-time data to track geo-hazards and deployment challenges specifically the requirement of wired connections in some conventional techniques. To address these challenges, wireless sensor networks have been used recently for subsurface monitoring. However, wireless sensor nodes in existing solutions only provide point measurements and are incapable of providing global measurement for characterization of subsurface medium.

The key contribution of this dissertation is to bridge the gap between real-time monitoring and global measurements by introducing a novel concept of Wireless Signal Networks (WSiNs) with a proof of concept for subsurface monitoring using actual wireless sensor nodes (i.e., MICAz) and a system design with a reconfigurable radio platform. Wireless signal networks use the real-time link quality signals among distributed wireless sensor nodes as the main indicator of an event in the physical domain. Our thesis is that "*the variation of the link quality between wireless sensor nodes can be used as an effective global sensing mechanism which reflects characteristics of geo-media subjected to various geo-events*". To prove this thesis, the dissertation proposes an accurate and simple radio propagation model for underground environments, and the model quantitatively explains that the changes of soil properties and conditions affect the link quality and strength of the radio waves within the region of the event. Then, the dissertation presents real-time global subsurface monitoring applications with wireless signal network concepts based on the proposed underground propagation model including experimental evaluations. Experiments demonstrated that calibrated wireless signal strength variations can be used as indicators to sense changes in the subsurface.

To extend underground communication distance, prolong network lifetime, and provide adaptive topology construction, we propose a system design for wireless signal networks with the reconfigurable radio platform. Based on the theoretical and empirical analysis of the radio propagation model, the dissertation proposes practical solutions of extending the underground communication distance and an evaluation platform for the system design with reconfigurable radio (i.e., Universal Software Radio Peripheral). The dissertation describes a novel topology control mechanism by introducing a new control dimension, i.e., frequency control, with the reconfigurable radio that supports underground communication distance extension, network lifetime enhancement, and adaptive topology construction in underground environments of high signal attenuation affected by geo-events.

Chapter 1

Introduction

1.1 Subsurface Monitoring Techniques

Electromagnetic (EM) wave propagation has been widely used in soil science as a means of geo-sensing and determination of some soil properties. For instance, moisture content and salinity of soil have been measured using different techniques including four-electrode sensors (surface array or insertion probes), remote electromagnetic induction sensors [1, 2], and Time Domain Reflectometric (TDR) sensors [3]. Also, Ground Penetrating Radar (GPR) and active microwave remote sensing have been implemented in soil moisture detection [4, 5]. In general, subsurface monitoring has been accomplished through destructive and non-destructive techniques including direct soil sampling, probing and soundings, and using geophysical mapping tools. Although these techniques have been successfully implemented to characterize the state of geo-media, there are challenges associated with these techniques including difficulties in providing real-time (i.e., event data reporting within a certain amount of time) data to track geo-hazard (e.g., landslides, slope failures) and deployment challenges specifically the requirement of wired connections in some conventional techniques.

To address some of these challenges associated with the aforementioned techniques, wireless sensors have been used recently for subsurface monitoring. Current applications of wireless sensors include measurements of earth-slope inclination, landslides, strong

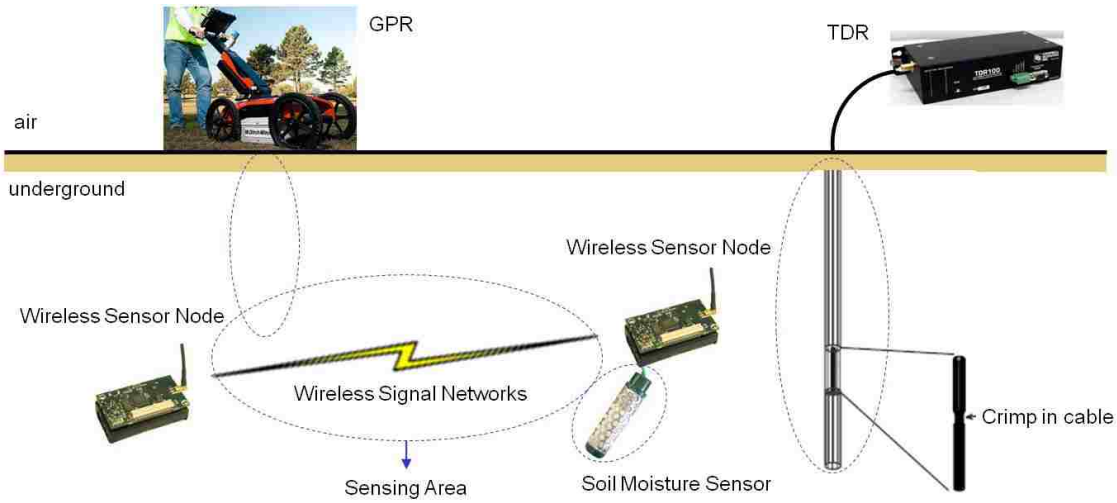

Figure 1.1: Sensing areas of subsurface monitoring techniques

ground motion, and soil-structure interactions [6, 7, 8, 9, 10]. In the examples cited above the sensors are attached to the exterior of the system of interest and embedded using supplementary frames and are designed to measure a specific property (point measurement) and transmit the collected data via wireless communication. Wireless sensor nodes in existing solutions, however, provide only point measurements and are incapable of providing global measurement for characterization of subsurface medium. This dissertation presents a novel concept of Wireless Signal Networks (WSiNs) to bridge the gap between real-time monitoring and global measurements. Figure 1.1 shows sensing areas of subsurface monitoring techniques such as GPR and TDR as well as wireless signal networks. GPR can provide global monitoring, however it has a difficulty in providing real-time data reporting. TDR can provide real-time data reporting, however it requires wired connections and has a difficulty in providing global subsurface monitoring. The wireless sensor node with sensing devices (e.g., a soil moisture sensor) provide a point sensing in real-time. As shown in Figure 1.1, wireless signal network can provide global sensing as well as real-time monitoring.

To show the benefit of global sensing with wireless signal network, a water leakage

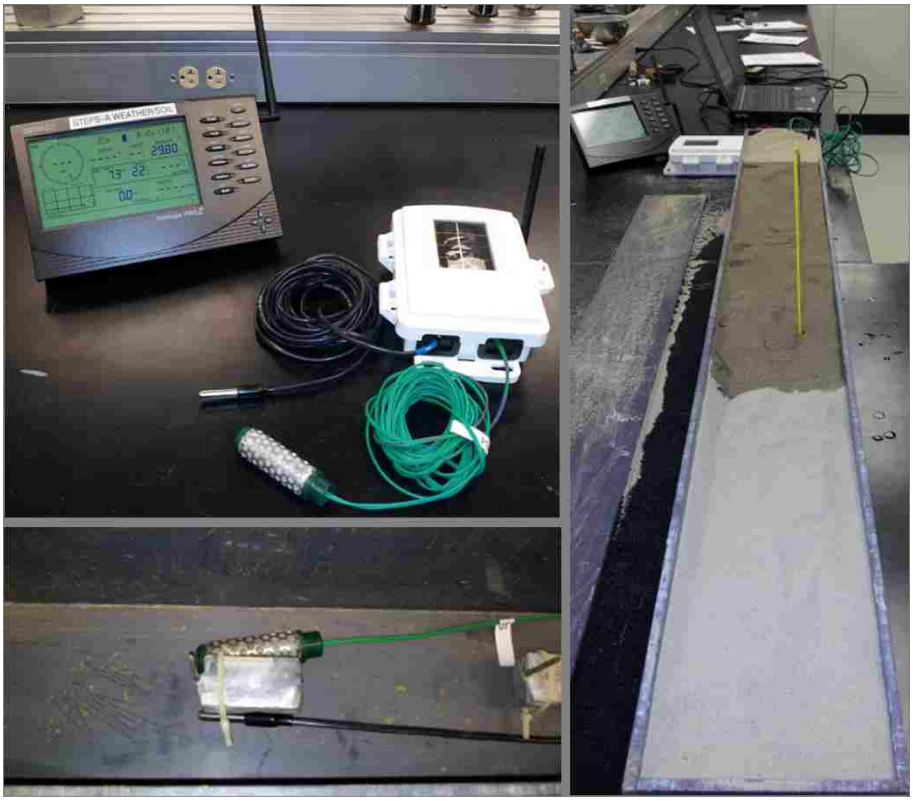

Figure 1.2: Commercial sensor suite, sensor installation, and water leakage event using test box

event is simulated and monitored with commercial sensor suite (i.e., Wireless Vantage Pro2 [11]) as well as wireless signal network using MICAz nodes. The commercial sensor suite, sensor installation, and water leakage event are shown in Figure 1.2. The commercial sensor suite is connected with a temperature sensor and a soil moisture sensor which represent point sensing. The details of experimental condition and the designed box are shown in Section 3.4.1. In the experiment, a sensor sends (S1) a packet at every 60 seconds and a receiver node (S2, located at 75 cm from the sender) calculated the received signal strength based on the received packet. At the same point of S2, a temperature sensor and a soil moisture sensor are installed as shown in Figure 1.2. Two water leakage events are generated to simulate a waterfront movement, and the measured water contents

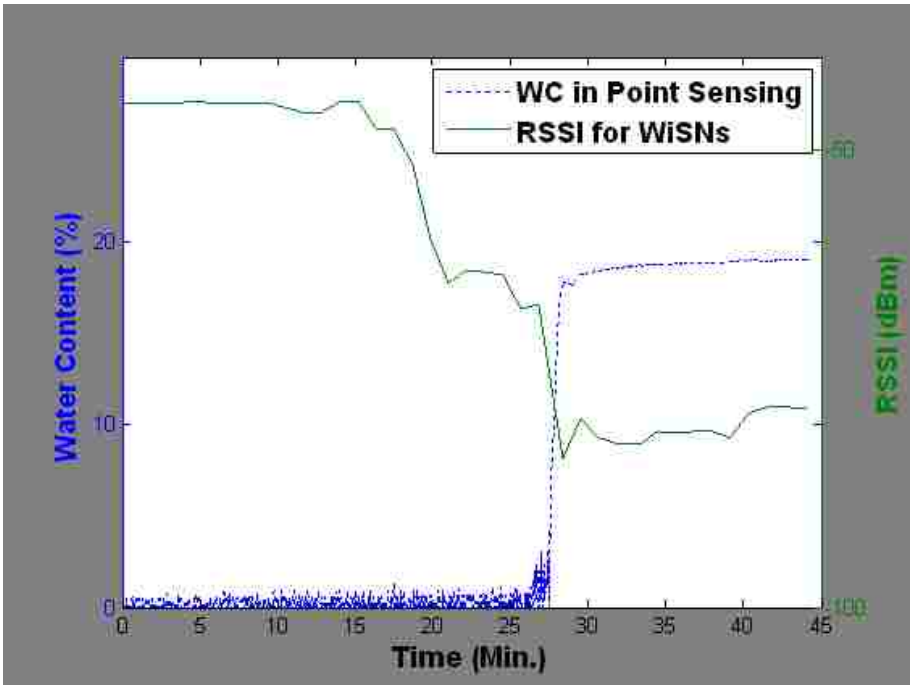

Figure 1.3: Commercial sensor suite, sensor installation, and water leakage event using test box

and received signal strengths are shown in Figure 1.3. The first water leakage event was made around the areas between S1 and S2 at 15 minutes, the second water leakage event was made around S2 at 25 minutes. As shown in Figure 1.3, the sensor node S2 has low received signal strength due to the first water leakage event while point sensing (soil moisture sensor) has no change. On the second water leakage event, both wireless signal network and point sensing can detect water leakage event. From this simulated event, wireless signal networks based on the monitoring with received signal strength provide global sensing in real-time.

1.2 Objectives and Contributions

The researches on the dissertation include five research objectives which are summarized as follows:

- The dissertation introduces Wireless Signal Networks (WSiNs) concept which uses the radio signal strength variation as the main indicator of an event in the physical domain of the wireless signal network. The dissertation provides solutions of application aspects of wireless signal networks including a survey of practical application and deployment challenges and solutions.

- The dissertation proposes an accurate and simple radio propagation model for underground low-power devices such as wireless sensor nodes and its performance evaluation by real wireless sensor nodes. The proposed model can be used to estimate communication distance of wireless underground sensor networks and to find out the way of extending communication radius underground in theoretical analysis.

- The dissertation includes subsurface event detection and classification methods using the proposed wireless underground signal networks and proposed underground propagation model through experimental evaluations. The dissertation provides a detailed list of network parameters and soil properties on how radio propagation is affected by soil properties in subsurface communication environments with experimental data.

- The dissertation proposes practical solutions of extending underground communication distance in wireless underground networks based on theoretical analysis and evaluation of radio propagation model. The dissertation presents a system design of an evaluation platform with USRP to extend underground communication distance and analyze the effects of soil properties on low frequency radio propagation. The system is called LUWSN (L:Low-frequency/Lehigh/LongLab).

- The dissertation proposes an energy efficient topology control with reconfigurable

radio to extend network lifetime of wireless sensor networks. For the energy efficient topology control, the dissertation proposes distributed topology control algorithms, reconfigurable radio topology control (RTC) and reconfigurable radio dynamic topology control (RDTC), which construct a minimum hop routing tree using multiple frequency bands.

The key contribution of this dissertation is to bridge the gap between real-time monitoring and global measurements by introducing a novel concept of Wireless Signal Networks (WSiNs) with a proof of concept for subsurface monitoring using actual wireless sensor nodes (i.e., MICAz), and a system design with a reconfigurable radio platform. To prove the proposed concept, the dissertation introduces an accurate underground radio propagation model with a different derivation method from previous works, and low frequency wireless sensor networks to extend underground communication distance for practical applications. The research methods and results are based on real wireless sensors (MICAz), so they can be used for real world implementations and a new underground networks design as well as the estimations of underground communication distance on wide range of frequency. The wireless signal/sensor networks based on the reconfigurable radio will address the existing problems such as extending network lifetime of wireless signal/sensor networks. While the previous researches assume the operating frequency is fixed or changed in narrow frequency bands, the reconfigure radio sensor networks are equipped with radio reconfiguration functionality in wide ranges of frequency bands. Thus, the approach using radio reconfiguration will address the problem (extending network lifetime) in a different angle and provide significant improvements. The proposed concepts of wireless signal networks and the system design methods are generic, so the research results can be used in different system such as wireless sensor network, cognitive radio, or software defined radio.

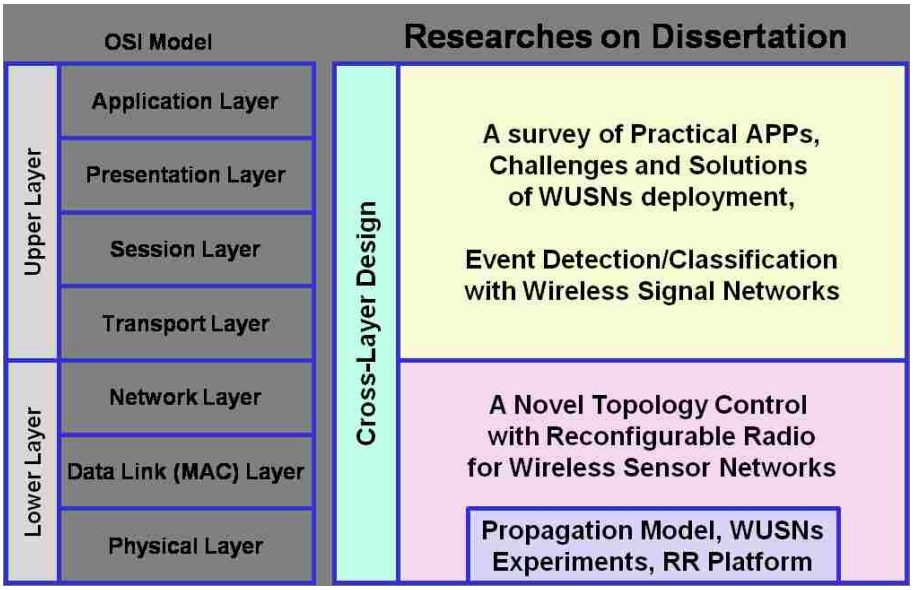

Figure 1.4: Researches on dissertation.

1.3 Research Approach

According to the traditional OSI layer model, the research can be grouped as three major parts such as 1) researches on physical layer such as radio propagation model and reconfigurable radio (or low frequency) sensor networks, 2) researches on an energy efficient topology control with reconfigurable radio for wireless signal/sensor networks, and 3) researches on application layer such as challenges and solutions of wireless underground sensor networks and subsurface event detection and classification using wireless signal networks. The researches on dissertation are shown in shown in Figure 1.4.

The researches on dissertation are organized as follows: In Chapter 2, the dissertation introduces Wireless Signal Networks (WSiNs) concept which uses the radio signal strength variation as the main indicator of an event in the physical domain of the wireless signal network. In Chapter 3, The dissertation proposes an accurate and simple radio propagation model for underground low-power devices such as wireless sensor nodes and its performance evaluation by real wireless sensor nodes. In Chapter 4, the dissertation

includes subsurface event detection and classification methods using the proposed wireless underground signal networks and proposed underground propagation model through experimental evaluations. In Chapter 5, the dissertation introduces a system design of reconfigurable radio sensor node which can extend underground communication distance, prolong network lifetime, and provide adaptive topology construction. In Chapter 6, the dissertation proposes an energy efficient topology control with reconfigurable radio to extend network lifetime of wireless sensor networks. Finally, the dissertation is concluded in Chapter 7.

Chapter 2

Wireless Signal Networks

2.1 Introduction

Wireless Underground Sensor Networks (WUSNs) [12] have abundant potential applications in monitoring subsurface geo-events. The key applications could be monitoring subsurface hazard and characterizing subsurface environments in real-time using WUSNs. However, it is difficult to monitor global subsurface hazard and characteristics due to the limited subsurface sensing capability of the sensor's equipments. To monitor global subsurface environments, the concept of Wireless Signal Networks (WSiNs) is introduced. The wireless signal networks use the signal strength variation in the soil medium as the main indicator of an underground event or a physical change in soil properties. The target applications of subsurface hazards monitoring include landslide, earthquake, and active fault zone monitoring which involve a lot of perturbation of earth masses and are characterized by the localization of sensors which allows sensors to estimate their locations using information transmitted by a set of seed sensors. Other potential applications of characterizing subsurface environments include monitoring of oil leakage from subsurface reservoirs, water leakage from underground pipelines, seepage in earth dams, and estimation of soil properties and conditions such as compaction, gradation, and salinity based on the received signal strength information. This dissertation summarizes practical potential applications of wireless signal networks based on the existing researches

and sensor network deployments. The installation and management of underground signal networks has more constraint than aboveground deployment, because digging a hole and finding sensor underground are not easy tasks. Even the sensor position is easily traceable; the sensor can be damaged when digging. This dissertation summarizes challenges and possible solutions on the deployment and management of underground signal network with wireless sensor nodes.

2.2 Concept of Wireless Signal Networks

Wireless Signal Networks (WSiNs) use the radio signal strength variation as the main indicator of an event in the physical domain of the wireless signal network. Soil properties such as density, water and mineral content are known to affect radio wave propagation. When and if these physical properties of the host soil change during the evolution of a geo-event (subsurface event), they in turn affect the transmission quality and strength of the radio waves within the region of the event. Using the new approach, the global subsurface monitoring in real-time can be achieved. Figure 2.1 shows the concept of subsurface monitoring with wireless signal networks for detection of landslide and chemical plume/oil leakage. The new approach could provide both point sensing and regional sensing between the underground transceivers, and real time measurements that potentially can be used for subsurface monitoring.

2.3 Subsurface Geo-applications

2.3.1 Subsurface Monitoring Applications

Wired and wireless sensor nodes are used for monitoring subsurface geo-event. Many applications of existing wired and wireless sensor networks can be replaced by WSiNs for wide ranges of global monitoring. The existing subsurface monitoring systems/researches and potential applications of WSiNs are as following:

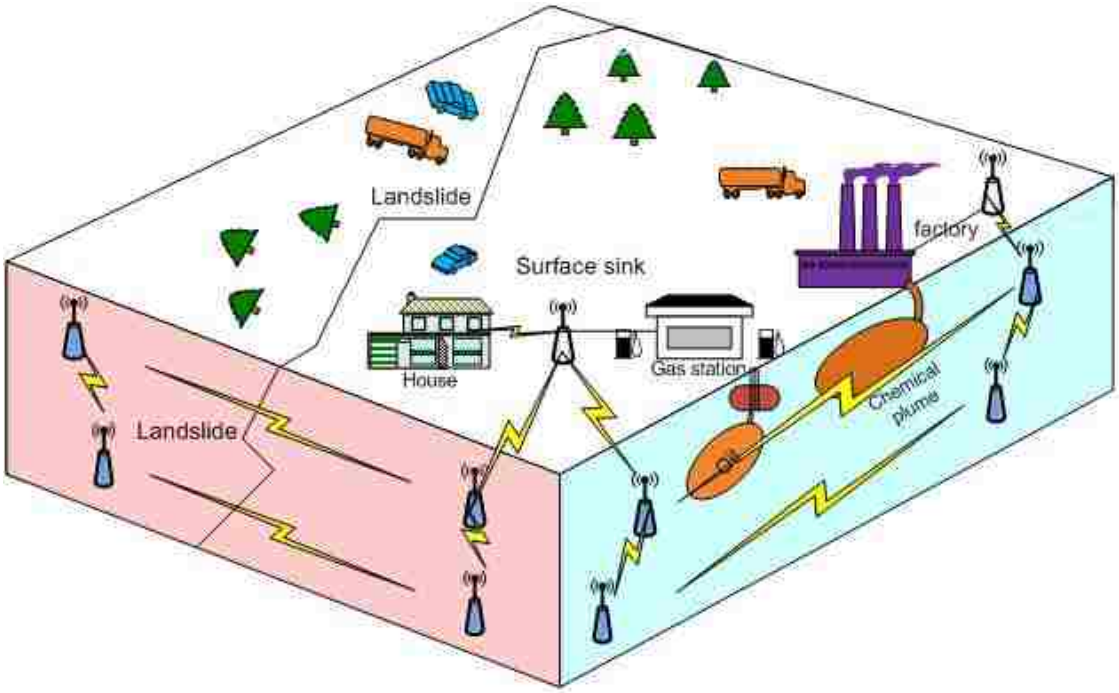

Figure 2.1: Subsurface monitoring with Wireless Signal Networks (WSiNs).

- Agriculture Application: WSiNs can be deployed to monitor underground soil conditions, such as water and mineral content, and to provide data for appropriate irrigation and fertilization. WSiNs can eliminate surface equipment such as the portion of sensor which extends above surface. With WSiNs providing local detailed data, individual sprinklers could be activated based on local sensors rather than irrigating an entire field in response to broad sensor data. The applications and experiences from a sugar farm deploying sensor networks are introduced in [13].

- Monitoring Structure Health: Monitoring the structural health of any underground components of an integrated structure such as building foundation, bridge pier, or dam's foundation is a good practical application of WSiNs. A customized wireless networked sensor can be built for structural health monitoring which sensor is called DuraNode in [14]. A wireless sensor network can be deployed for structural health

monitoring of civil structures such as theater in [15].

- Mine Application: Mine is a good place to deploy wireless underground sensor networks. The radio propagation can be either in soil or in tunnel on mine structure. WSiNs can help rescuers with a general area to search for survivors in collapsed building and mine. For an example of mining case study, safety assurance and rescue communication systems in high-stress environments are introduced in [16]. As in systems deployed above ground, a fixed infrastructure can provide routine long-distance communication in harsh mine environments. Signals can be sent over electrical conductors such as twisted pair and coaxial cables, and via optical fibers. With the location information from sensor nodes, a coal mine personnel global positioning system can be built [17].

- Sport Field Application: WSiNs can be used for monitoring sports field, where they can be used to monitor soil conditions at golf courses, soccer fields, baseball fields, and grass tennis courts.

- Security Application: The data provided from sensor nodes can be useful information for home and commercial security, where sensors could be deployed underground around the perimeter of a building in order to detect intruders. Wireless pressure sensors deployed at a shallow depth along the length of a border could be used to alert authorities to illegal crossings.

- Underground Infrastructure Monitoring: WSiNs are applicable to monitor pipes, electrical wiring, and liquid storage tanks underground. The water pipe monitoring under the road is a good example of underground infrastructure monitoring [18, 19, 20, 21]. A wireless sensor network configuration for water distribution monitoring system is introduced in [22]. An overview of an automatic underground distribution fault location system is introduced in [23] where an example of a one-line diagram from another intranet web application is shown for the feeder with an estimated fault location. WSiNs can be used for underground oil tank monitoring. An automatic oil leak detection system for an underground tank which can be applied to a practical application of WSiNs is introduced in [24].

- Natural Disaster: The target applications for subsurface hazards include a landslide, an earthquake, and monitoring active fault zone which involve a lot of shifting and moving of earth masses and are characterized by the localization of sensors. WSiNs can be used for detecting landslide which concept is introduced as Senslide in [25]. The design, development, and evaluation of a tilt and soil moisture sensor network for slope monitoring applications are introduce in [26]. Sensor networks can be used for monitoring volcanic eruptions. The volcano monitoring sensor-network architecture is introduced in [27] where the network consists of 16 sensor nodes, each with a microphone and seismometer, collecting seismic and acoustic data on volcanic activity.

- Environmental Monitoring: Monitoring the presence and concentration of various toxic substances are important for soil near rivers and aquifers, where chemical runoff could contaminate drinking water supplies. Sensor networks can be used for monitoring outdoor water quality. The paper [28] investigates a wireless sensor network deployment - monitoring water quality, e.g. salinity and the level of the underground water table. The goal is to collect real time water quality measurements together with the amount of water being pumped out in the area, and investigate the impacts of current irrigation practice on the environments, in particular underground water salination.

- Home Application: Wireless sensor nodes can be used for home security and gardening. A sensor deployed in shallow depth around house can detect intruder by the pressure sensor and generate alarm signal. The sensor with moisture sensor can provide water content of the soil to control sprinklers. Monitoring and preventing overflow of a septic tank in home is another application of wireless signal networks.

- Subway security monitoring: Rail-based mass transit systems are vulnerable to many criminal acts, ranging from vandalism to terrorism. Wireless sensor technology can be used for subway security monitoring and underground tunnel/rail monitoring. Sensor networks can be used as dependable integrated surveillance systems for the physical security of metro railways in [29].

Table 2.1: Practical subsurface monitoring applications

Application Calories	Description on Applications
Agriculture	Monitoring underground soil conditions, such as water and mineral content to provide data for appropriate irrigation and fertilization
Structure Health	Monitoring the structural health of subsurface structures (i.e. foundations, reservoirs, pipelines), sensitive structures (i.e. bridge, dam) or deep foundations (piles)
Mine/Tunnel	Underground minefield monitoring, Coal mine personnel global positioning system
Sport Field	Lawn and garden monitoring, Sports field monitoring
Security	Monitor the aboveground presence and movement of people or objects, Border patrol
Underground Infrastructure	Water pipe monitoring under the road, Water distribution monitoring system, Underground power distribution fault location system, Underground oil tank monitoring
Natural Disaster	Monitoring landslide and land subsidence Monitoring the movement of a glacier Monitoring volcanic eruptions
Environmental Monitoring	Monitoring the presence and concentration of various toxic substances, Monitoring outdoor water quality
Home	Home security, gardening, Septic tank monitoring
Subway	Subway security monitoring, Underground tunnel/Rail monitoring

Wireless signal networks with wireless sensor nodes can be used in many practical applications for monitoring subsurface geo-event. Table 2.1 shows the application categories and the description on the practical subsurface monitoring application for wireless signal and underground wireless sensor networks.

2.3.2 Subsurface Monitoring of WSiNs

Wireless sensor node can adopt existing sensing technologies and devices such as light sensor, accelerometer, moisture sensor, ammonia/gas detection sensor, pressure sensor,

Table 2.2: Category of subsurface monitoring

Category of Monitoring	Characteristic	Potential Applications
Soil Condition	Soil properties and conditions such as compaction, gradation, pH level, and salinity	Oil leakage from subsurface reservoirs, Water leakage from underground pipelines, Seepage in earth dams, Sea water intrusion near sea shore
Soil Movement	Perturbation of earth masses	Landslide, Land subsidence Earthquake, Active fault zone monitoring

temperature sensor, humidity sensor, seismic sensor, fiber optical sensor, etc. The sensing devices of sensor node such as moisture sensor or temperature sensor could provide point sensing due to the underground sensing environments. However, it is difficult to monitor global subsurface hazard and characteristics due to the limited subsurface sensing capability of the sensor's equipments. With the concept and application of the wireless signal networks, the global subsurface monitoring in real-time can be achieved. The wireless signal network uses the electromagnetic (EM) signal strength variation as the main indicator of an event in the physical domain. Soil properties such as density, water and mineral content are known to play important roles in determining losses of a propagating EM wave. When and if these physical properties of the host soil change during the evolution of a geo-event, they in turn affect the transmission quality and strength of the EM waves within the region of the event. Wireless signal networks have abundant potential applications in monitoring subsurface geo-event. The key applications could be monitoring subsurface hazard and characterizing subsurface environments in real-time using WSiNs. The subsurface monitoring can be categorized into two classes as show in Table 2.2.

Table 2.3: Challenges and solutions on deployment of WSiNs

Challenges on deployment	Descriptions	Open Issues and Solutions
Installation and Management	Difficult to install manage sensors	Good network and topology design minimizing installation and management costs
Battery Power	Hard to replace battery	Use high capacity battery, Optimization to minimize power consumption of sensing and operation
Communication Radius	Short communication radius due to high attenuation of radio signal	Use low radio frequency to extend communication radius communication radius
Event Detection	Difficult to differentiate simultaneous underground events	Design event classification methods based on probability theory based on probability theory
Good Applications	Need good examples of WSiNs deployment	Provide good potential practical applications

2.4 Deployment Challenges and Solutions of WSiNs

The deployment of sensor networks in challenging environments such as underground incurs new problems. Table 2.3 shows the challenging issues and potential solutions of WSiNs deployment.

2.4.1 Installation and Management

The installation and management of WSiNs is much more difficult than aboveground networks because digging a hole and finding sensor underground are not easy tasks. Even the sensor position is easily traceable; the sensor can be damaged when digging. Thus, before deployment underground sensor networks, the network and topology should be designed to minimize installation and management costs. For example, the sensor in high energy consumption can be deployed in shallow depth which will be easier to manage.

2.4.2 Battery Power

Replacing battery of underground sensors is quite difficult because digging a hole and finding sensor underground are not easy tasks. Even the sensor position is easily traceable; the sensor can be damaged during the digging. To avoid replacing battery, high capacity battery and power saving sensor operation such as sleep mode can be used. If sensor nodes adopt high capacity battery such as D batteries (15000 mAh) instead of widely used AA batteries (2000$\sim$2400 mAh), the sensor nodes' lifetime can be extended about 7 times longer. For the sake of minimizing energy consumption of underground sensors operation, sleep mode and long data reporting interval can be adopted. We estimate that the sensors' expected lifetime is about 4 years when two D batteries are used, once or twice packet sending per hour, 1 second sniff period. The sensors sleep during the sniff period and then wake up at the end of the sniff period to detect clear channel and initiate data transmission or listen for data [30]. The value of average power consumption is based on Crossbow's power calculation spreadsheet [31, 32]. If the two D batteries are attached in parallel, the expected sensors' lifetime can be extended.

2.4.3 Communication Radius

In the air, the received signal strength is decaying with distance square, which is introduced by the Friis radio transmission formula. The received signal strength in soil is decaying much faster than air due the high attenuation of radio propagation in soil medium. The received signal strength in soils is defined as follows [33]:

$$P_r(d) = K\frac{e^{-2\alpha d}}{d^2} \tag{2.1}$$

where $K = \frac{A_e cos\theta_\eta}{2|\eta|}(\frac{Ids\mu_0\omega}{4\pi})^2$ is a coefficient not affected by distance and α is the attenuation constant of the medium. The attenuation constant α characterizing the soil properties is defined as follows:

$$\alpha = Re(\gamma) = \omega\sqrt{\frac{\mu\epsilon}{2}\left[\sqrt{1+\left(\frac{\sigma}{\omega\epsilon}\right)^2}-1\right]} \tag{2.2}$$

, where γ is the propagation constant, ω is angular frequency, ϵ is the permittivity, and μ is the magnetic permeability of the soil, and σ is the electric conductivity of the medium. In case of 2.4 GHz MICAz and 433 MHz MICA2, the communication radius are about 20cm and 30cm in wet clay type soil (electrical conductivity = 780 mS, relative permittivity = 30) as shown in Figure 5.2(a).

If the underground sensors use a low frequency, the communication radius can be extended more efficiently. There are candidates of low frequency bands for underground communication such as low frequency ISM (industrial, scientific and medical) bands of 125 KHz, 134 KHz, 6.78MHz, and 13.56MHz. ISM bands are radio bands reserved internationally for the use of radio frequency for industrial, scientific and medical purposes. Based on the theoretical estimation using Equation 2.1, we can achieve 1.6$\sim$2.3m communication with 13.56MHz and 6.78MHz bands, and 31$\sim$32m communication with 134KHz and 125KHz bands even in wet clay underground with 1 Watt Tx power and the same MICA's antenna gain as shown in Figure 5.2(b) and 5.2(c).

2.4.4 Event Detection

The wireless sensor nodes adopt moisture sensors for water leakage detection and accelometer to detection soil movement for landslide and earthquake. In addition to these devices' point sensing capability, the combined information of functional signal with sensing devices will provide more accurate event detection. The received signal strength with respect to distance from the source can be considered as information to be classified for different events. The received signal strength information can be classified by minimum distance classifier using Bayesian decision theory. In the application of Bayesian theory to runtime wireless underground sensor networks, the computational power is an important factor to be considered because wireless sensor nodes have limited battery power and low computational power. To use the information for the event detection, a new event detection method for wireless underground sensor networks should be devised.

2.4.5 Good Applications

The design of good applications is an important issue for wireless underground sensor networks, because the enhanced technology and concept could be useless unless there is no good application. Thus, the dissertation provides a summary of potential practical applications of wireless signals networks. The representative applications of wireless signal networks are experimentally evaluated by laboratory simulations in Chapter 4.

2.5 Summary

In this chapter, the concept of Wireless Signal Networks (WSiNs) is introduced. The chapter provides a summary of existing subsurface monitoring applications which can be used for potential applications of wireless signal networks. The existing subsurface monitoring applications for wireless signal networks can be categorized into two categories: monitoring soil condition and monitoring soil movement. The dissertation summarizes challenge and possible solutions of wireless signal networks based on theoretical and empirical analysis.

Chapter 3

Underground Radio Propagation Model

The theory and experimental data of the underground radio propagation are important for the applications of wireless communications as well as wireless sensor networks. The dissertation introduces an accurate underground radio propagation model for low-power devices such as wireless sensor nodes and evaluates its performance by real wireless sensor nodes. The proposed model describes underground radio signal propagation that is proportional to $e^{-2\alpha d}/d^2$ where d represents the distance and α represents the attenuation constant reflecting the soil properties. The received signal strength in a logarithmic scale expression is a linear function of α at a fixed distance. To estimate the underground radio signal propagation, the proposed model requires two soil properties which are electrical conductivity (σ) and permittivity (ϵ) comparing with a free-space radio propagation model. To evaluate the proposed underground radio propagation model, experiments measuring the radio signal strength with underground sensor nodes were conducted in various sub-surface conditions. Comparing the theoretical estimations of the underground radio propagation and the measured data, the proposed theoretical model fits the measured data well. In the comparisons of theoretical estimations with received signal strength measurements, the soil properties are controlled and measured in both laboratory and field experiments for accurate evaluations.

3.1 Introduction

A group of wireless sensor nodes deployed underground called Wireless Underground Sensor Networks (WUSNs) provides useful information of subsurface environments such as water and mineral content for agriculture, oil leakage from an oil reservoir, or land movement for earthquake monitoring [12]. Spatially distributed underground sensor nodes monitor subsurface conditions and report the information in real-time to the sink or a master node with localized interactions. To deploy a wireless underground sensor network such as monitoring of soil water contents in [34, 35], it is important to understand and model the underground radio propagation between underground sensor nodes. With the underground radio propagation model, network designers can estimate underground communication radius and network capacity. The properties of underground communication medium (i.e. soil) are different from air and the evaluation of the underground radio signal propagation model is required to control the soil properties to verify their effects. But, there is limited research evaluating the underground radio propagation models with measured data in laboratory and field using wireless underground sensors.

The main contribution of this chapter in the dissertation is that it provides an accurate underground radio propagation model with comparisons to measured data in subsurface environments. The dissertation provides the details of developing the underground radio propagation model which can be used for applications of wireless underground sensor networks such as underground sensor node localization and subsurface monitoring. The proposed model is generic and applicable to a wide range of frequencies besides the one used by the current wireless sensors. The proposed underground radio propagation model was evaluated by comparing laboratory and field measurements with the data estimated by the theoretical model. To the best of our knowledge, this is the first comparison study to verify the underground radio propagation model for subsurface (underground to underground) communication in both laboratory and field (actual underground) with wireless sensor nodes operating at 2.4GHz frequency bands.

The remainder of this chapter is organized as follows. In Section 3.2, the related work is introduced. In Section 3.3, the underground radio propagation model for wireless underground sensor networks is presented. Then, in Section 3.4, the proposed underground

radio propagation model is evaluated by the comparisons with the data from laboratory and field experiments. Finally, the chapter is concluded in Section 3.5.

3.2 Related Works

3.2.1 Free-space Propagation

The Received Signal Strength (RSS) between the transmitter and the receiver on the clear and unobstructed line-of-sight (LOS) path can be predicted by a free-space radio propagation model. A well-known radio transmission formula was introduced by H. T. Friis in 1946 [36]. The received power in free space is given by the Friis free space equation as follows:

$$P_r(d) = \frac{P_t G_t G_r \lambda^2}{(4\pi)^2 d^2 L} \tag{3.1}$$

where $P_r(d)$ is the received power which is a function of the transmitter-receiver distance, P_t is the transmitted power, G_t is the transmitter antenna gain, G_r is the receiver antenna gain, d is the distance between the transmitter and receiver, L is the system loss factor not related to propagation ($L \geq 1$), and λ is the wavelength [37]. Log-distance path loss models based on measurements are widely used in practical path loss estimation. The average path loss ($\overline{PL}$) between the transmitter and the receiver is expressed as follows:

$$\overline{PL}(d) \propto \left(\frac{d}{d_0}\right)^n \tag{3.2}$$

or

$$\overline{PL}(dB) = \overline{PL}(d_0) + 10nlog\left(\frac{d}{d_0}\right) \tag{3.3}$$

where n is the path loss exponent that indicates the rate at which the path loss increases with the distance, d_0 is the close-in reference distance which is determined from measurements close to the transmitter, and d is the transmitter-receiver distance [37].

3.2.2 Underground Propagation

Soil Properties on Radio Propagation

The radio signal experiences reflection, diffraction, and scattering over the ground communication as well as in the underground communication. In underground wireless networks, reflection occurs when a propagating electromagnetic wave is confronted by objects such as rocks or the surface between the earth and air. The underground propagation is characterized by the soil properties such as the permittivity (ϵ), permeability (μ), and electrical conductivity (σ). For lossy dielectrics, the permittivity and electrical conductivity are dependent on the operating frequency. These two properties characterize the displacement (polarization) current and the conduction current which incur the power losses of the electromagnetic wave in the soil [38]. Magnetic permeability of soils is very close to the permeability of free space [39]. From these facts, we can infer that the permittivity and electrical conductivity are crucial parameters affecting underground radio propagation.

Modified Friis Model

Researchers have studied a channel model of an underground wireless sensor network using the path loss model [40, 41, 42]. The model is based on the Friis equation [36] and provides an equation describing the received signal strength at a distance d from the transmitter. From the results of the papers, the received signal is described as follows:

$$P_r = P_t + G_r + G_t - [6.4 + 20log(d) + 20log(\beta) + 8.69\alpha d] \tag{3.4}$$

where P_t is the transmit power, G_r and G_t are the gains of the receiver and transmitter antenna respectively, d is the distance in meters, α is the attenuation constant in $1/m$ and β is the phase shifting constant in $radian/m$. In the theoretical research [40] trying to provide the characteristics of a wireless channel for underground sensor networks, a correction factor is added to the Friis equation to apply additional path loss in soils. The additional path loss in the equation depends on the attenuation constant α and the phase shifting constant β, which values depend on the dielectric properties of soil. Based on

the Peplinski's paper [43], the dielectric properties of soil in the 0.3∼1.3 GHz band were calculated in the researches. In the calculation of the path loss, the parameters for underground environments such as operating frequency, the composition of soils, the bulk density, and the volumetric water content are considered. In addition to the attenuation of the radio signal in soil, two channel models, reflection from ground surface and multi-path fading, are introduced based on [37]. These models are evaluated by the theoretical analysis of 300∼900 MHz bands and the follow-up works [44, 45] provide empirical results using MICA2. Recent paper [46] introduces an additional component, lateral waves, in addition to the direct propagation and reflected signal from the surface on the underground communication.

CRIM-Fresnel Model

For the quantification of signal attenuation in soil, [47] investigates the impact of soil depth, soil water content, and soil electrical conductivity on the signal transmission strength using a soil box in the laboratory environment. To approximate the signal attenuation from underground to above ground communications, [47] introduces that the total signal attenuation A_{tot} is the sum of soil attenuation as well as signal reflection as following:

$$A_{tot} = \alpha d + R_c \tag{3.5}$$

where α is the soil attenuation in dB/m from [48], d is the soil depth in meters, R_c is the attenuation due to the reflection. The model is based on the commonly used complex refractive index model (CRIM) which calculates the soil dielectric permittivity from the permittivity of the solid (ϵ_s), water (ϵ_w), and air (ϵ_a) phase at a specific frequency, and assumes that water is the only source of dielectric losses. [47] claims that, [40] uses a more elaborate dielectric mixing model, however, the empirical dielectric mixing model of [43] is not supported by a sufficiently large database, thus the combined CRIM-Fresnel model approach is better suited to get a first indication of the attenuation of radio waves in soils. Recent paper [49], based on the modified Friis model and the combined CRIM-Fresnel model, introduces an underground wave propagation model which takes into consideration the attenuation due to signal reflection, the phase shifting constant, and

signal refraction. Its estimation of the signal attenuation is similar to the modified Friis model.

In our laboratory and field experiments with wireless sensor nodes (MICAz) operating on 2.4 GHz, we observed mismatches on the comparisons of measured data to the existing models. This mismatch and lack of soil property explanation on the radio propagation lead us to design a new generic form of underground radio propagation model and conduct experiments which explain the effects of soil properties affecting underground radio signal propagation. The proposed model is based on [50] which described the electric-field propagation through earth from a vertical electric dipole and presented experimental data over the frequency range from 1$\sim$10 MHz. The model is revisited to produce the received power form of the underground sensor nodes and the proposed model is validated on the frequency bands used by the current wireless sensors. The dissertation presents a generic received power model which can be compared with the path loss model and provides valid derivation on the wide range of frequencies (1MHz$\sim$2.5GHz). The proposed underground radio propagation model derived from an electric dipole is evaluated with measurements of MICAz operating on 2.4GHz in both laboratory and field with the explanation of the effects of soil properties on the radio propagation.

3.3 An Underground Radio Propagation Model

3.3.1 Underground Network Model

Wait and Fuller [50] considered the electromagnetic fields of a vertical electric dipole in a homogeneous conducting half-space using simplifying approximations based on large effective refractive index of the earth. The effective refractive index is a number quantifying the phase delay per unit length in a waveguide relative to the phase delay in a vacuum. Sommerfeld [51] assumes that the Hertz vector of underground radio propagation has only a z component Π, which is referred to as the *potential*. This is conveniently decomposed by writing $\Pi = \Pi^p + \Pi^s$, where Π^p is the primary potential of the source and Π^s is the secondary potential. The latter accounts for the presence of the air interface. Symbols

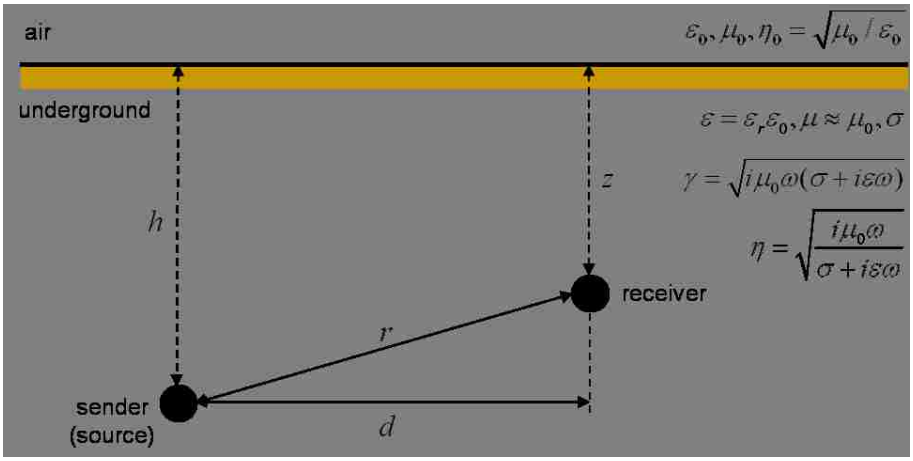

Figure 3.1: Symbols used for deriving underground radio propagation model

used in the underground radio propagation model are shown in Figure 3.1. In the underground network model, the underground medium has permittivity $\epsilon = \epsilon_r \epsilon_0$, permeability μ_0, and electrical conductivity σ, where ϵ_r is the relative permittivity of the underground medium, ϵ_0 $(8.85 \times 10^{-12} F/m)$ is the permittivity of air, and μ_0 $(4\pi \times 10^{-7} H/m)$ is the permeability of air.

3.3.2 Underground Radio Propagation

In an underground network, a source is imagined to be a vertical electric dipole of length ds and carrying a current I. For a time factor $e^{i\omega t}$ in cylindrical-coordinates, the formal exact expression for the primary potential from a Sommerfeld integral is described as follows [50]:

$$\begin{aligned} \Pi^p &= \frac{Ids}{4\pi(\sigma + i\epsilon\omega)} \frac{e^{-\gamma r}}{r} \\ &= \frac{Ids}{4\pi(\sigma + i\epsilon\omega)} \int_0^\infty \frac{e^{-u|z-h|}}{u} J_0(\xi d)\xi d\xi \end{aligned} \tag{3.6}$$

where d is the radial distance from the source, $\gamma = \sqrt{i\mu_0\omega(\sigma + i\epsilon\omega)}$ is the complex propagation constant, $r = \sqrt{d^2 + (z-h)^2}$, $u = \sqrt{\xi^2 + \gamma^2}$, and $J_0(\xi d)$ is the Bessel

function of order zero. The integration variable ξ can be identified with the sine of a plane wave spectrum of complex angle θ via $\xi = -i\gamma \sin\theta$. The secondary potential underground is described as follows [50]:

$$\Pi^s = \frac{Ids}{4\pi(\sigma + i\epsilon\omega)} \int_0^\infty \frac{e^{-u(z+h)}}{u} R(\xi) J_0(\xi d) \xi d\xi \tag{3.7}$$

where $R(\xi) = \frac{u - Ku_0}{u + Ku_0}$ is a Fresnel reflection factor, $u_0 = \sqrt{\xi^2 + \gamma_0^2}$, $\gamma_0 = i\omega\sqrt{\epsilon_0\mu_0}$, and $K = \frac{\sigma + i\epsilon\omega}{i\epsilon_0\omega}$.

The vertical electric-field component, E_z, at the receiver is the observable quantity from the primary and secondary potentials as follows [50]:

$$\begin{aligned} E_z &= E_z^p + E_z^s = \left(-\gamma^2 + \frac{\partial^2}{\partial z^2}\right)\left[\Pi^p + \Pi^s\right] \\ &= \frac{Ids}{4\pi(\sigma + i\epsilon\omega)d^3}(C^p + C^s) \end{aligned} \tag{3.8}$$

where

$$C^p = \left(-\Gamma^2 + \frac{\partial^2}{\partial D_0^2}\right)\left[\frac{e^{-\Gamma\Re}}{\Re}\right], \tag{3.9}$$

and

$$C^s = \int_0^\infty \frac{e^{-UD}}{U} R(x) J_0(x) x^3 dx \tag{3.10}$$

where C^p and C^s are the primary and secondary contributions, $\Gamma = \gamma d$, $D_0 = \frac{|z-h|}{d}$, $\Re = \sqrt{D_0^2 + 1}$, $x = \xi d$ is the integration variable, $U = \sqrt{x^2 + \Gamma^2}$, $D = \frac{z+h}{d}$, $R(x) = \frac{U - KU_0}{U + KU_0}$, and $U_0 = \sqrt{x^2 - (\frac{\omega d}{c})^2}$. After the mathematical calculations, the result of the primary contribution is described as follows:

$$C^p = e^{-\gamma r}\left(\frac{d}{r}\right)^3 \{2(1 + \gamma r) - \left(\frac{d}{r}\right)^2 \left[3(1 + \gamma r) + (\gamma r)^2\right]\}. \tag{3.11}$$

The secondary contribution C^s could be neglected if the air interface was sufficiently removed from the source and observer locations (i.e., deep burial depths). If $z = h$ (the same depth for the sender and receiver) and the burial depth is deep enough (for example, $10\lambda = 1.25m$ for sandy soils or $5\lambda = 0.625m$ for clay type soils with MICAz operating on 2.4GHz) , the electric-field can be simplified as follows:

$$E_z = \frac{Ids}{4\pi(\sigma + i\epsilon\omega)d^3}\{-e^{-\gamma d}\left[1 + \gamma d + (\gamma d)^2\right]\}. \tag{3.12}$$

With the radiating electric-field component, the power density can be calculated with intrinsic wave impedance [52]. The received signal power in $Watts$ can be calculated as follows:

$$P_r = A_e \frac{|E_z|^2}{2\,|\eta|} cos\theta_\eta \tag{3.13}$$

where A_e is the effective antenna area of the receiver, $\eta = \sqrt{\frac{i\mu\omega}{\sigma + i\epsilon\omega}}$ is the intrinsic wave impedance of the medium, and θ_η is the phase angle of the intrinsic impedance $\eta = |\eta| e^{j\theta_\eta}$. For a thin linear half-wave antenna in a wireless sensor network, the effective antenna area is determined by the wavelength as follows: A_e=$0.13\lambda^2$ [38]. The result of the received signal of the wireless underground sensor node with a whip antenna is expressed as follows:

$$P_r = \frac{0.13\lambda^2 cos\theta_\eta}{2\,|\eta|} \left| \frac{Ids\{-e^{-\gamma d}[1 + \gamma d + (\gamma d)^2]\}}{4\pi(\sigma + i\epsilon\omega)d^3} \right|^2 . \tag{3.14}$$

If $|\gamma d| \gg 1$, the received signal strength at distance d can be simplified as follows:

$$\begin{aligned} P_r(d) &\simeq \frac{A_e cos\theta_\eta}{2\,|\eta|} \left| \frac{-Ids \times i\mu_0\omega e^{-\gamma d}}{4\pi d} \right|^2 \\ &= K \left| \frac{e^{-\gamma d}}{d} \right|^2 = K \left| \frac{e^{-2\gamma d}}{d^2} \right| \\ &= K \frac{e^{-2\alpha d}}{d^2} \end{aligned} \tag{3.15}$$

where $K = \frac{A_e cos\theta_\eta}{2|\eta|} (\frac{Ids\mu_0\omega}{4\pi})^2$ is a coefficient not affected by distance and $\alpha = Re(\gamma) = \omega \sqrt{\frac{\mu\epsilon}{2} \left[\sqrt{1 + \left(\frac{\sigma}{\omega\epsilon}\right)^2} - 1 \right]}$ is the attenuation constant of the medium.

The received signal of the wireless underground sensors is proportional to $e^{-2\alpha d}/d^2$ where d represents the distance between the sender and the receiver and α represents the attenuation constant which is determined by the soil properties such as permittivity and electric conductivity. In the simplification a condition, $|\gamma d| \gg 1$, is required. The physical meaning of $|\gamma d|$ is the signal attenuation magnitude with respect to distance, where the higher value the higher attenuation in the medium. In case the radio signal attenuation is high such as underground communications, the received signal strength

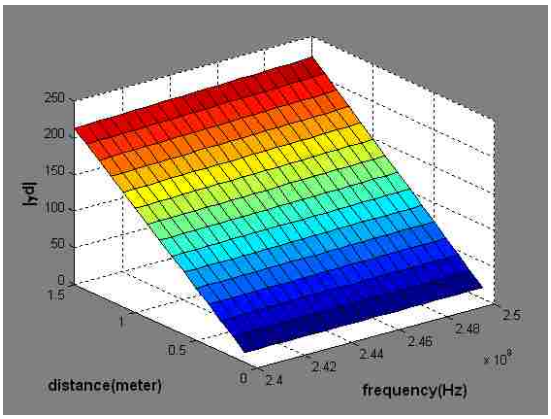

(a) 2.4∼2.5GHz bands

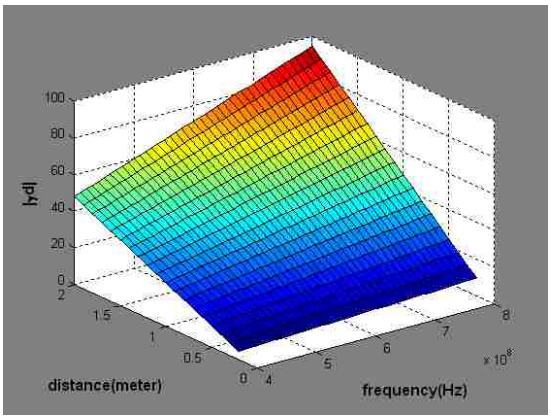

(b) 400∼800MHz bands

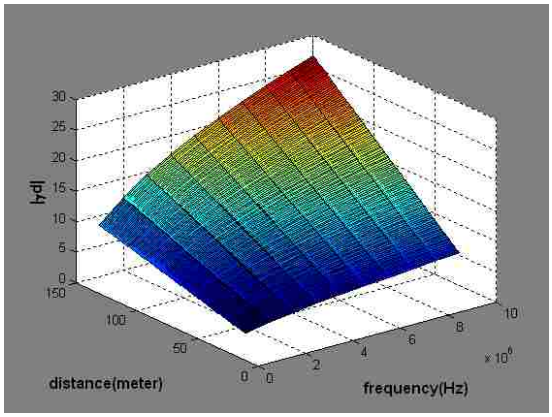

(c) 1∼10MHz bands

Figure 3.2: The values of $|\gamma d|$ in three different frequency ranges

form can be simplified as Equation 3.15. To verify the condition, we calculated and plotted the $|\gamma d|$ in three different frequency ranges with respect to distance in Figure 3.2. In the sensor network frequency ranges of 2.4GHz (MICAz) and 400MHz (MICA2), the value of $|\gamma d|$ is greater than 1 at different distances including close distances. In cases with low frequencies such as 1∼10MHz bands, the simplified form holds if the distance

is greater than 30 meters, which is 0.1λ of the 1Mhz frequency.

3.3.3 Logarithmic Scale Expression

With the proposed underground radio propagation model, the received power can be expressed in a logarithmic scale as follows:

$$\frac{P_r(d)}{P_r(d_0)} \simeq \left(\frac{d_0}{d}\right)^2 e^{-2\alpha(d-d_0)} \tag{3.16}$$

or

$$\begin{aligned}\left[\frac{P_r(d)}{P_r(d_0)}\right]_{dB} &\simeq 10log\left[\left(\frac{d_0}{d}\right)^2 e^{-2\alpha(d-d_0)}\right] \\ &= -20log\left(\frac{d}{d_0}\right) - 8.69\alpha(d-d_0)\end{aligned} \tag{3.17}$$

where d_0 is the close-in reference distance which is close to the transmitter, and d is the transmitter-receiver distance. The logarithmic scale expression has a similar form to the log-normal shadowing model with a pass loss exponent n=2 and an additional path loss term instead of a shadowing deviation. The relative logarithmic expression is consistent with the result form of Equation 3.4 reported in [40, 41, 42], even though the derivation methods are different. Without the reference distance notation, the Equation 3.15 can be expressed in logarithmic scale as following:

$$P_r(d)_{dB} = 10logK - 20logd - 8.69\alpha d. \tag{3.18}$$

At the fixed distance from the source, the received signal strength is a function of the attenuation constant α and the intrinsic wave impedance η (in the constat K of Equation 3.15) which are dependent on the electrical conductivity σ and permittivity ϵ of the soil. Because the attenuation factor is dominant on the signal attenuation of the underground radio propagation, the received signal strength can be expressed by a linear function of α at fixed distances such as $P_r(\alpha)_{dB} = K' - 8.69d\alpha$ where $K' = 10logK - 20logd$. Figure 3.3 shows the linear relation between the received signal strength and the attenuation constant (α) at the fixed distance where α values are calculated from Table 4.2. Using

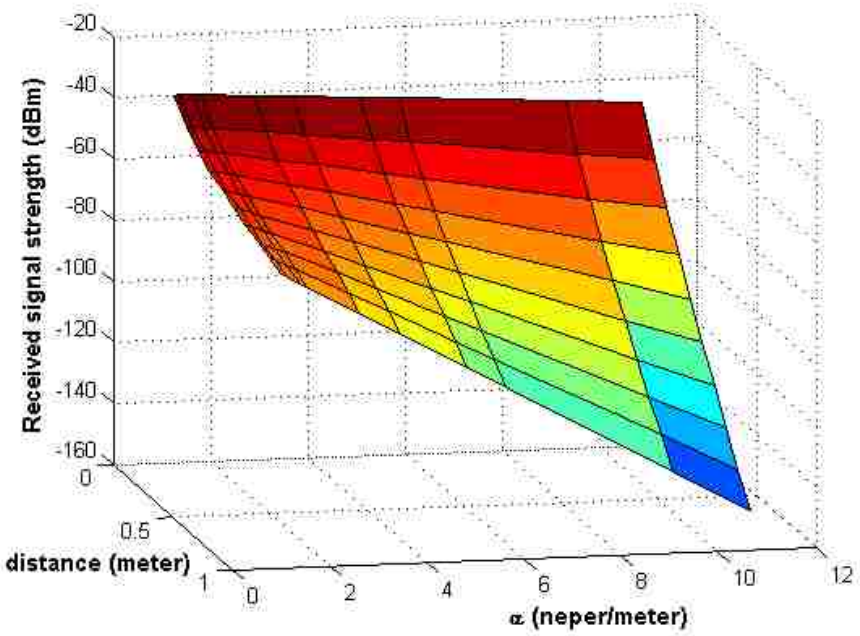

Figure 3.3: Received signal strength with attenuation constant (α) at the fixed distance

received signal strength at the fixed distance, the attenuation constant α can be estimated as following: $\alpha \approx (K' - P_r)/8.69d$. In the subsurface monitoring applications using the received signal strength variation as a main indicator of subsurface events introduced in [53], the subsurface events (i.e., soil properties change) can be detected by the attenuation constant deviation as follows: $\alpha(d, t + \Delta t) \geq \zeta \times \alpha(d, t)$, where t is time and ζ is the deviation criterion which can be empirically determined based on the underground environments.

3.3.4 Effects of Soil Properties and Frequency

The underground received signal in the proposed equation experiences signal attenuations depending on the transmission power, the operating frequency, and the underground medium's properties, which are permittivity and electric conductivity. To evaluate the

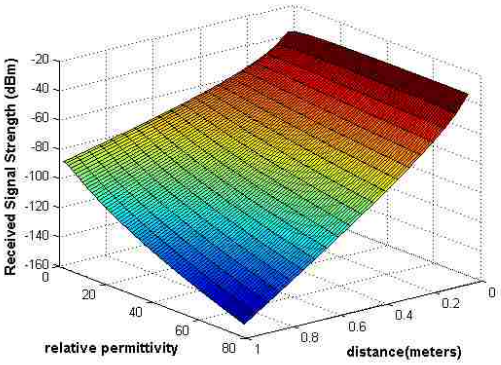

(a) RSS with relative permittivity (ϵ_r) of soil and distance (d)

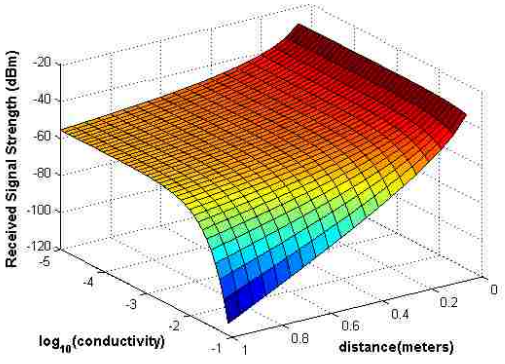

(b) RSS with electric conductivity (σ) of soil and distance (d)

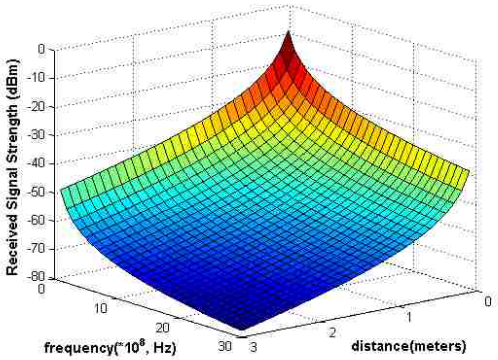

(c) RSS with operating frequencies and distance (d)

Figure 3.4: Relationships between the Received Signal Strength (RSS) and communication distance, soil properties, and frequency

effect of permittivity, we calculated and plotted the received signal strength of 2.4 GHz sensor nodes with respect to distance (0.05$\sim$1 meters) in Figure 3.4(a).

The transmission power is set to be 0dBm in all comparisons in Figure 3.4. The

range of relative permittivity (ϵ_r) is 2$\sim$79 (ex, 1: air, 80: water) with a loss tangent ($tan\delta$=ϵ''/ϵ'=0.05, estimated from [43]) where ϵ=$\epsilon' - i\epsilon''$. In Figure 3.4(a), the received signal strength decreases as the relative permittivity increases in the permittivity range of soils (relative permittivity of saturated sandy soil: 19$\sim$30 [54]).

To investigate the effect of electric conductivity, we calculated the received signal strength with relative permittivity of 20 (Figure 3.4(b)). The maximum communication distance of the underground sensor network is expected to be around 1 meter in 2.4 GHz [45, 55, 56]. So, we chose the short distance of 0.05$\sim$1 meters with various electric conductivities. The range of electric conductivity is $10^{-1}\sim10^{-5}$ (ex, electric conductivity of drinking water: $0.0005\sim0.05$, electric conductivity of soil: $\sim10^{-1}$ from Table 4.2 and [57]). In Figure 3.4(b), the received signal strength dramatically changes in the range of conductivity between 10^{-1} and $10^{-2.5}$ S/m. Increasing the distance in the range of electric conductivity between 10^{-1} and $10^{-2.5}$ S/m causes the signal strength to decay quickly due to high attenuations in the soil. Because the transmission power is set to be 0dBm in the comparisons, the received signal strength converges to Tx power level (0dBm) as the distance goes to 0.

The effects of the operating frequency (100MHz$\sim$3GHz) with fixed Tx power (0dBm) are shown in Figure 3.4(c) with fixed electric conductivity ($10^{-2}S/m$) and relative permittivity of 20. The received signal strength decreases as the operating frequency is getting higher because the higher frequency has more attenuation in the soil medium. Thus, the lower frequency band can achieve the longer communication distance on the underground communication if the antenna gain and Tx power are same.

3.4 Performance Evaluations

To evaluate the accuracy of the proposed underground radio propagation model, various experiments in the laboratory and in the field were conducted using MICAz (2.4GHz). The MICAz sensor nodes are with CC2420 which is 2.4 GHz IEEE 802.15.4 compliant RF transceiver and includes a digital direct sequence spread spectrum baseband modem. The operating frequency was configured to be 2.48GHz which is Zigbee channel

26 and non-overlapping with 802.11b (WiFi). All wireless sensor nodes are calibrated and selected to be working in 1$\sim$2 dBm error bounds on the received signal strength measurement. A wireless sensor nodes (sender) sends a packet at every 15 seconds, and the receivers sample the received signal strength from the received packets and store the date on the flash memory in which data can be retrieved in the laboratory with serial or ethernet programming boards connected to the PC. As an underground medium, two types of sand were used: uniform size construction sands (D_{10}=0.2mm, D_{30}=0.34mm, and D_{60}=0.67mm) and (D_{10}=0.40mm, D_{30}=0.51mm, and D_{60}=0.62mm) where D_x is the diameter of the soil particles for which $x\%$ of the particles are finer.

3.4.1 Experimental Conditions

Laboratory tests

To control the soil properties, a small plastic (PVC) box with dimensions 118$\times$13$\times$13cm was made as shown in Figure 3.5(a) and 3.5(b) and filled with controlled soils. In each experiment, physical soil properties (e.g. particle size distribution, soil density) and temporally dynamic variables (e.g. soil water content, salinity, soil temperature, etc.), which affect the electric conductivity and permittivity of the medium, were controlled. The validity of using the PVC box for the measurements is evaluated by comparing with actual underground measurements in the appendix. The electric conductivity values of the soil in all experiments were measured as shown in Table 4.2 and the relative permittivity of the soil is estimated between 19$\sim$30 based on [54].

Field test

The field tests were conducted at a remote corner of the athletic field facilities of Lehigh University. This area was selected because of its isolation from existing Wi-Fi interference and surface noise, distance from major underground facilities, and type of the sandy soil encountered which matched reasonably well with the sand used in laboratory experiments. The field tests were conducted at the burial depth of 140cm for thermal and moisture isolation as well as isolation from EM interferences. A square trench of

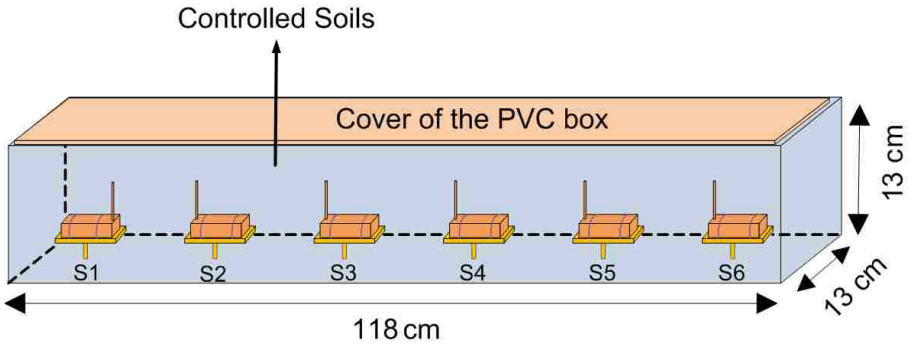

(a) Designed PVC box to install sensors (one transmitter (S1) and five receivers)

(b) PVC box with sensors before soil filling

(c) Installed sensors in the box with temperature probes before burying

Figure 3.5: Details of laboratory and field test preparation

150×150cm was excavated to 140cm depth. The soil properties inside the PVC box were controlled and the surrounding soil and environmental conditions are monitored during the field experiments. The small test box underground was also equipped with two thermocouples underneath the top cap to monitor the temperature of the test sand as shown in

Figure 3.5(c). The field tests were conducted for the duration of 4 days, during which the transceivers sampled and stored data at 15 second intervals.

3.4.2 Comparison of Results

The received signal strengths with 0dBm Tx power in the laboratory and field tests were measured for 5%, 8%, 12%, 15%, and 20% wet sand and compared with the theoretical received signal strength estimation using Equation 3.15 (proposed model) and Equation 3.4 (comparison model) in dBm scale, and the measured electric conductivity of sand summarized in Table 4.2. In the comparisons, the average absolute deviation (D in dBm scale) or mean absolute error (MAE) between the measured data and the theoretical estimations on N positions is calculated as follows:

$$D = \frac{1}{N}\sum_{i=1}^{N} |P^i_{measured} - P^i_{estimated}|. \tag{3.19}$$

Then, the accuracy (A, %) based on mean absolute percentage deviation (MAPD) or mean absolute percentage error (MAPE) is calculated as follows:

$$A = [1 - \frac{1}{N}\sum_{i=1}^{N} |\frac{P^i_{measured} - P^i_{estimated}}{P^i_{measured}}|] \times 100. \tag{3.20}$$

MAPE is commonly used to evaluate cross-sectional estimation/forecast and expressed in generic percentage terms that will be understandable to a wide range of users [58].

In the comparisons, the electric conductivity of wet sand was in the range of 20$\sim$300mS/m which were measured values as shown in Table 4.2, and the permittivity of the wet sand was in the range of 19$\sim$30 [54] which were estimated values according to changes of moisture content and salinity.

The theoretical estimation (σ=86.96mS/m, ϵ_r=19), laboratory measurements, and field measurements for the 12% wet sand with 5000ppm salinity are compared in Figure 3.6. The average deviation between the laboratory and field measurements was 5.2dBm which was the amount of deviation seen in different laboratory experiments. The average deviation and accuracy between the theoretical estimation of the proposed radio propagation model and the field measurement were 4.36dBm and 93.26% respectively, and the

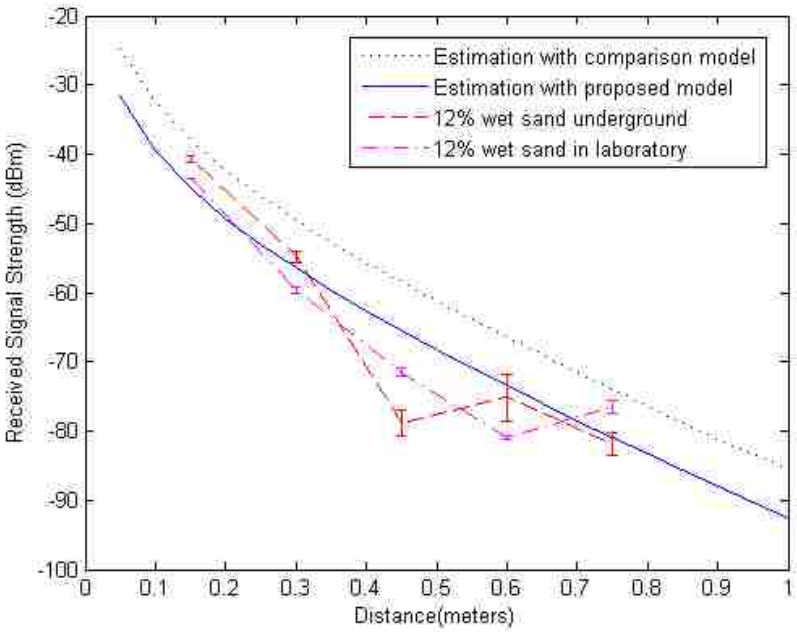

Figure 3.6: Comparison of theoretical estimations and field/laboratory measurements: 12% wet sand with salinity (5000ppm)

average deviation and accuracy between the estimation and the laboratory measurement were 4.49dBm and 93.56% respectively. The average deviation and accuracy between the theoretical estimation of the comparison model and the field measurement were 8.96dBm and 87.35%, and between the estimation and the laboratory measurement were 9.11dBm and 85.84% respectively. In both field and laboratory measurements, the proposed model more accurately estimates the received signal strength.

The theoretical estimations (5% wet sand: σ=23.42mS/m, ϵ_r=19; 8% wet sand: σ=37.61mS/m, ϵ_r=19; 15% wet sand: σ=123.61mS/m, ϵ_r=30; 20% wet sand: σ=283.77mS/m, ϵ_r=30), laboratory measurements of 5% wet sand with 1000ppm salinity, 8% wet sand with 5000ppm salinity, 15% wet sand with 1000ppm salinity, and 20% wet sand with 5000ppm salinity are compared in Figures 3.7(a), 3.7(b), 3.7(c), and 3.7(d). The average deviation and accuracy between the theoretical estimation of the proposed model and

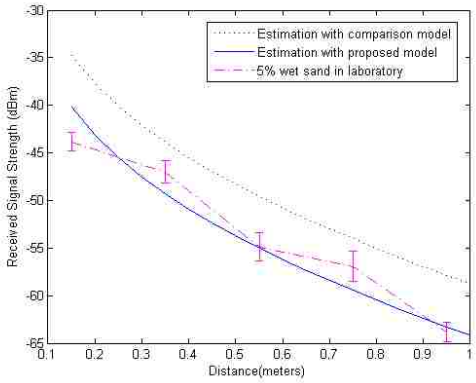

(a) 5% wet sand with salinity (1000ppm); theoretical estimations vs. laboratory measurements

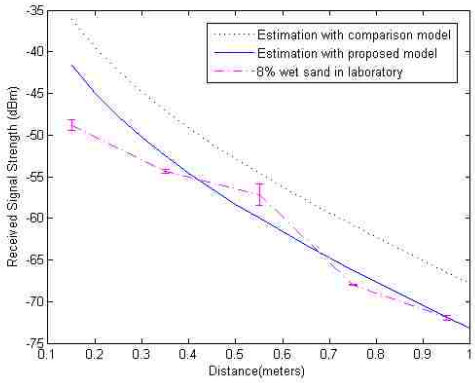

(b) 8% wet sand with salinity (5000ppm); theoretical estimations vs. laboratory measurements

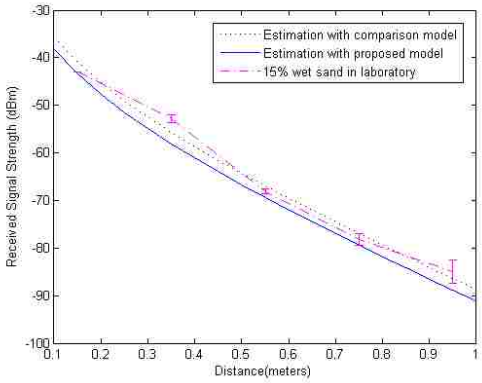

(c) 15% wet sand with salinity (1000ppm); theoretical estimations vs. laboratory measurements

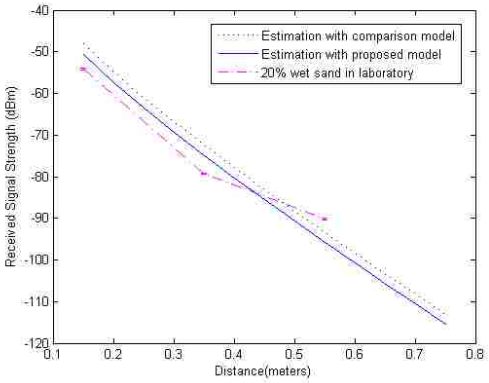

(d) 20% wet sand with salinity (5000ppm); theoretical estimations vs. laboratory measurements

Figure 3.7: Comparison of theoretical estimations and measured data

the 5% wet sand measurement were 1.92dBm and 96.24%, and between the estimation of the comparison model and the measurement were 4.46dBm and 91.89%, respectively. The average deviation and accuracy between the theoretical estimation of the proposed

Table 3.1: Comparison of theoretical estimations and measured results (F:Field, L:Laboratory, D:Deviation, A:Accuracy)

Model	Results	5%L	8%L	12%F	12%L	15%L	20%L	Average
Proposed Model	D (dBm)	1.92	3.19	4.36	4.49	1.77	6.01	3.62
	A (%)	96.24	94.01	93.26	93.56	97.43	91.95	94.41
Comparison Model	D (dBm)	4.46	10.25	8.96	9.11	5.12	8.44	7.72
	A (%)	91.89	82.59	87.35	85.84	92.89	88.54	88.18

model and the 8% wet sand measurement were 3.19dBm and 94.01%, and between the estimation of the comparison model and the measurement were 10.25dBm and 82.59%, respectively. In 8% wet sand comparison, the comparison model shows relatively low accuracy on the estimation. The average deviation and accuracy between the theoretical estimation of the proposed model and the 15% wet sand measurement were 1.77dBm and 97.43%, and between the estimation of the comparison model and the measurement were 5.12dBm and 92.89%, respectively. In 15% wet sand comparison, two models show accurate estimations. The average deviation and accuracy between the theoretical estimation of the proposed model and the 20% wet sand measurement were 6.01dBm and 91.95%, and between the estimation of the comparison model and the measurement were 8.44dBm and 88.54%, respectively. The sensors located at 75cm and 95cm lost the signal from the source due to high attenuation in wet soil and no data was recorded.

The comparison results are summarized in Table 3.1 which confirms that the theoretical received signal strength estimation fits the measured data well within a 3.62dBm deviation or with an accuracy of 94.41% on average. The smaller average absolute deviation or higher accuracy represents the estimation is statistically more accurate based on all measurements. Thus, the proposed underground radio propagation model provides more accurate fit to the measured data in all laboratory experiments. The accurate radio propagation model can be used for the applications of subsurface event classification, where the estimation error on the radio propagation affects the classification error.

3.4.3 Comparison with Underground Measurement

To control and maintain the soil properties such as water content and relative density during experiments, plastic (PVC) boxes should be used as shown in Figure 3.5(b) in the performance evaluation. In the measurements, the radio signals could be reflected from the surfaces of the box, however, the reflected signals are expected to be negligible because of the high attenuation of the small amounts of the reflected signals. The reflection coefficient (R) between the soil and the PVC box can be calculated according to the Fresnel equation as following: $R \approx (\sqrt{\epsilon_{r,soil}} - \sqrt{\epsilon_{r,PVC}})^2/(\sqrt{\epsilon_{r,soil}} + \sqrt{\epsilon_{r,PVC}})^2 = 0.1192$ where $\epsilon_{r,soil} = 19$, $\epsilon_{r,PVC} = 4.5$ [47, 54, 59]. To investigate the effect of the actual reflection, we compared the data using the box with actual underground measurements. To realize actual underground communications, we directly installed sensor nodes underground near the field test location where the soil is a wet clay type soil which is more realistic soil sample for underground environments. Using the underground clay type soil samples, however, it is difficult to characterize and control the soil properties for various experiments. In the preliminary test with the wet clay type soil samples, the maximum underground communication distance of MICAz is about 30cm. So, a square trench of 60$\times$100cm was excavated to the depth of 60cm for the actual underground environment in which there is no reflected signal from the surface. For the comparison, the PVC box was filled with the same wet clay type soil on the ground. The Received Signal Strength (RSS) of an underground sensor node located from 7.5cm from the sender was -39dBm whereas RRS of a sensor inside the box was -36.26dBm where the deviation was 2.74dBm. At the location of 25cm from the sender, the RSS of an underground sensor node was -77.89dBm whereas RRS of a sensor inside the box was -72.22dBm where the deviation was 5.67dBm. The average deviation between actual underground and PVC box measurements was 4.2dBm which was the amount of deviation seen in the experiments depending on the minor environmental condition changes (e.g., relative density, temperature, and small antenna angle change), and could not provide significant effects on the performance evaluations. The slightly lower received signal strength on the actual underground is originated from not only no reflected signals from the surfaces, but also soil compaction due to the soil mass which effect can be seen at Figure 4.2(d). From

the comparisons and analysis, the measurement using PVC box is a valid method for the performance evaluation.

3.5 Underground Wireless Sensor Network Design Guidance: Required Number of Sensor Nodes

In the application of wireless underground sensor network, the topology construction is an important task due to the high attenuation of the wireless signal. Using the proposed underground radio propagation model in Equation 3.15, the distance from the radio signal source can be calculated by $d = W\left(\sqrt{\frac{\alpha^2}{K \times P_r}}\right)/\alpha$, where W is the Lambert W function. When Tx power (P_t) and the minimum sensible power (P_{min}= -94dBm in MICAz) are known, the required number of underground sensor nodes are estimated based on the distance formulation.

The wireless underground sensor networks can be used for underground infrastructure monitoring applications such as monitoring pipes, electrical wiring, and liquid storage tanks underground. Monitoring the structural health of any underground components of an integrated structure such as building foundation, bridge pier, or dam's foundation is a good practical application of wireless underground sensor networks. The connected shapes of these underground infrastructure can be modeled by three representative topologies: 1) a connected barrier (line), 2) a polygon, and 3) a circle.

1. Required number of sensor nodes for a connected barrier: Let d_i is the communication distance between i^{th} and $(i+1)^{th}$ nodes. To provide a connected network over M meters, $\sum_{i=1}^{N-1} d_i \geq M$, where N is the required number of sensor nodes. If the soil properties are consistent over the area (i.e., $d_1 = d_2 = \cdots = d_{N-1} = d$), the required number of sensor nodes for the line network is expressed as follows:

$$N \geq \lceil \frac{M}{W\left(\sqrt{\frac{\alpha^2}{K \times P_{min}}}\right)/\alpha} \rceil + 1. \tag{3.21}$$

2. Required number of sensor nodes for a polygon: The perimeter of a building foundation can be modeled by a polygon. To construct a network for the polygon in a

consistent soil medium, the required number of sensor nodes is expressed as follows:

$$N_k \geq \sum_{i=1}^{k} N_i - (k-1) \tag{3.22}$$

$$= \sum_{i=1}^{k} \lceil \frac{M_i}{W\left(\sqrt{\frac{\alpha^2}{K \times P_{min}}}\right)/\alpha} \rceil - 2k + 1 \tag{3.23}$$

where a polygon has k sides and N_i is the required number of sensor node for i^{th} side which length is M_i meters.

3. Required number of sensor nodes for a circle: The perimeter of underground water or oil tank can be imagined as a circle. If the soil properties are consistent, the required number of sensor nodes for a circle network with a radius M_r is expressed as follows:

$$N_c \geq \lceil \frac{360}{tan^{-1}(d/M_r)} \rceil \tag{3.24}$$

$$= \lceil \frac{360}{tan^{-1}(\frac{W\left(\sqrt{\frac{\alpha^2}{K \times P_{min}}}\right)}{\alpha M_r})} \rceil. \tag{3.25}$$

3.6 Summary

This chapter provides theories and measured results to improve the understanding of underground radio signal propagation of wireless sensor networks. Based on the theories, we developed the received signal strength expression as well as the logarithmic scale expression of the underground radio propagation with respect to the distance between the sender and the receiver. The proposed underground radio propagation model is accurate due to its derivation based on theoretical studies of how radio propagate in subsurface environments. The proposed model was validated using laboratory and field measurements. The estimated received signal strength from the underground radio propagation model provides a very good fit to the measured data of the wireless underground sensor networks. Based on the proposed propagation model and measurements, the required numbers of sensor nodes for three underground network topologies are presented.

Chapter 4

Subsurface Event Detection and Classification

Subsurface environment sensing and monitoring applications such as detection of water intrusion or a landslide, which could significantly change the physical properties of the host soil, can be accomplished using a novel concept, Wireless Signal Networks (WSiNs). The wireless signal networks take advantage of the variations of radio signal strength on the distributed underground sensor nodes of WSiNs to monitor and characterize the sensed area. Experiments demonstrated that calibrated wireless signal strength variations can be used as indicators to sense changes in the subsurface environment. The concept of WSiNs for the subsurface event detection is evaluated with applications such as detection of water intrusion, relative density change, and relative motion using actual underground sensor nodes. To classify geo-events using the measured signal strength as a main indicator of geo-events, we propose a window-based minimum distance classifier based on Bayesian decision theory. The window-based classifier for wireless signal networks has two steps: event detection and event classification. With the event detection, the window-based classifier classifies geo-events on the event occurring regions that are called a *classification window*. The proposed window-based classification method is evaluated with a water leakage experiment in which the data has been measured in laboratory experiments. In these experiments, the proposed detection and classification method based on wireless

signal network can detect and classify subsurface events.

4.1 Introduction

Wireless sensor networks have the potential to be implemented in subsurface sensing and monitoring applications, which are called Wireless Underground Sensor Networks (WUSNs) [12]. The key applications could be monitoring subsurface hazard and characterizing subsurface environments in real-time using wireless sensor nodes. In the applications of subsurface hazard monitoring, wireless sensor networks can be used for slope monitoring or predicting landslide. Subsurface wireless sensor nodes can adopt existing sensing devices (e.g., MICA2/z with MTS300/310/400/410 for light, temperature, humidity, barometric pressure, seismic, acoustic, sounder, and accelerometer [60]). However, the sensor nodes only provide point measurements and are incapable of providing global measurement for characterization and monitoring of subsurface medium. To characterize and monitor subsurface environments globally, the concept of Wireless Signal Networks (WSiNs) is introduced in this chapter. The WSiNs use the wireless signal strength variation between the distributed sensor nodes as the main indicator of a subsurface event or physical change in the host medium properties.

The target applications of subsurface hazards monitoring include landslide, earthquake, and active fault zone monitoring which involve a lot of perturbation of earth masses and are characterized by the localization of sensors which allows sensors to estimate their locations using information transmitted by a set of seed sensors. Other potential applications of characterizing subsurface environments include monitoring of oil leakage from subsurface reservoirs, water leakage from underground pipelines, seepage in earth dams, and estimation of soil properties and conditions such as compaction, gradation, and salinity based on the Received Signal Strength (RSS) information. The received signal strength with respect to distance from the source can be considered as information to be classified for different events. The received signal strength information can be classified by minimum distance classifier using Bayesian decision theory. In the application of Bayesian theory to runtime wireless underground sensor networks, the computational

power is an important factor to be considered because wireless sensor nodes have limited battery power and low computational power. In the dissertation, window-based minimum distance classifier is proposed for energy and computational efficient classifier for wireless signal networks maintaining high accuracy with less computation. This chapter in the dissertation makes three research contributions.

- A detailed list of network parameters and soil properties is provided with experimental data on how radio propagation is affected by soil properties in subsurface communication environments. With the comprehensive analysis of network parameters and soil properties in subsurface communication environments, network designers and researchers can estimate underground communication radius and network capacity, and use the experimental data for their underground wireless network design.

- The WSiN concept is evaluated for the event detection of subsurface applications such as detection of water intrusion, relative density change, and relative motion using actual underground sensor nodes. For the event detection concept and experiment, a new type of subsurface sensing system is developed.

- A window-based minimum distance classifier based on Bayesian decision theory is evaluated with the water leakage experiment. The received signal strength information over the existing underground communications of wireless sensor nodes is used as a tool for subsurface event detection and classification with high accuracy and less computation.

To monitor underground environments, the underground radio propagation model can be used by underground wireless signal networks which use the wireless signal strength variation in the soils as the main indicator of an event. By analyzing the received signal strength, the wireless sensor networks can collect additional information from the wireless data carrier. The targeted events are subsurface hazards such as a landslide or earthquake which involve a lot of shifting and moving of earth masses, and the intrusion of a chemical plume which would dramatically change the physical properties of the host soil as shown in Figure 2.1. These events would affect the transmission of radio waves and the received

signal strength in the region. Because the underground received signal strength deviation is very small, the subsurface events can be detected by the signal strength deviation as follows: $P_r(d, t + \Delta t) \geq \zeta \times P_r(d, t)$, where ζ is the deviation criterion which can be empirically determined based on the underground environments. If the sensor nodes are equipped with a moisture sensor or an accelerometer, the wireless signal networks will provide more accurate detections such as the soil parameter variation and distance from the signal source. Using the underground radio propagation model in Equation 3.15, the distance from the source can be calculated by $d = W\left(\sqrt{\frac{\alpha^2}{K \times P_r}}\right)/\alpha$, where W is the Lambert W function. At the fixed distance from the source, the received signal strength is a function of the attenuation constant α and the intrinsic wave impedance η (in the constat K of Equation 3.15) which are dependent on the electrical conductivity σ and permittivity ε of the soil. If the soil condition is changed due to the event such as water leakage on the medium between sensors, the sensor can detects the event based on the decreased received signal strength and classify the event based on the reference data which can be generated by Equation 3.15 or empirical data.

4.2 Parameters and Properties affecting Underground Radio Propagation

In the wireless underground sensor network deployments and experiments, the received signal is affected by network parameters and soil properties. From our measured data and existing works [43, 45, 61], there are the network parameters and soil properties that affect the received signal strength. The dissertation provides a detailed list of the network parameters and soil properties on how radio propagation is affected by soil properties in subsurface communication environments with experimental data. The experimental conditions for the measurements are described in Section 3.5 and the PVC box shown in Figure 3.5(a) and 3.5(b) is used to evaluate the soil and network parameters affecting on the received signal strength. The summarized parameters and the effects on the received signal strength are presented in Table 4.1.

Table 4.1: Parameters affecting the received signal strength in underground communications

Parameters		Effects on received signal
Network Parameters	Tx Power	Tx power ↑ ⇒ received signal ↑
	Distance	Distance ↑ ⇒ received signal ↓
	Burial depth	Burial depth ↓ ⇒ received signal ↑
	Antenna orientation	Angle change ⇒ Different strength
Soil Properties	Soil Gradation	Particle size ↑ ⇒ received signal ↑
	Water content	W.C. ↑ ⇒ received signal ↓
	Salinity	Salinity ↑ ⇒ received signal ↓
	Relative density	Relative density ↑ ⇒ received signal ↓
	Temperature	Temperature ↓ ⇒ received signal ↑

4.2.1 Network Parameters

Transmit Power

The received signal strength in underground communication is proportional to the transmission power ($P_r \propto P_t$) which is the same as in air communication. The received signal strength of higher TX power (0 dBm) is greater than lower TX power (-5 dBm) in the sandy soil which contains 12 % water content shown in Figure 4.1(a).

Distance between sender and receiver

The received signal strength in underground communication is proportional to $e^{-2\alpha d}/d^2$ which means the signal decays as the distance increases. Due to the attenuation factor ($e^{-2\alpha d}$) in the soil, the rate of decay is much faster than in air communication. The decaying received signal strengths are shown in Figures 3.4(a), 3.4(b), 3.3, and 4.1(a).

Burial depth

As the burial depth increases, there is no reflected signal from the surface between underground and air. To evaluate the effects of burial depth in underground sensor networks,

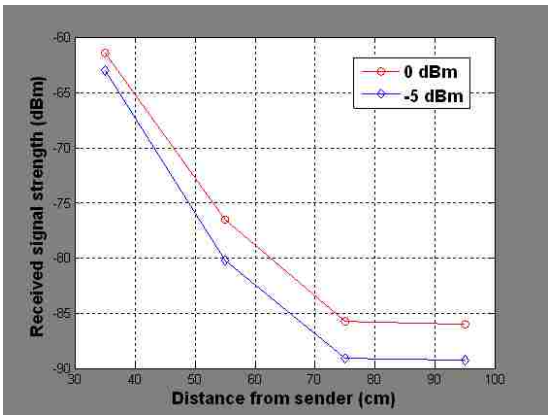

(a) TX powers

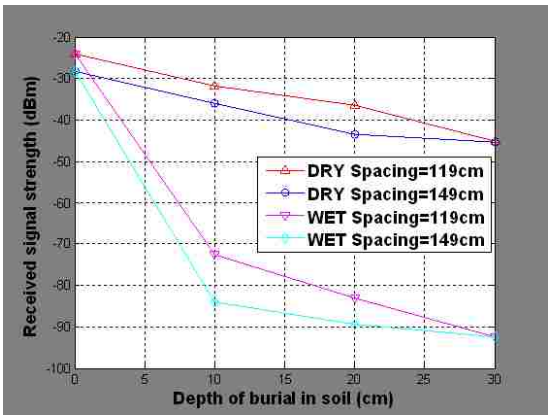

(b) Burial depths

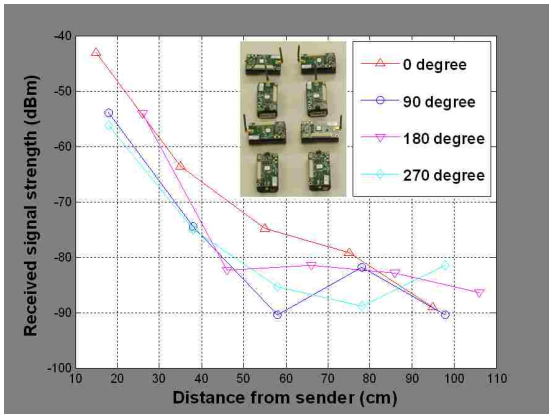

(c) Antenna angles

Figure 4.1: Received signal strength variations with wireless network parameters

the received signal strength was measured at different burial depths in a large soil box with dimensions 122cm long, 86cm wide, and 51cm deep. The box was filled with construction sand (D_{50}=0.56mm) with two different levels of Water Content (W.C.): dry and 8% water content. As shown in Figure 4.1(b), the signal strength decreases as the burial depth increases. The trend is more significant for wet sand.

Antenna orientation

In wireless communication, the antenna is an important component affecting the received signal strength. In wireless underground sensor networks, the orientation of the antenna angle also affects the signal strength at the receivers. The antenna angle is defined as the rotation angle (counter clock wise for the sender, clock wise for the receiver) from the position that the sender and receiver antennas are face-to-face as shown in Figure 4.1(c). To evaluate the effects of antenna orientation, the received signal strengths are measured at four different angles in wet sand with 12% moisture content. In the measurement, the angle 0° means the sender and receiver antennas are facing each other, and the sender and receiver are rotating at different angles counter clock wise and clock wise respectively. In Figure 4.1(c), the received signal strength has about 10 dBm difference at different angles. In all other measurements, the 0° antenna angle is used.

4.2.2 Soil Properties

The received signal strength is affected by the soil properties such as physical soil properties (e.g. particle size distribution, soil density) and temporally dynamic variables (e.g. soil water content, salinity, soil temperature, etc.) which are affecting the electric conductivity and permittivity of the soil. To evaluate the variation of the received signal strength and apply the changing electric conductivity to the proposed theoretical model, the electric conductivity of the soil was measured for different water contents and salinity based on ASTM (American Society for Testing and Materials) G187 standard [62] and the results are shown in Table 4.2.

Soil gradation

The received signal strengths in two types of sand with different gradations were compared. The comparisons of the received signal strength for the fine and medium sands at 12% water content are shown in Figure 4.2(a). The average particle size (D_{50}) of fine

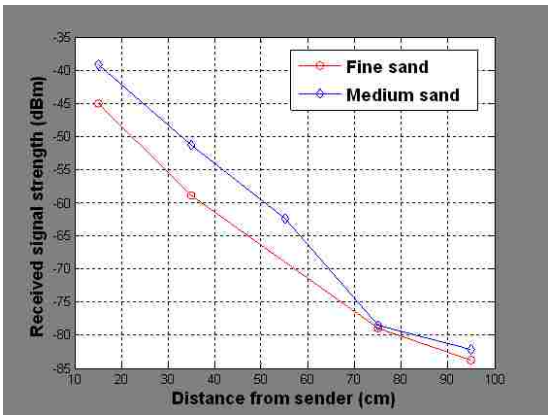

(a) Soil gradation

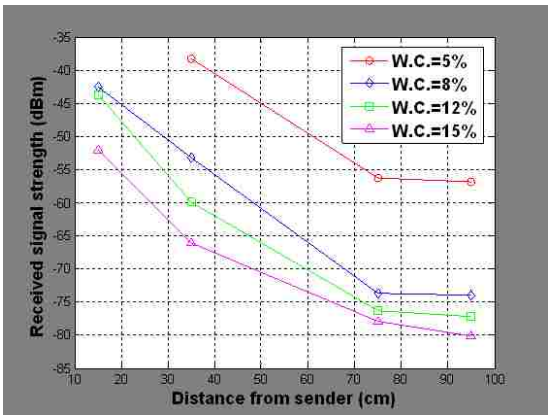

(b) Water contents (W.C.)

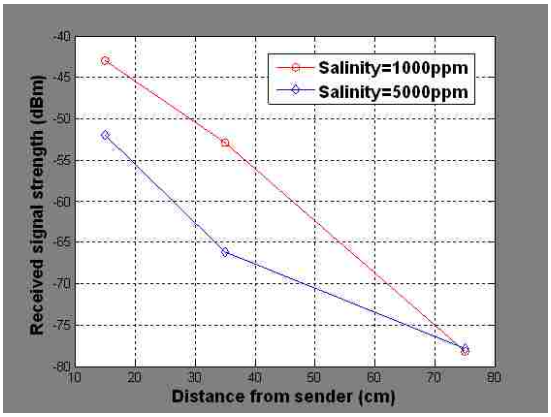

(c) Salinity

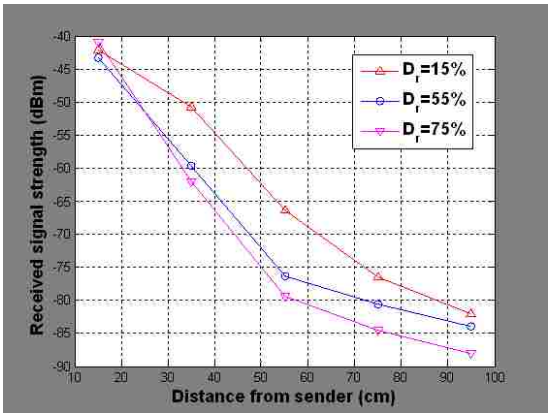

(d) Relative density

Figure 4.2: Received signal strength variations with changing soil properties

and medium sand was 0.58 and 0.98 mm respectively. The received signal strength increases as the particle size in the soil increases. This may be attributed to the fact that, in the same soil type and condition, the soil with smaller particle size has higher electrical conductivity which incurs higher attenuation in the radio signal propagation.

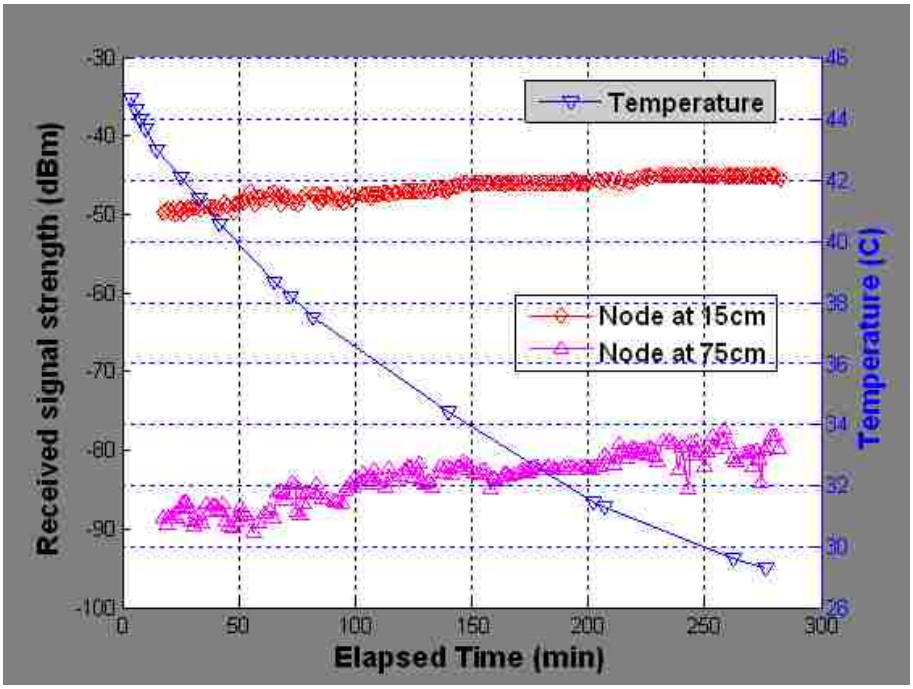

Figure 4.3: Received signal strength variations with temperature changes

Water content

The increase in the water content increases the electric conductivity of the soil as presented in Table 4.2. The increased conductivity induces more attenuation on the underground radio propagation. The received signal strengths for different water contents were measured and the results for water contents of 5%, 8%, 12% and 15% are shown in Figure 4.2(b). As seen in Figure 4.2(b), the received signal strength decreases as the water content increases.

Salinity

As the salinity of the soil increases, the electric conductivity of the soil increases (see Table 4.2). The received signal strengths for different salinity levels were measured and the results for salinity levels of 1000 and 5000 ppm at a water content of 15% are shown

Table 4.2: Electric conductivity of the soil used in received signal strength measurements

Soil Type	Water Content(%)	Salinity(ppm)	Electric Conductivity(mS/m)
Fine Sand	5	1000	23.42
		5000	26.67
	8	1000	33.16
		5000	37.61
	12	1000	65.36
		5000	86.96
	15	1000	123.61
		5000	146.05
	20	1000	238.66
		5000	283.77

in Figure 4.2(c) where the received signal strength decreases as the salinity increases.

Relative density

The received signal strengths for different relative densities (D_r, an index that quantifies the state of compactness between the loosest and densest possible state of coarse-grained soils) were measured at constant water contents. The results for specimens of fine sand at relative densities of 15, 55, and 75% by compaction at constant water content of 12% are shown in Figure 4.2(d). As shown in Figure 4.2(d), the received signal strength of the loose sand at 15% relative density is higher than the denser sands of 55% and 75% relative densities. The received signal strength decreases as relative density increases and the the influence of signal attenuation is significant at longer distance.

Temperature

To evaluate the effects of underground temperature, the received signal strengths were measured as the temperature dropped in a simulation test and the results are shown in Figure 4.3. As seen in Figure 4.3, the received signal strength increases as the temperature drops because the electrical conductivity of the soil decreases slightly while the temperature dependence of the soil bulk dielectric permittivity is negligible for small and

medium moisture soils [63, 64, 65].

4.3 Subsurface Event Detection and Classification

The received signal strength with respect to distance from the source can be considered as information to be classified for different events. The received signal strength information can be classified by minimum distance classifier using Bayesian decision theory. In the application of Bayesian theory to runtime wireless underground sensor networks, the computational power is an important factor to be considered because wireless sensor nodes have limited battery power and low computational power. A MICAz sensor node has a low-power microcontroller (ATmega128L) which speed is 4 or 7 MHz [60]. The CPU-heavy computational works cannot be done while it sends or receives data due to its hardware and software architecture. When sensor nodes send and receive data, the received signal strength information can be collected. The MICAz sensor node consumes power as follows: 0 dBm TX: 17.4 mA, -10 dBm TX: 11 mA, and receive mode 19.7 mA [60]. In all experiment, 0 dBm TX power is used. In this dissertation, window-based minimum distance classifier is proposed for energy and computational efficient classifier for wireless sensor networks maintaining high accuracy with less computation. The window-based classifier for wireless signal networks has two steps: event detection (based on the deviation criterion) and event classification (minimum distance classification). With the event detection (i.e., time), the window-based classifier classifies geo-events on the event occurring regions (i.e., location) that are called a *classification window*. The proposed window-based classification method is evaluated with a water leakage simulation in which the data has been measured in laboratory experiments.

4.3.1 Event Detection (window selection)

Because the wireless sensor has limited battery and computational power, it is not reasonable to classify events at every sensing time. When the sensor node sends or receives data, it cannot compute the probabilities for the event classification. So, if the strength of the received signal does not change from previously collected data at a specific location,

there is not new geo-hazard or event in the soil medium and the event classification is not required. Thus, it is important to detect the region of the event occurring with a simple classification such as two-category case (ω_1: event, ω_2: no-event) in which ω_1 can be assigned to binary value 1 and ω_2 to binary value 0. The subsurface event ω_1 at k^{th} position ($1 \leq k \leq N$) can be detected by the signal strength deviation from existing M sample average at the n^{th} sensing time t_n as follows:

$$|x_k(t_n) - [\sum_{j=n-1}^{n-M} x_k(t_j)]/M| \geq \xi \tag{4.1}$$

where ξ is the deviation criterion. The deviation criterion can be empirically decided (ex, 3 5 dBm) based on the measured data which has small variation in soil.

4.3.2 Event Classification on Selected Window

There are N positions to sense geo-events in underground wireless signal networks. Let $\{\omega_1, \omega_2, \ldots, \omega_c\}$ be the finite set of c states of events. $P(\omega_j)$ describes the prior probability that the event is in state ω_j. The variability of a measurement in probabilistic terms is expressed as x which is considered a random variable whose distribution depends on the state of event which is expressed as $p(x|\omega_i)$. If we have an observation x for which $P(\omega_i|x)$ is greater than $P(\omega_j|x)$, there would be a higher possibility that the true state of the event is ω_i. Thus, choosing ω_i minimizes the probability of error. In the classification with more than one measurement, the scalar x is replaced by the feature vector $\vec{x}$, where $\vec{x}$ is in an N-dimensional Euclidean space R^N. The posterior probability $P(\omega_i|\vec{x})$ can be computed from $p(\vec{x}|\omega_i)$ by Bayes formula:

$$P(\omega_i|\vec{x}) = \frac{p(\vec{x}|\omega_i)P(\omega_i)}{p(\vec{x})} \tag{4.2}$$

where $p(\vec{x}) = \sum_{j=1}^{c} p(\vec{x}|\omega_j)P(\omega_j)$. Bayes formula shows that by observing the value of $\vec{x}$ we can convert the prior probability $P(\omega_i)$ to the a posteriori probability $P(\omega_i|\vec{x})$ - the probability of the state of event being ω_i given that feature value $\vec{x}$ has been measured. $p(\vec{x}|\omega_i)$ is called likelihood of ω_i with respect to $\vec{x}$. The Bayes decision rule emphasizes the role of the posterior probabilities, and the evidence factor $p(\vec{x})$ is unimportant as far

as making a decision is concerned. To represent event classifiers, a set of discriminant functions $g_i(\vec{x})$ is used, where $i = 1, \ldots, c$. The classifier is said to assign a vector $\vec{x}$ to class ω_i if $g_i(\vec{x}) > g_j(\vec{x})$ for all $i \neq j$. For the minimum error rate classification, discriminant functions are defined as follows [66]:

$$\begin{aligned} g_i(\vec{x}) &\triangleq P(\omega_i|\vec{x}) = \frac{p(\vec{x}|\omega_i)P(\omega_i)}{\sum_{j=1}^{c} p(\vec{x}|\omega_j)P(\omega_j)} \\ &\triangleq p(\vec{x}|\omega_i)P(\omega_i) \\ &\triangleq \ln p(\vec{x}|\omega_i) + \ln P(\omega_i) \end{aligned} \tag{4.3}$$

where $\sum_{j=1}^{c} p(\vec{x}|\omega_j)P(\omega_j)$ does not affect on the decision and can be ignored. The log scale expression of discriminate functions does not affect the decision as well, and will be used to develop a minimum distance classifier. The measured received signal of wireless sensors is assumed to be independent and normal (or gaussian) distribution [67, 68, 69, 70, 71, 72]. That is, each measurement is statistically independent and its probability density function is normally distributed. Thus, the discriminant function can be evaluated with the densities $p(\vec{x}|\omega_i)$ which are multivariate normal - that is, $p(\vec{x}|\omega_i) \sim N(\vec{\mu_i}, \sum_i)$ where $\vec{\mu_i}$ is the mean vector and $\sum_i$ is the covariance matrix. The general multivariate normal density in N dimensional is written as

$$p(\vec{x}) = \frac{1}{(2\pi)^{N/2}|\Sigma|^{1/2}} \exp[-\frac{1}{2}(\vec{x} - \vec{\mu})^t \Sigma^{-1}(\vec{x} - \vec{\mu})] \tag{4.4}$$

where $\vec{x}$ is N-dimensional column vector, $\vec{\mu}$ is the N-dimensional mean vector, Σ is the N-by-N covariance matrix, $|\Sigma|$ and Σ^{-1} and are its determinant and inverse, respectively [66]. With multivariate normal density, the discriminant function is express as follows:

$$g_i(\vec{x}) = -\frac{1}{2}(\vec{x} - \vec{\mu_i})^t \Sigma^{-1}(\vec{x} - \vec{\mu_i}) - \frac{N}{2}\ln 2\pi - \frac{1}{2}\ln|\Sigma_i| + \ln P(\omega_i). \tag{4.5}$$

When the features are statistical independent and each feature has the same variance σ^2, the covariance matrix is expressed as $\Sigma_i = \sigma^2 I$ where I is the identity matrix. Then, the discriminant functions are simplified as follows [66]:

$$g_i(\vec{x}) = -\frac{\|\vec{x} - \vec{\mu_i}\|^2}{2\sigma^2} + \ln P(\omega_i) \tag{4.6}$$

where $\|\cdot\|$ denotes the Euclidean norm, that is,

$$\|\vec{x} - \vec{\mu_i}\|^2 = (\vec{x} - \vec{\mu_i})^t(\vec{x} - \vec{\mu_i}). \tag{4.7}$$

If the prior probabilities $P(\omega_i)$ in the log scale expression are the same for all c classes, the $\ln P(\omega_i)$ term becomes unimportant additive constant that can be ignored. In this case, the optimum decision rule can be a minimum distance classifier. To classify a feature vector $\vec{x}$, we measure the Euclidean distance $\|\vec{x} - \vec{\mu_i}\|$ from each $\vec{x}$ to each of the c mean vectors, and can assign $\vec{x}$ to the category of the nearest mean. The subsurface events can be classified based on the training data ($\vec{\mu_i}$) and measured received signal strengths ($\vec{x}$). The training data can be generated from empirical data or theoretical estimation such that the event ω_i has training data $\vec{\mu_i}$. Then, the measurement $\vec{x}$ can be classified to the event ω_i which has the minimum distance between $\vec{x}$ and $\vec{\mu_i}$ or the highest probability that the true state of the event is ω_i. Based on the minimum distance classifier, the decision boundary can be calculated. For example, the received signal strengths of two events (two different water content measurements using MICAz where 12% is measured water content in normal condition and 15% is the water content after the water leakage event) at 5 positions and the connected decision boundary of minimum distance classification for 5 positions are shown in Figure 4.4.

After detection of a subsurface event, the event is classified based on the selected window. The minimum-error-rate classification can be achieved by using the discriminant functions with $\vec{x} = x_k \in \Psi$ where Ψ is a set of W features in classification window which size is W. The window based selection reduces the error rate of the classification. Suppose that we observe a particular x_k and that we contemplate taking decision α_i. If the true state of the event is ω_j, the classification has the loss $\lambda(\alpha_i|\omega_j)$. Because $P(\omega_j|x_k)$ is the probability that the true state of event is ω_j, the expected loss associated with taking decision α_i on selected window, R_W, is

$$\begin{aligned} R_W(\alpha_i|\vec{x}) &= \sum_{k=1}^{W}\sum_{j=1}^{c}\lambda(\alpha_i|\omega_j)P(\omega_j|x_k) \\ &\leq \sum_{k=1}^{N}\sum_{j=1}^{c}\lambda(\alpha_i|\omega_j)P(\omega_j|x_k) = R_N(\alpha_i|\vec{x}) \end{aligned} \tag{4.8}$$

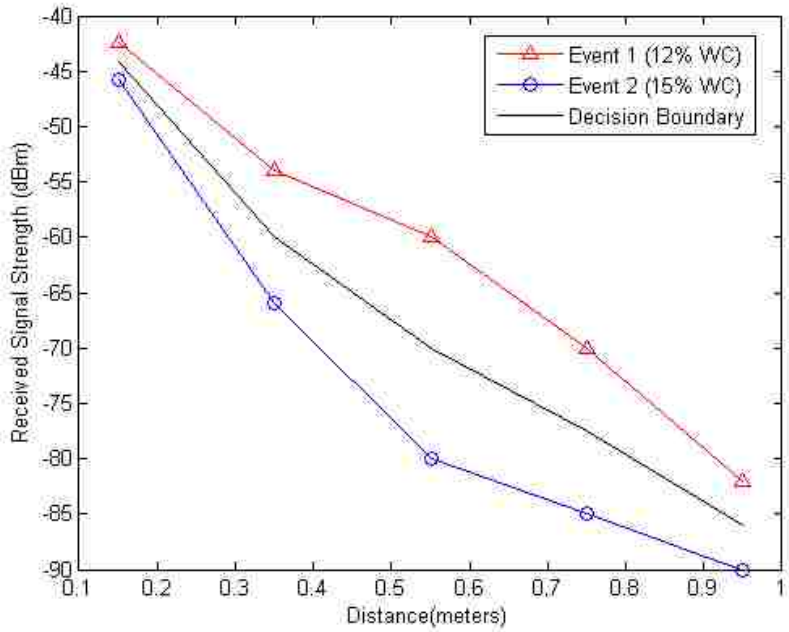

Figure 4.4: An example of decision boundary of minimum distance classifier for water leakage event.

where R_N is the expected loss of whole range (N classifications) and $W \leq N$. The expected loss of window classifier R_W is lower than the expected loss of whole range classifier R_N as shown in Equation 4.8. For example, the minimum distance classifier on all sensing positions has higher error rate due to the variation of received signal strength in no event region. The Figure 4.5 shows the window for minimum distance classifier and error prone points from the water leakage event. The window-based computation has lower computational cost than whole range computation. That is to say, the computational cost of minimum distance classifier as number of multiplications with c classes and N features is $O(cN)$ as the number of multiplications where as the window based minimum distance classification with window size of W is $O(cW)$, where $W \leq N$.

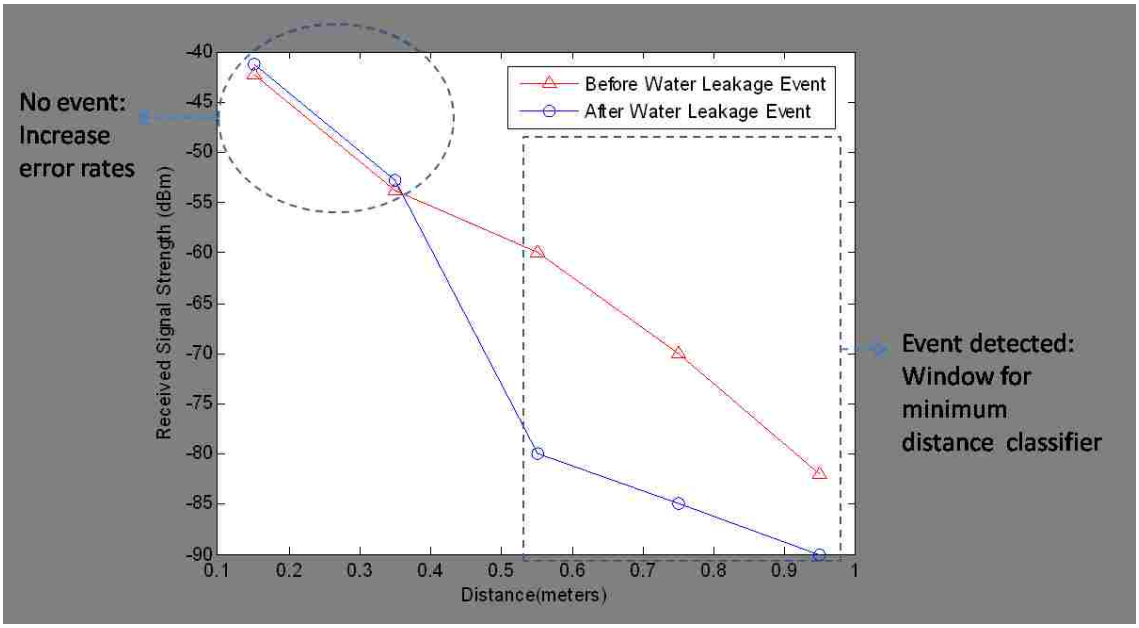

Figure 4.5: A window for minimum distance classifier.

4.4 Performance Evaluations

The concept of wireless signal networks for subsurface event detection and classification is validated with widely used sensor nodes (i.e., MICAz) because of their stability for the measurements of received signal strength. The MICAz sensor nodes are with the CC2420 RF transceiver which includes a digital direct sequence spread spectrum baseband modem. The operating frequency was configured to be 2.48GHz which is Zigbee channel 26 and non-overlapping with 802.11b (WiFi). All wireless sensor nodes are calibrated and selected to be working in 1$\sim$2 dBm error bounds on the received signal strength measurement. A wireless sensor nodes (sender) sends a packet periodically (at every 15 seconds for subsurface event detection simulation), and the receivers sample the received signal strength from the received packets and store the date on the flash memory in which data can be retrieved in the laboratory with serial or ethernet programming boards connected to the desktop. As an underground medium, two types of sand were

used: uniform size construction sands (D_{10}=0.2mm, D_{30}=0.34mm, and D_{60}=0.67mm) and (D_{10}=0.4mm, D_{30}=0.51mm, and D_{60}=0.62mm) where D_x is the diameter of the soil particles for which $x\%$ of the particles are finer.

4.4.1 Subsurface Event Detection

The simulation tests were designed to demonstrate the functionality of the WSiNs to detect transient changes in host soil within the network domain. Using Equation 4.1 and the decision rule, the subsurface events can be detected based on the empirically or theoretically determined deviation criterion ξ (ex, 3$\sim$5 dBm). Three subsurface event simulations were conducted to generate transient changes within host soil mass (coarse sand, D_{10}=2.2mm, D_{30}=2.9mm, D_{50}=3.3mm, and D_{60}=3.8mm where D_x is the diameter of the soil particles for which $x\%$ of the particles are finer) in the large soil box shown in Figure 4.6. These events were (1) water intrusion, (2) relative density change, and (3) relative motion.

Detection of water intrusion

Water intrusion events were simulated by gradually injecting water between the nodes. Figures 4.7(a) and 4.7(b) show the network system configuration and results of water intrusion simulation respectively. All transceivers were buried at a depth of 20 cm at the locations shown in Figures 4.7(a). The initial water content of soil was 6%. First event was started at 17 minute (elapsed time) where water was injected between the sender and node R2 (Receiver 2). Next event was started at 19 minute where water was injected between the sender and node R4. Last event was started at 32 minute where water was injected between the sender and node R5. As it can be seen from Figure 4.7(b), there is a significant decrease in the received signal strength right after the water injection in all three cases. However, there is no change in the received signal strength at node R3 (fairly constant) which was not located in the region of events. Average water content of soil located between the sender and R2/R4/R5 after the injection event was determined as 12%, 11%, and 16% respectively. The increased water content of soil increased the permittivity and electrical conductivity of the medium, resulting in decrease of received

Figure 4.6: Large soil box for simulations of subsurface event detection.

signal strength. Important to note is that the magnitude of signal depletion is proportional to the magnitude of change in the water content (comparing nodes R2 and R5). Also, since node R4 was located at farther distance than the other nodes, it has a lower value of received signal strength.

Detection of relative density change

Relative density change simulation through soil compaction was conducted by applying vibration at the soil surface using magnetic vibration equipment. All transceivers were buried at a depth of 20 cm with network configuration as shown in Figure 4.8(a). Each shaded area between the sender and receivers (starting from node R2 toward R5) in Figure 4.8(a) were compacted for about 2 minutes starting at 27, 32, 36, and 38 minute. The water content of the soil was 5%. As it can be seen in Figure 4.8(b), the change

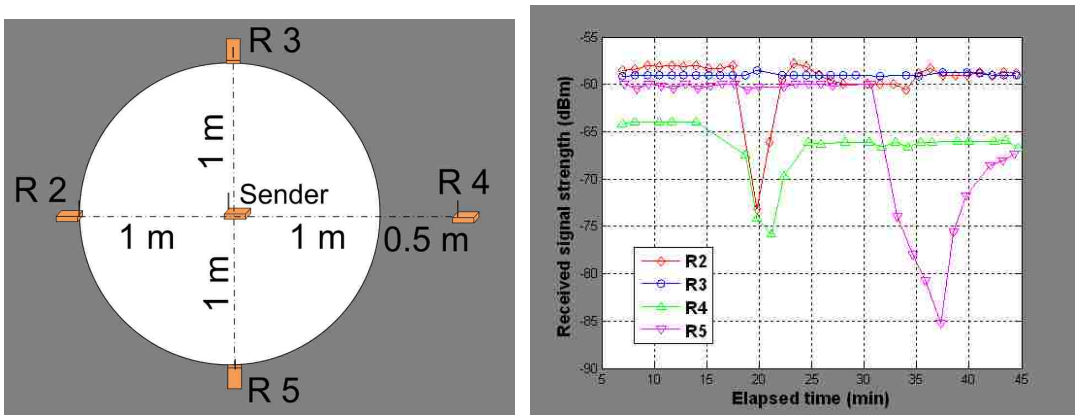

(a) Configuration for water intrusion

(b) Results of water intrusion detection

Figure 4.7: Simulations of subsurface event detection (water intrusion).

in the compactness of soil is detected by marked drops in signal strengths at all nodes. As it was shown in the parametric test results in Table 4.1, the increase in soil density reduces the signal strength. The drop in received signal strength may be attributed to the increase in electrical conductivity of the medium. Compacted soil has more surface particle contacts compared to the loose soil and provides more electron flow resulting in higher electrical conductivity of the compacted media. Consequently, the received signal strength decreases as the soil compactness (relative density) increases.

Detection of relative motion

In this simulation, the sender and the nodes R2, R3, R4, and R5 were located in the same plane at a depth of 15 cm from the surface and the nodes R6, R7, R8, and R9 were located at the same plane at a depth of 45 cm from the surface as shown in Figure 4.9(a). The soil mass was held using a wooden facing in the front while the other sides remained continuous. The event started at 27 minute by removing the front facing. Relative motion simulation results are shown in Figure 4.9(b). The received signal strength at nodes R2,

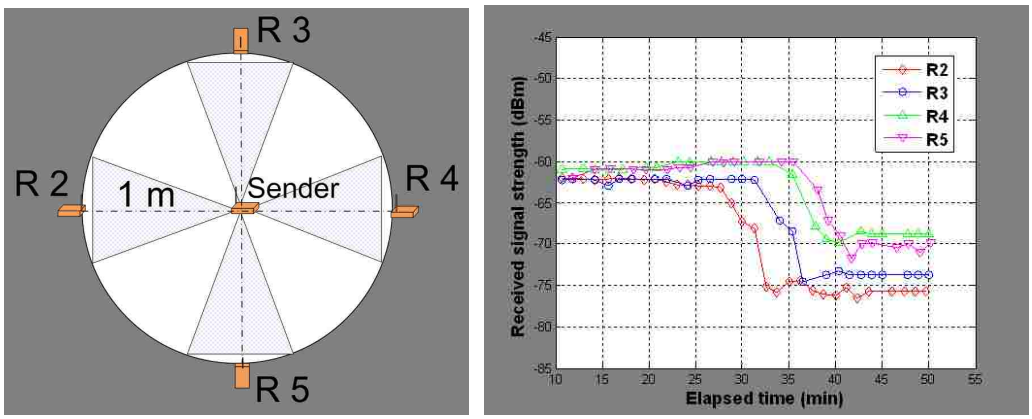

(a) Configuration for relative density change

(b) Results of relative density change detection

Figure 4.8: Simulations of subsurface event detection (relative density change).

R3, R6, and R7 remained fairly constant. Since neither the physical properties of the soil nor the distance between the sender and receiver changed within these regions, no change was recorded in the received signal strength. At nodes R4 and R5 that were directly affected by the event, the received signal strength dropped and remained constant in Figure 4.9(b). The drop is attributed to a combination of different factors including change in the distance between the sender and receivers, antenna orientation, and density of soil between the sender and receivers. In contrast, an increase in the received signal strength at nodes R8 and R9 was detected. This increase may be attributed to the removed mass of soil initially located on top of these nodes. The important point to notice is that the event could be detected through changes in the received signal strength of the nodes within the network domain.

4.4.2 Subsurface Event Classification

For the sake of better and accurate control on the soil properties comparing with the large soil box shown in Figure 4.6, a small plastic (PVC) box with dimensions $118 \times 13 \times 13$cm

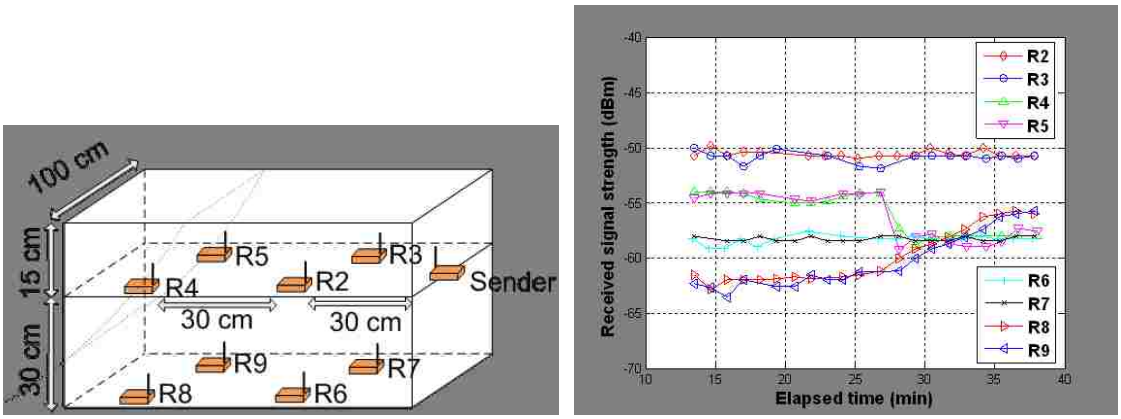

(a) Configuration for relative motion change

(b) Results of relative motion change detection

Figure 4.9: Simulations of subsurface event detection (relative motion change).

was made as shown in Figure 3.5(a) and 3.5(b) and filled with controlled soils. In the experiment, physical soil properties (e.g. particle size distribution, soil density) and temporally dynamic variables (e.g. soil water content, salinity, soil temperature, etc.), which affect the electric conductivity and permittivity of the medium, were controlled. To evaluate the proposed classifier, we apply the classifier into a water leakage simulation where soil properties are controlled where the soil is fine sand (D_{10}=0.4mm, D_{30}=0.5mm, D_{50}=0.58mm, and D_{60}=0.62mm).

In the experiment, sensors (S2$\sim$S6) sent a packet at every 60 seconds and the receiver node (S1) calculated the received signal strength based on the received packet. Based on the collected received signal strength information, the node S1, which can be a sink node or an intermediate node that can send or receive data, estimates the location of water leakage event and classifies the water contents on the soil media between the transmitters and receiver. In the water leakage experiment, the soil in the box contained 12% water content before the water leakage event. The water leakage event was start at 26 minutes after experiment start by injecting water into the regions between 40cm and 60cm from the first node (S1). After the water leakage event, the average volumetric water content

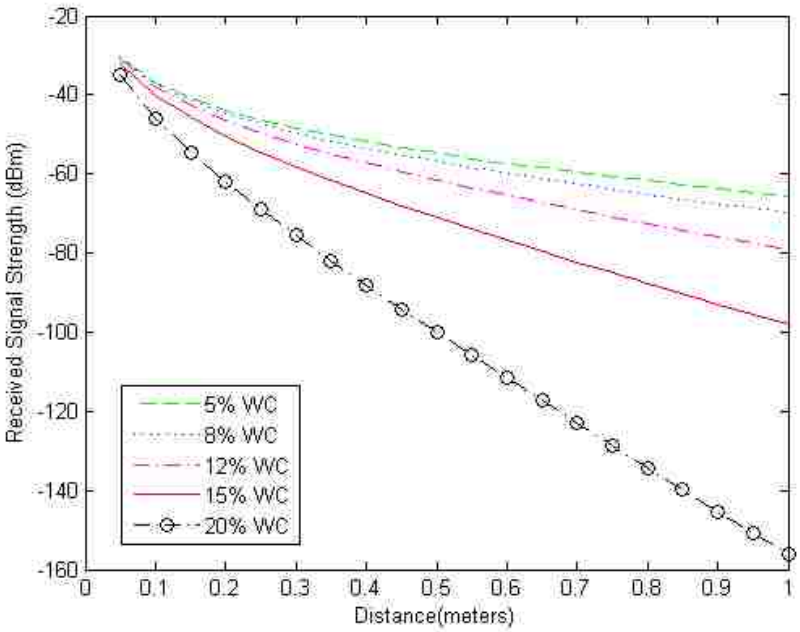

Figure 4.10: Received signal strength estimation with different water contents.

of the soil in the box was 15%.

Reference data generation

In the evaluation, we classify the geo-events based on training data which can be the measured data or theoretically estimated data. Because we have an accurate underground radio propagation model, we generate the estimated received signal strength with different water content as the reference data (training data for the event classification) which are shown in Figure 4.10. In the estimation using Equation 3.15, the electric conductivity values of the soil in all experiments were measured as shown in Table 4.2 and the relative permittivity of the soil is estimated between 19∼30 based on [54].

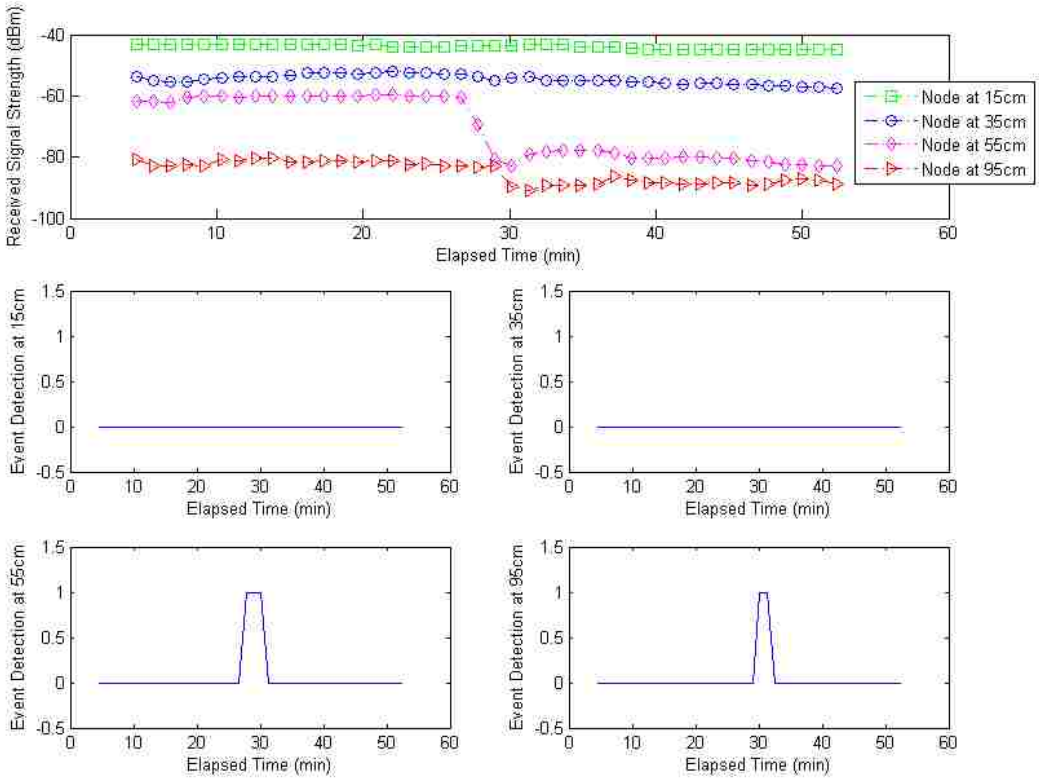

Figure 4.11: RSS measurements in water leakage simulation (top) and event detection signals from different location (nodes at 55cm and 95cm generate event detection signals).

Event classification of water leakage simulation

The Figure 4.11 shows the time evolution of the received signal strength when the water leakage event was conducted. With the water leakage event at 26 minute, the nodes at 55 cm and 95 cm have low received signal strength due to high signal attenuation from increased water content. As a result, the node at 55cm generates event detection signal at 26, 27, and 28 minutes and the node at 95cm generates event detection signal at 28 and 29 minutes based on Equation 4.1 and the decision rule, where the deviation criterion ξ is 3 and the previous sensing time M is 3. Thus, the minimum distance classification will

Table 4.3: Comparisons of Minimum Distance Classifier (MDC).

Time (min.)	Event Detection	Window-based MDC		Whole Range MDC	
		Classified	Result	Classified	Result
26	Node at 55cm	15% WC	No Error	12% WC	False Class.
27	Node at 55cm	15% WC	No Error	12% WC	False Class.
28	Node at 55cm, 95cm	15% WC	No Error	15% WC	No Error
29	Node at 95cm	15% WC	No Error	15% WC	No Error

be conducted only from 26 minute to 29 minute.

When events are detected, the window-based minimum distance classifier classifies the event based on the measured data of the detected region by calculating the minimum distance between the detected event and the reference data using Equation 4.6. Figure 4.12 shows the received signal strength between 26 and 29 minutes where the event detection signals are generated. In Figure 4.12, the red circle represents the data in the classification window that can be used in the minimum distance classification. The detected events at 26, 27, 28, and 29 minutes are classified as 15% water leakage event based on the window-based minimum distance classifier as shown in Figure 4.12. In case of whole-range minimum distance classification, the detected events are classified as 12% water leakage event at 26 and 27 minutes and 15% water leakage event at 28 and 29 minutes. We compared window-based minimum distance classification and whole-range minimum distance classification and summarized the result in Table 4.3. The proposed method generates four event detections during the water leakage simulation. At event detection, the window-based minimum distance classification detects the leakage event correctly with 100% accuracy where as the whole range minimum distance classification has 50% accuracy (50% false classification). The window-based minimum distance classification has 68% less computation than the whole range minimum distance classification in the simulation.

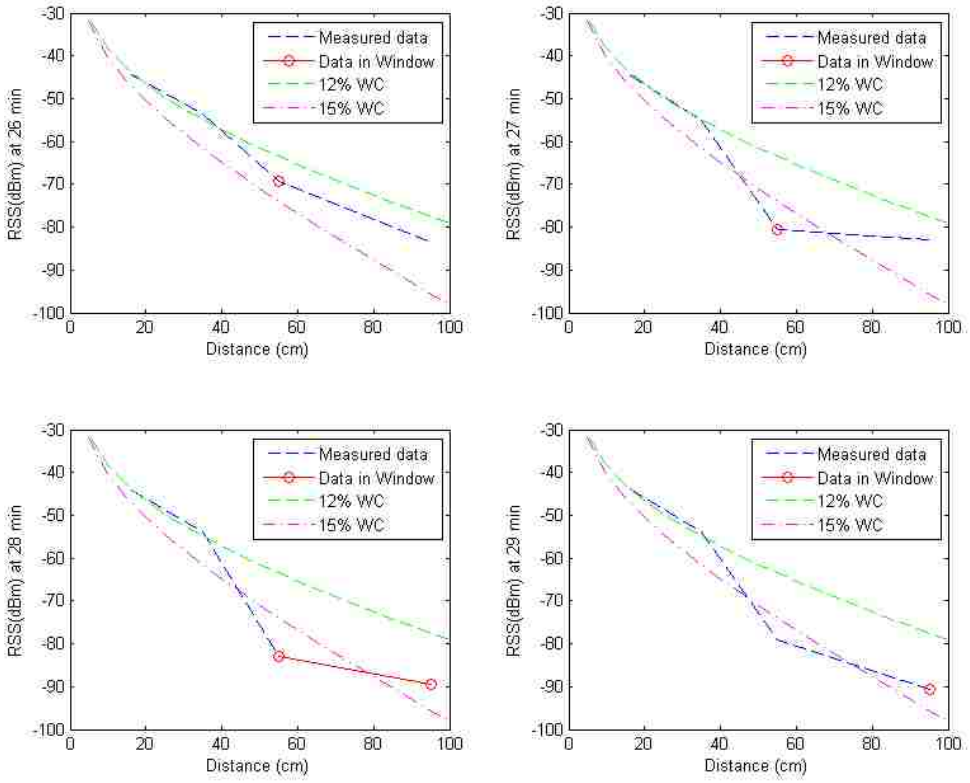

Figure 4.12: Event classification based on received signal strength between 26 and 29 minutes (detected events at 26, 27, 28, and 29 minutes are classified as 15% water leakage event with window-based minimum distance classifier).

4.5 Summary

The received signal strength information of underground sensors is used to characterize the geo-event in the proposed wireless signal network. This chapter presents a detailed list of network parameters and soil properties affecting underground radio propagation with experimental data. To evaluate the concept of WSiNs for subsurface event detection, three event detection experiments (water intrusion, relative density change, and relative motion)

were conducted using MICAz. In this chapter, the window-based minimum distance classifier is proposed to detect and classify geo-events of wireless underground sensor networks. The window-based minimum distance classifier accurately detects geo-events and classifies the water leakage event into different water contents. From the theoretical analysis and experiment, the proposed window-based minimum distance classifier has less computation and higher accuracy than whole range minimum distance classifier.

Chapter 5

Reconfigurable Radio Platform

Reconfigurable Radio (RR) is a generic concept based on technologies such as Software Defined Radio (SDR) and Cognitive Radio (CR) whose systems exploit the capabilities of reconfigurable radio and networks for self-adaptation to a dynamically-changing environment with the aim of improving system performance and spectrum utilization [73]. Cognitive radio is a paradigm for wireless communication in which either a network or a wireless node changes its transmission or reception parameters to communicate efficiently avoiding interference with licensed or unlicensed users [74]. A software-defined radio system, or SDR, is a radio communication system where components that have been typically implemented in hardware (e.g. mixers, filters, amplifiers, modulators/demodulators, detectors, etc.) are instead implemented by means of software on a personal computer or embedded computing devices [75]. The term of reconfigurable radio system is introduced in ETSI (European Telecommunications Standards Institute) and the relationship is shown in Figure 5.1. We use USRP (Universal Software Radio Peripheral) board for the evaluation platform of reconfigurable radio as shown in following Figure 5.3 [76]. We will design an optimizing reconfigurable radio platform for underground wireless sensor networks which have a reasonable communication radius to be used for practical underground monitoring applications.

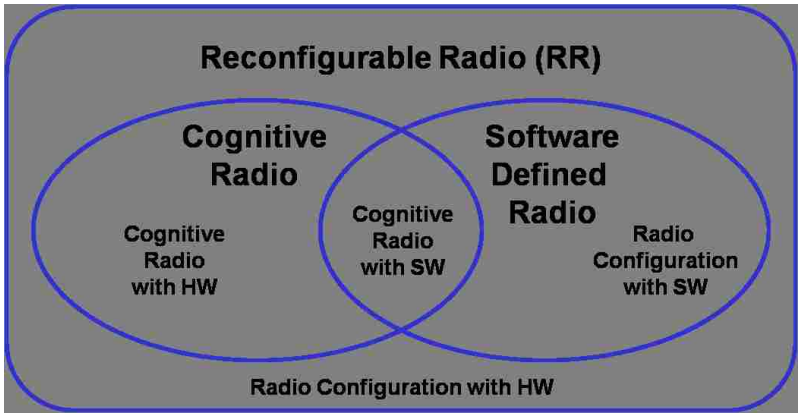

Figure 5.1: The concept and relationship of reconfigurable radio

5.1 Applying Reconfigurable Radio System to Wireless Signal Networks

The reconfigurable radio system can be used in the intelligent infra structure monitoring such as bridge and subsurface monitoring using wireless signal. In subsurface monitoring, the radio signal experiences high attenuation in soils. According to the soil condition, the system can choose different frequency bands to maintain longer and reliable communication. In the infra structure monitoring such as bridge monitoring, the reconfigurable radio capabilities can reduce power consumption on data sending operations with an energy efficient topology control. For example, large amounts of data can be transmitted in relatively smaller number of transmissions or short time with high frequency which has high data transmission capability. An energy efficient topology control with reconfigurable radio is introduce in Chapter 6. Another example is long distance communication with low frequency avoiding data relays which can reduce data collecting time and intermediate node's and overall network power consumption. In wireless signal networks, the lower frequency bands provide longer communication distance while higher frequency bands provide more sensitive response due to the attenuation characteristics in the underground medium. The benefits using reconfigurable radio are as follows:

- Longer distance and reliable communication in high attenuating condition such as underground with lower frequency bands
- Save power on the network operation using lower or higher frequency bands according to the network environments
- Interference avoidance among adjacent nodes using multiple frequency bands
- Increase network capacity using higher frequency bands
- Provide more sensitive sensing on wireless signal networks using higher frequency bands
- Provide adaptive topology construction using multiple frequency bands

5.2 Extending Underground Signal Propagation

The communication radius in soil is much shorter than air due the high attenuation of radio propagation in soil medium. Based on the underground radio propagation model and the field measurements, the communication radius of the commercial wireless sensors such as 2.4 GHz MICAz and 433 MHz MICA2 with 1mW Tx power are about 20cm and 30cm in wet clay type soil (measured electrical conductivity = 780 mS, estimated relative permittivity = 30) sampled in Lehigh University Goodman Campus as shown in Figure 5.2(a).

To overcome the high attenuation and extend communication radius in soil, three parameters can be controlled such as using high transmission power, using high gain antenna, and using low radio frequency. In case of high transmission power and high gain antenna, the benefit of extending communication radius is not enough to design practical underground applications. If the underground sensors use a low frequency, the communication radius can be extended more efficiently. There are candidates of low frequency bands for underground communication such as low frequency ISM (industrial, scientific and medical) bands of 125 KHz, 134 KHz, 6.78MHz, and 13.56MHz. ISM bands are radio bands reserved internationally for the use of radio frequency for industrial, scientific

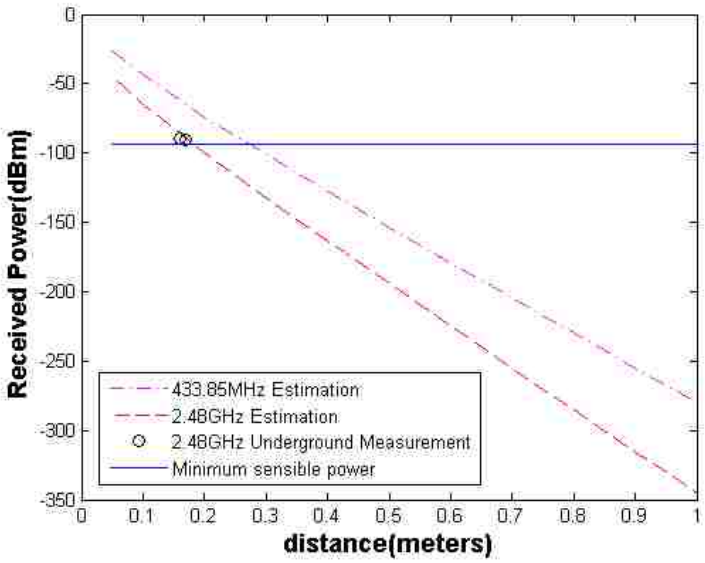

(a) With 2.48 GHz and 433.85 MHz

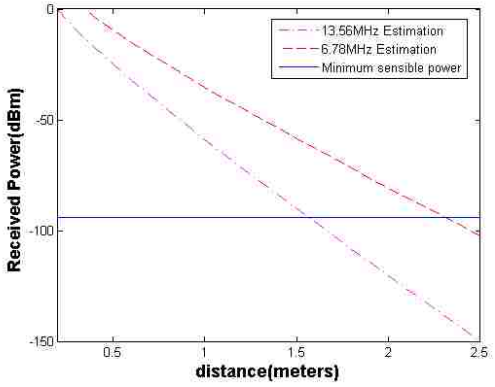

(b) With 13.56 MHz and 6.78 MHz

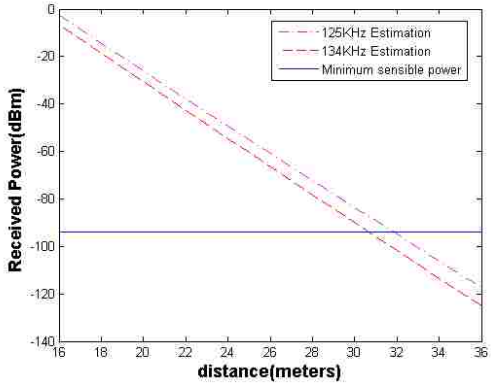

(c) With 125 KHz and 134 KHz

Figure 5.2: Underground radio signal attenuation

and medical purposes.

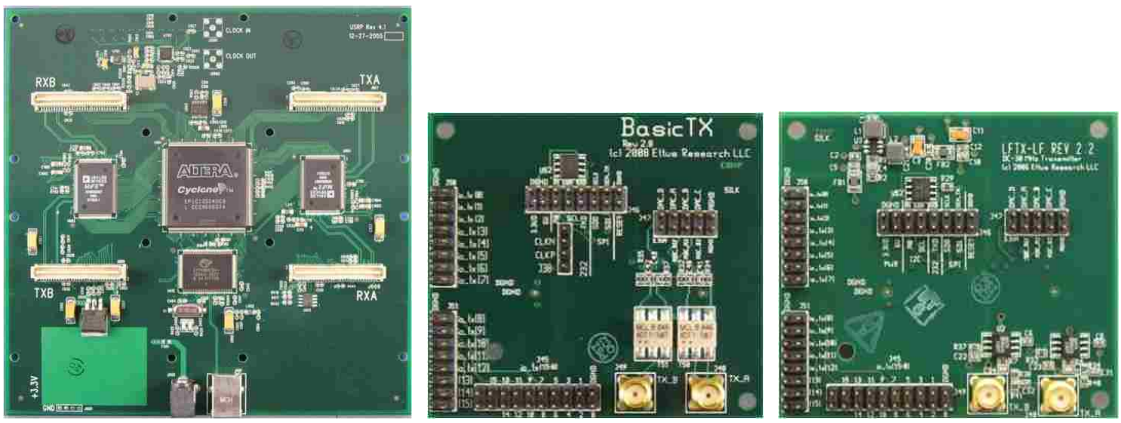

(a) USRP Mother Board

(b) Basic TX Daughter Board

(c) LFTX-LF Daughter Board

Figure 5.3: USRP mother board, basic TX and LFTX boards

Based on the theoretical estimation using Equation 3.15, we can achieve 1.6∼2.3m communication with 13.56MHz and 6.78MHz bands, and 31∼32m communication with 134KHz and 125KHz bands even in wet clay underground with 1 Watt Tx power and the same MICA's antenna gain as shown in Figure 5.2(b) and 5.2(c).

5.3 Experimental Low Frequency Platform using USRP

USRP (Universal Software Radio Peripheral) is an experimental platform of a GNU radio or software-defined radio (SDR) system where components that have been typically implemented in hardware (e.g. mixers, filters, amplifiers, modulators/demodulators, detectors, etc.) are instead implemented by means of software on a personal computer or embedded computing devices [75]. We use USRP boards and two daughter boards for the evaluation platform of low frequency operation via radio reconfiguration as shown in Figure 5.3. The BasicTX and BasicRX boards are designed for use with external RF frontends operating from 1 to 250 MHz frequency bands [77]. LFTX and LFRX are similar

Figure 5.4: USRP setup for low frequency communications

to the BasicTX and BasicRX, but the operating frequency bands are from DC to 30 MHz with differential amplifiers and low pass filters [77].

We verified the USRP system can work on the low frequency bands which are suitable for underground communications. Using two USRP mother boards equipped with BasicTX/RX and LFTX/RX daughter boards, the communication systems working on low frequency bands are established as shown in Figure 5.4. We tested three candidates of low frequency bands such as 13.56MHz ISM band, 6.78MHz ISM band, and 190KHz LowFER band. In the experiments, the receiver showed increased signal level when it is receiving data as shown in Figure 5.5. In the experiment, we use VERT400 antenna which is 144 MHz, 400 MHz, and 1200 MHz Tri-band 7-inch omnidirectional vertical antenna. In the project, we will find suitable low frequency antenna for better gain to extend underground communication distance. In the experiments, one host PC (Linux OS) is sending data while another host PC is receiving the date. Instead of printing received data, the receiver can run spectrum analyzer to show the RF signal level. The receiver shows increased signal level when it is receiving data.

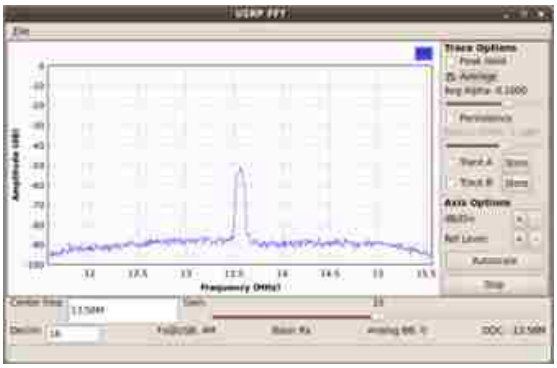

(a) 13.56MHz ISM band

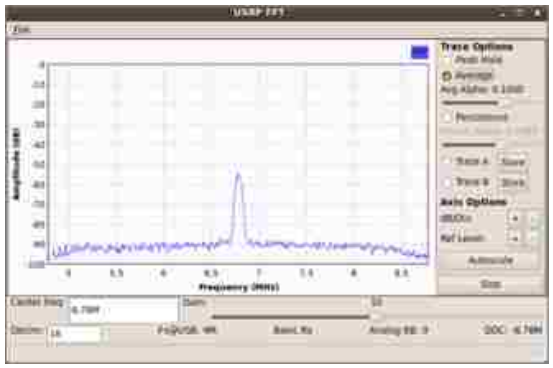

(b) 6.78MHz ISM band

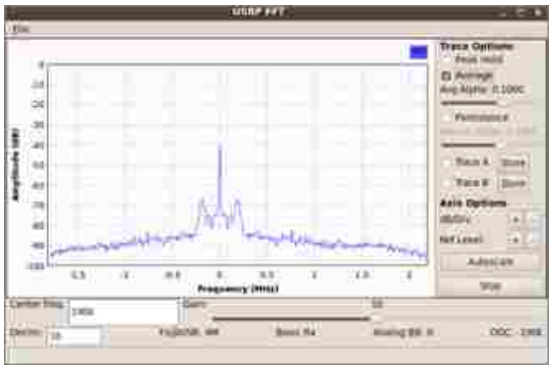

(c) 134KHz ISM band

Figure 5.5: USRP spectrum analyzer on low frequency receiver

5.4 Low Frequency Sensor Node Design

To realize low frequency underground wireless signal/sensor networks, we designed a new hardware platform which is called Reconfigurable Radio Sensor Networks (RRSNs) based on the MICA2/MICAz and USRP platforms. The main processing parts (i.e., CPU, memory, etc.) of the reconfigurable radio sensor are coming from MICA2/MICAz and the reconfigurable radio parts for the low frequency operation are coming from USRP system.

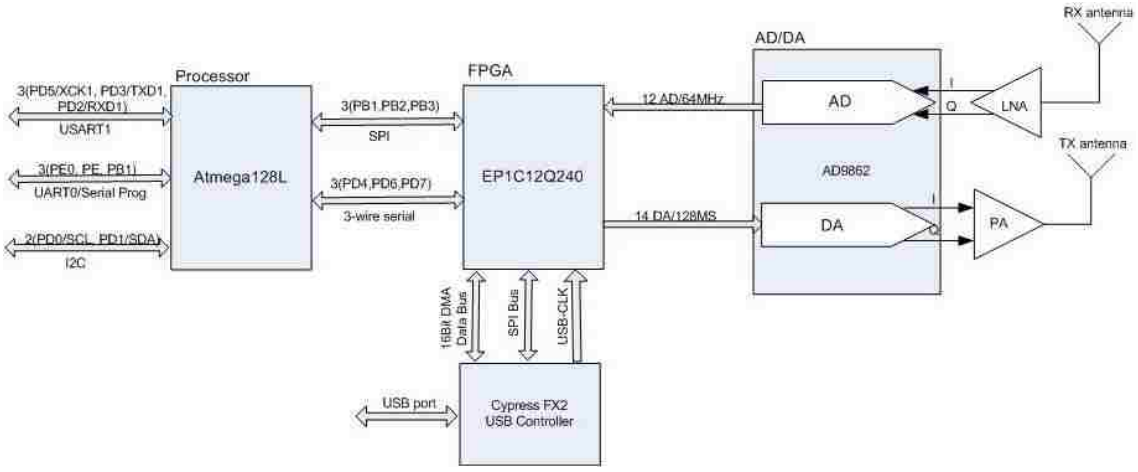

Figure 5.6: The block diagram of reconfigurable radio sensor node

The significant difference of reconfigurable radio low frequency sensor from USRP is the implementation of radio communication system. Because the sensor node has low computational CPU, it cannot implement the communication system in softwares. In the reconfigurable radio sensor networks, the traditional radio communication blocks (e.g. mixers, filters, amplifiers, modulators/demodulators, detectors, etc.) are implemented in FPGA (Field Programmable Gate Array). The reconfigurable radio sensor node can have multiple radio communication blocks working on different frequency bands ranging from KHz to GHz. Depending on the requirements of communication spectrum, the sensor node can be equipped with multiple RF front ends. The main block diagram of reconfigurable radio sensor node is shown in Figure 5.6.

This prototype operates as a stand-alone wireless sensor with a low frequency radio transceiver. It consists of two parts, a main board and a daughter board. The main board(processor board) integrates microprocessor, FPGA and AD/DA converter. The daughter board, or the RF front end, includes the amplifiers and antennas. This split design approach combined with software radio implemented in FPGA gives the prototype huge flexibility in wireless communication. With different sets of daughter boards, the prototype can use a wide frequency band ranging from a few MHz to hundreds of

MHz for communication.

The Atmega128L low power microprocessor provides a rich set of standard interfaces that are wired to a common connector on the main board. This connector can interface with a variety of sensor boards which use standard data ports such as I2C, UART or SPI. Also, Atmega128L is connected to FPGA via two serial ports, one for data communication and the other for configuration. The low power Cyclone FPGA used on the main board is the core part for radio communication. In fact, modulation/demodulation, source coding/decoding and channel coding/decoding are all implemented in FPGA. An additional microcontroller Cypress FX2 is built on the main board to support FPGA programming thorough USB port. The wide band AD/DA converter AD9862 sits between FPGA and RF front end. Two AD converters and two DA converters are integrated on the chip and it makes conversions between digital signals and analog signals. The daughter board is actually the RF front end which includes the transmitter part and receiver part. The transmitter consists of a power amplifier and a transmit antenna. The receiver contains a low noise amplifier and a receiver antenna. The selection of antennas and design of amplifiers vary according to the communication frequency band chosen.

5.5 A Novel Topology Control with Reconfigurable Radio

The wireless sensor network that is using reconfigurable radio functionality is called a *reconfigurable radio sensor network* (RRSN) where the transmission range can be dramatically changed due to the wide ranges of operating frequency selection. Taking the advantage of changing the operating frequency over a wide frequency range will let wireless sensor networks enhance energy efficiency as well as satisfy given network performance requirements. Current sensor systems such as MICAz and MICA2 are working on fixed ultra-high frequency (UHF) bands of 2.4GHz and 300$\sim$900 MHz. If the sensors use lower frequencies in ISM (Industrial, Scientific and Medical) or license free bands, they can achieve better propagation and longer communication distance. This is beneficial because it extends network lifetime in the environments of high signal attenuation, such as

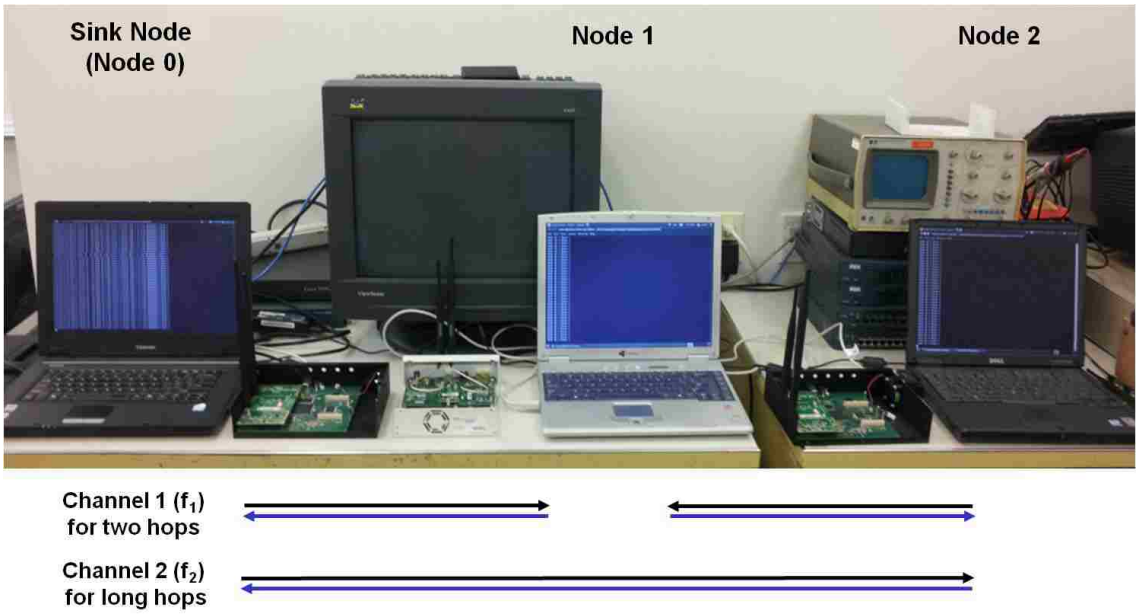

Figure 5.7: Implementation of topology control algorithm with USRP systems

being underground, in a dense forest, and in industrial fields. Especially low frequency is strong in the environments of high signal attenuation such as underground, dense forest, and industrial fields. In such highly attenuating environments, a sensor network needs the radio reconfiguration to the lower frequency bands to achieve long communication distance for the energy efficiency.

For an energy efficient topology control, the dissertation introduces a new control dimension, *frequency control*, with an advanced radio technology, *reconfigurable radio*, where the transmission range can be dramatically changed by the operating frequency selection over a wide frequency range. For the energy efficient topology control, the dissertation presents distributed topology control algorithms, reconfigurable radio topology control (RTC) and reconfigurable radio dynamic topology control (RDTC), which construct a minimum hop routing tree using multiple frequency bands. The detail algorithms are shown in Chapter 5. The proposed topology controls with reconfigurable radio are implemented using 3 USRP nodes as shown in Figure 5.7.

The topology control algorithms are implemented with two python files such as *topology_sink.py* for a sink node and *topology_node.py* for relay/regular nodes. The python file for the sink node requires input arguments especially the number of nodes on the network to finish network setup procedure. The python file for the sink node requires two important input arguments such as the node ID and a trigger of topology update. The system consists of three phases as follows:

- Setup phase
- Static phase
- Dynamic phase

As a simple scenario, the packet includes five fields as follows:

- Size (2 bytes)
- Node ID (1 byte)
- Hop Count(1 byte)
- Packet type (1 byte)
- Data (variable)

In the packet, the packet type (1 byte) represents the following meaning:

- 0x01: Route Request (RREQ)
- 0x02: Route Reply (RREP)
- 0x03: Route Established (ESTABLISHED)
- 0x04: Topology Change (TC)
- 0x05: Topology Update (TU)
- 0x06: Topology Update Finish (TUF)

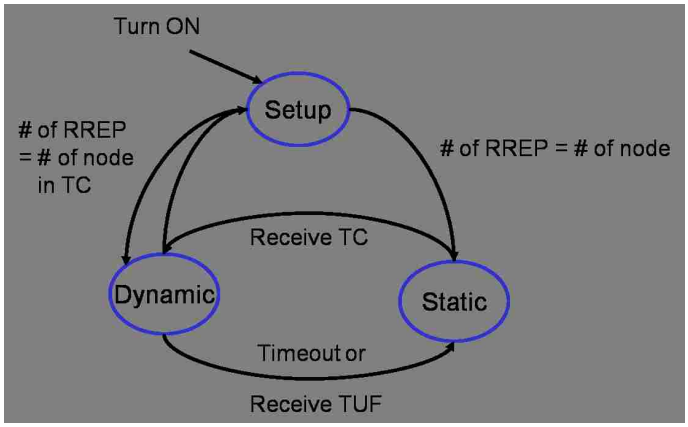

Figure 5.8: The state diagram of sink node

- 0x10: Data

When the power is up, all nodes are starting at setup phase. With packet exchanges of route request and reply, the sink node and regular node change their state to static state. In static state, nodes are periodically reporting data and the relay nodes relay the date when they have leaf nodes. The state diagrams of sink and regular nodes are shown in Figure 5.8, 5.9(a), and 5.9(b). A relay node can trigger the topology update when its remaining power is lower than a threshold (e.g., 20%). The operation of this node is called master mode in the topology update. Depends on the topology update trigger, the node state branches master and slave mode during topology update. The operation of the leaf nodes on the relay node (master mode) is called slave mode. In the implementation of RTC algorithm, USRP system was configured to be operating on 2.4GHz ISM bands (f_1). In the implementation of RDTC algorithm, USRP system was configured to be operating on 915MHz ISM bands (f_2). The experiments comply with the FCC's guidelines.

5.6 Summary

This chapter introduces a new concept of Low Frequency Wireless Signal Networks (LFWSiNs) and Reconfigurable Radio Sensor Networks (RRSNs) with theoretical estimations and practical experimental solutions. The chapter presents the design and development of reconfigurable radio sensor networks in progress for low frequency wireless signal networks which can be used for subsurface monitoring applications. For an energy efficient topology control using RRSNs, the dissertation introduces a new control dimension, frequency control, and presents distributed topology control algorithms which are implemented using 3 USRP nodes.

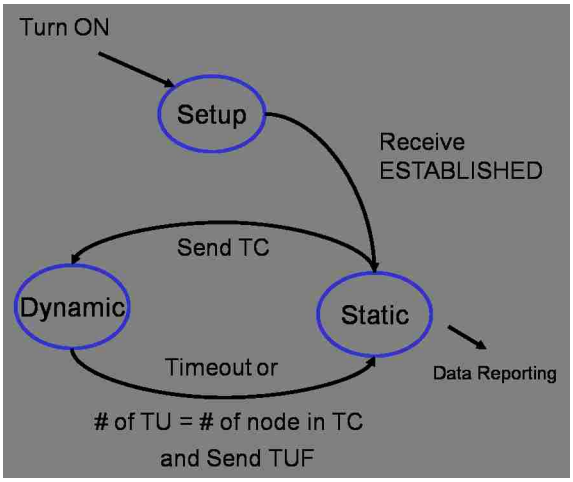

(a) The node state in master mode (triggering topology update)

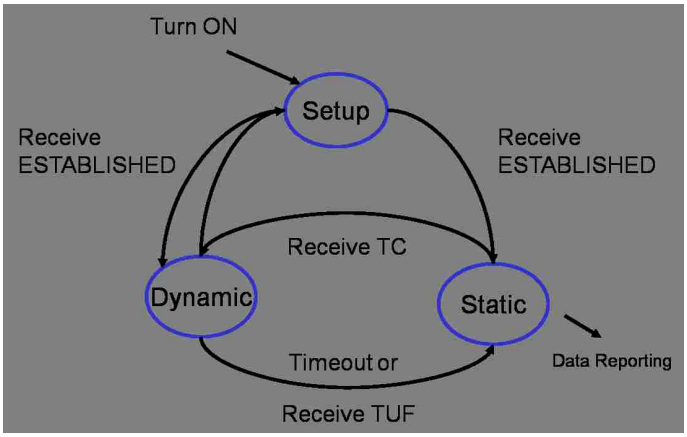

(b) The node state in slave mode (leaf nodes of the relay node in master mode)

Figure 5.9: The state diagram of relay and regular nodes. The node state branches master and slave mode during topology update.

Chapter 6

Topology Control with Reconfigurable Radio

Topology control in wireless sensor networks has been studied to extend network lifetime without affecting important network performance. Existing topology controls grant sensor nodes a sense of control parameters, such as adjusting the transmission power or switching power mode between sleep mode and active mode, to achieve energy savings and prolong network lifetime. However, existing topology controls assume that the operating frequency is fixed or can be changed in a narrow range of frequencies, thus the communication distance is not radically changed because of the radio propagation characteristic. For an energy efficient topology control, the dissertation introduces a new control dimension, *frequency control*, with an advanced radio technology, *reconfigurable radio*, where the transmission range can be dramatically changed by the operating frequency selection over a wide frequency range. The dissertation formulates a network lifetime maximization problem while maintaining the successful data relay based on the proposed network, channel, and power consumption models of the reconfigurable radio senor networks. For the energy efficient topology control, the dissertation presents distributed topology control algorithms, reconfigurable radio topology control (RTC) and reconfigurable radio dynamic topology control (RDTC), which construct a minimum hop routing tree using multiple frequency bands. Simulation results show that the proposed

topology controls can extend the lifetime 1.98 times longer than the existing approaches under three simulated conditions for aboveground communications on average. In underground communications, the proposed topology controls can extend the lifetime 2.91 times longer than the existing approaches under three simulated conditions on average.

6.1 Introduction

6.1.1 Topology Control and its Research Problems

A wireless sensor network (WSN) consists of spatially distributed autonomous sensors to monitor physical or environmental conditions such as temperature, vibration, motion or pollutants and to report the monitored data to the sink. In a battery operated wireless sensor network, a critical issue is maximizing lifetime of the sensor node. In a hope to extend the lifetime of battery powered wireless sensor nodes, topology control has been receiving more and more attention. In wireless sensor networks, *topology control* is a technique to alter the arrangement of the network elements such as links, nodes, etc., which will achieve energy conservation and will extend network lifetime without affecting important network performance such as connectivity [78]. The *network lifetime* in the dissertation is defined as the battery exhaustion of the first sensor node, which can be characterized as either the first failure of the packet delivery or the time until the network partition due to battery outage [79]. The dissertation addresses a problem, maximizing network lifetime while maintaining *successful data relay*, which is defined as the amount of data generated from all nodes equal to the amount of data collected at the sink node.

6.1.2 Related Works

The topology control grants sensor nodes a sense of control over certain parameters, such as adjusting the transmission power to control the transmission range [80] or switching the power mode between sleep mode and active mode [81] as shown in Figure 6.1, to achieve energy savings and prolong network lifetime. Based on the power adjustment and the power mode switching techniques, various energy efficient topology control methods

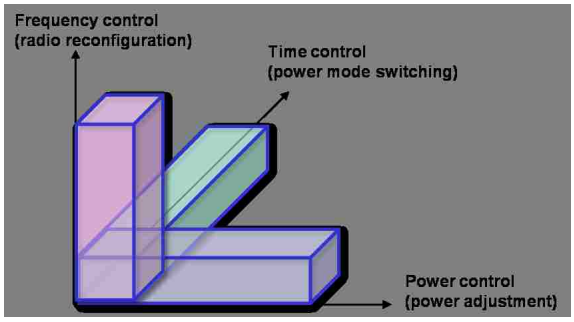

Figure 6.1: Control dimensions for topology control.

have been proposed. An important performance parameter in wireless sensor networks that periodically monitor environments is the amount of data collected from all wireless sensor nodes [82]. To report the event data with limited local topology information on a large number of nodes, a forwarding scheme based on the partial topology knowledge is introduced as a way for energy efficient routing [83]. For a packet forwarding scheme considering sleep-wake scheduling of sensor nodes, an anycast packet forwarding scheme is developed while reducing event reporting delay [84]. The relay nodes near the sink will tend to deplete their energy budget faster than other nodes due to the relaying data, which is known as an energy hole around the sink [85]. The selection and management of the relay nodes are important because it will prolong the network lifetime. With an aim to maximize network lifetime, an algorithm for optimum location and power allocation for each cooperative relay node is introduced [86].

6.1.3 A New Approach

In previous research, the topology control schemes use power controls (transmission power adjustment) and time controls (power mode switching) to extend network lifetime. There are limitations on maximizing the network lifetime and maintaining connectivity because the change of the topology or neighbor set is limited with the control of the transmission power and sleep-wake scheduling. The dissertation introduces a new control

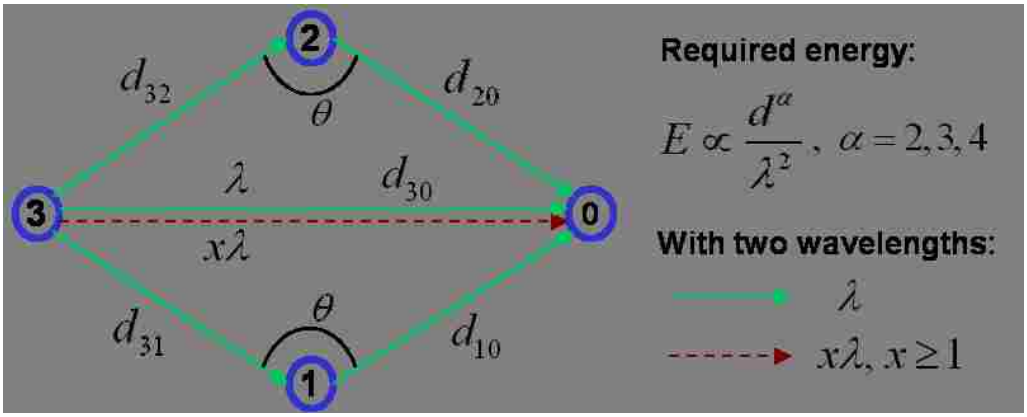

Figure 6.2: A four node example for the comparison of the network lifetime.

dimension, *frequency control* as shown in Figure 6.1, with an advanced radio technology, *reconfigurable radio*, where the transmission range can be dramatically changed by selecting an operating frequency selection over a wide range from KHz to GHz. The proposed topology control is different from existing frequency control approaches, such as a topology control using multiple channels among non-overlapping channels on the same frequency band (i.e., 2.4GHz or 5GHz band) presented in [87], because of the wide ranges of operating frequency selection. In wireless communications, the received power (P_{Rx}) is inversely proportional to the distance (d) and proportional to the wavelength (λ) such as $P_{Rx} \propto \lambda^2/d^L$, where L is the path loss exponent from the Friis transmission equation [37]. To achieve *communication distance* (defined as the distance satisfying $P_{Rx} \geq P_{threshold}$), the required energy (transmission power) increases exponentially with the order L as the distance increases such as $E \propto d^L/\lambda^2$.

In a four node example, as shown in Figure 6.2, nodes 1, 2, and 3 send data to the sink node 0. The nodes 1 and 2 can be relay nodes of node 3 with a topology control. The example shows that the radio reconfiguration can extend the network lifetime comparing with power and time controls, even without a relay node, by increasing wavelength. The network lifetime is induced by a node with the maximum power consumption, such as

T_{net}=B/P_{max}, where B is the energy of the battery. For the sake of simplicity, we assign d_{31}=d_{10}=d_{32}=d_{20}=2, $\theta = 120°$, λ=1, x=2, L=2, and B=120. Without any control method, the required power for the direct communication from node 3 to node 0 using λ is P^{None}=12, which is P^{None}_{max}. Thus, the network lifetime is T^{None}_{net}=10. In the example with a topology control based on the power control introduced in [80, 85], a relay node is required for the network energy efficiency because of $\cos\theta < 0$. The maximum power consumption of the topology control with the power control is P^{PC}_{max}=8 on a relay node, either node 1 or 2. In this case, the network lifetime is T^{PC}_{max}=15. In the topology control with the sleep management introduced in [81, 84] where both node 1 and 2 are relay nodes using sleep mode in turn, the maximum power consumption is P^{TC}_{max}=6 at either node 1 or 2. Thus, the network lifetime is T^{TC}_{max}=20. If node 3 uses a frequency with the wavelength of 2λ to communicate with node 0 after radio reconfiguration, the maximum power consumption of the topology control using the frequency control is P^{FC}_{max}=3. In this case, the network lifetime is T^{FC}_{max}=40 which is 2.67 times longer than the power control and 2 times longer than the time control. This simple example shows that the topology control with radio reconfiguration is more energy efficient when comparing with power and time controls. The energy saving effect is getting more significant as x increases. Each control dimension is complementary to each other. Thus, the combination of the control dimensions is more beneficial to the energy efficient topology control.

6.1.4 Contributions

The contributions of the dissertation for the energy efficient topology control using reconfigurable radio are as follows:

- The dissertation presents the system model which includes network, channel, and power consumption models for the reconfigurable radio system, as well as it formulates a network lifetime maximization problem considering the successful data relay.

- The dissertation presents the reconfigurable radio topology control (RTC) algorithm, including a minimum hop routing tree construction on the reconfigurable

radio sensor networks.

- The dissertation proposes the dynamic topology control (RDTC) algorithm including pruning and grafting the local leaf branches of a low power relay node to further extend the network lifetime.

From the simulation results, the proposed topology control based on the reconfigurable radio can double the network lifetime comparing with the topology control methods based on the power and time controls. To the best of our knowledge, this is the first research applying radio reconfiguration from wide range of frequencies to address the problem of maximizing network lifetime as a energy efficient topology control in wireless sensor networks.

The rest of the dissertation is organized as follows. In Section 6.2, the dissertation introduces the reconfigurable radio sensor networks with the description of an example of the hardware design, the advantages, and the challenges. Section 6.3 outlines the system model for the reconfigurable radio sensor networks. In Section 6.4, the dissertation formulates a problem to maximize the network lifetime. Then, in Section 6.5, the dissertation provides the energy efficient topology control algorithms including a routing tree construction on the reconfigurable radio sensor networks. In Section 6.6, the dissertation provides the performance evaluations and discussion. Finally, the Section 6.7 concludes the chapter.

6.2 Reconfigurable Radio Sensor Networks

6.2.1 Reconfigurable Radio and its Hardware Platforms

Reconfigurable radio is a wireless communication paradigm in which either a network or a wireless node changes its communication parameters, such as operating frequency and modulation/demodulation, with the aim of system performance improvements. Software-defined radio (SDR) system can be a good example of the system using the reconfigurable radio functionality adapting to a dynamically-changing environment. A SDR system is a radio communication system where components that have been typically implemented in

hardware (e.g. mixers, filters, amplifiers, modulators/demodulators, detectors, etc.) are instead implemented by means of software on a personal computer or embedded computing devices [75]. The wireless sensor network that is using reconfigurable radio functionality is called a *reconfigurable radio sensor network* (RRSN) where the transmission range can be dramatically changed due to the wide ranges of operating frequency selection. Taking the advantage of changing the operating frequency over a wide frequency range will let wireless sensor networks enhance energy efficiency as well as satisfy given network performance requirements. Current sensor systems such as MICAz and MICA2 are working on fixed ultra-high frequency (UHF) bands of 2.4GHz and 300∼900 MHz. If the sensors use lower frequencies in ISM (Industrial, Scientific and Medical) or license free bands, they can achieve better propagation and longer communication distance. This is beneficial because it extends network lifetime in the environments of high signal attenuation, such as being underground, in a dense forest, and in industrial fields. Especially low frequency is strong in the environments of high signal attenuation such as underground, dense forest, and industrial fields. In such highly attenuating environments, a sensor network needs the radio reconfiguration to the lower frequency bands to achieve long communication distance for the energy efficiency.

USRP (Universal Software Radio Peripheral) is an experimental platform of a GNU radio or software-defined radio system. USRP can be an example platform for the reconfigurable radio system, however it requires a host PC to implement the communication components in softwares. The sensor node cannot implement the communication components in softwares because it has a low-power processor. To show the feasibility of the stand-alone sensor node with reconfigurable radio functionality, called *reconfigurable radio sensor node*, a new hardware platform design based on the MICA2/MICAz and USRP platforms was introduced in [53]. In the proposed platform, the main processing parts (i.e., CPU, memory, etc.) of the reconfigurable radio sensor node are designed like MICA2/MICAz nodes and the reconfigurable radio parts for the radio reconfiguration are designed like USRP system. The significant difference of reconfigurable radio sensor platform from USRP is the implementation of radio communication components. In the reconfigurable radio sensor nodes, the traditional radio communication blocks (e.g. mixers, filters, modulators/demodulators, detectors, etc.) will be implemented in FPGA (Field

Programmable Gate Array). The reconfigurable radio sensor node can have multiple radio communication blocks and be equipped RF front ends working on different frequency bands ranging from KHz to GHz depending on the number of required frequency bands.

6.2.2 Benefits and Challenges of Applying Reconfigurable Radio in Wireless Sensor Networks

The benefits of reconfigurable radio on the topology control can be described as follows:

- It significantly reduces the transmission power to communicate at the same distance by using larger wavelengths or lower frequency bands. The required energy (transmission power) to achieve the communication distance increases exponentially with the order L as the distance increases such as $E \propto d^L/\lambda^2$. The effect of soaring required energy can be significantly alleviated by increasing the wavelengths (λ) or lowering the operating frequency (f).

- It reduces the number of relay nodes through long distance communication while maintaining connectivity for the data relay, which is more energy efficient. This effect is more significant in areas of high signal attenuation such as being underground or in industrial fields. In the example shown in Figure 6.2 where $d_{30}^L > d_{31}^L + d_{10}^L$ using a single frequency with a wavelength λ, the relay node is required for the network energy efficiency. By radio reconfiguration on the link between the sender and the receiver to $x\lambda$, the relay node is not required for the energy efficiency when $\sqrt{\frac{d_{30}^L}{d_{31}^L+d_{10}^L}} \leq x$.

- It avoids interference from adjacent nodes in a wireless network using multiple frequency bands. In Figure 6.2, after the radio reconfiguration on the link between the node 3 and 0 to a frequency different from the link between the node 1 and 0 or the node 2 and 0, the interference will be reduced.

- It provides a dynamic or adaptive network topology. In the ad-hoc mesh network, the relay nodes around the sink node will use more power to relay traffic, which is known as an energy hole. The topology change with the reconfigurable radio makes

the sensor network able to avoid high burden relay nodes to transmit data to the sink. When a relay node has low remaining power or is faulty, the network topology should be updated to extend network lifetime further. By radio reconfiguration and changing communication distance, the energy holes on the topology can be distributed to extend network lifetime.

- The relay nodes having a large amount of data in close distance where the signal attenuation is small can benefit from using high frequency to transmit data. In the boundary of the two different media (e.g., near the surface), the relay node can use two different frequency bands to relay the data such as high frequency bands for data relay in aboveground communications and low frequency bands for underground communications.

While having advantages, there are trade-offs of using a reconfigurable radio on the topology control such as increasing 1) the complexity and power consumption on the hardware, and 2) the control overhead and complexity. The reconfigurable radio sensor networks have not been yet deployed, however recent advances in SDR technology can be used in the design of the practical energy efficient radio reconfiguration system. The dissertation introduce a solution for reconfigurable radio sensor nodes by presenting block diagram and prototype. To address the control overhead and complexity of reconfigurable radio sensor networks, the dissertation proposes a system model, a route construction scheme, and distributed relay selection algorithms. In addition to the technical challenges, there is a consideration on the radio reconfiguration. Because the data rate of the low frequency carrier is limited, applications requiring a high data rate such as surveillance system using wireless sensor networks have a limitation on the frequency candidates for the radio reconfiguration. The new topology control with reconfigurable radio, which has advantages and challenges, provides longer network lifetime on the evaluations in Section 6.5.

6.3 System Model

6.3.1 Network Model

We consider a wireless sensor network with N nodes and a sink node which are not mobile. Sensors are powered by batteries that are not rechargeable and not replaceable. All sensor nodes are static and all wireless links are bidirectional, which is common in current sensor networks [88]. Each node holds its device ID and there are two types of sensor nodes: relay nodes and device nodes. The device nodes periodically sense the environment and report the sensing results to the sink node through the relay nodes, which are decided on the route construction. The relay nodes relay the data from peer-relay and/or device nodes to the sink node, as well as the nodes sense the environment and report the results to the sink node. Sensor nodes are equipped with reconfigurable radio and can change their operating frequencies among M license-free frequency bands, such as 5.8GHz, 2.4GHz, 433MHz, 13.5MHz, 6.78MHz, and 134KHz ISM bands. The definition of the network lifetime can be extended as the fraction of alive nodes or the time until the network fails to construct a backbone for the performance comparisons. The radio reconfiguration to transmit the data is not frequently performed to save energy due to the control overhead.

To deliver the sensor data, each node knows its next-hop node to the sink via neighbor discovery and route construction. Due to the radio reconfiguration capability with multiple radio frontends, the sensor node can send and receive data via different radio frontends similar to those in a USRP system. During its data transmission periods, a device node communicates with a delay node in a chosen operating frequency through one radio frontend with its other radio frontend(s) turned off. The relay node may have multiple radio frontends turned on at the same time when it communicates with neighboring nodes (device and/or relay nodes) in multiple frequency bands. The medium access control is based on CSMA/CA (Carrier Sense Multiple Access with Collision Avoidance). Assume that all sensor nodes wake up at the same scheduled time from a sleep mode for environmental sensing and data reporting based on time synchronization and scheduling.

The proposed networks operate in three phases: a setup phase, a static phase, and

a dynamic phase. In the setup phase, the relay nodes are selected and the routes from any node to the sink node are constructed. In the static phase, every node senses the environment and reports the sensor data to the sink node periodically. All nodes use the sleep mode to prolong network lifetime in the static phase. To minimize the power consumption during the idle periods, the device nodes switch to the sleep mode right after data reporting and receiving an ACK from the precedent relay node. The relay nodes switch to the sleep mode after finishing data reporting and relaying. If a relay node has its battery-power level decreased to a certain threshold, the networks enter into the dynamic phase where the relay node's local topology will be reconstructed to reduce the data transmissions and thus energy consumption burden of the low-power relay node. If the local topology is successfully reconstructed, the low-power relay becomes a device node.

6.3.2 Channel Model

The channel model used in the dissertation is as follows [37]:

$$P_{Rx} = \frac{P_{Tx} \times \lambda^2}{A \times PL(d)}, \tag{6.1}$$

where P_{Rx} is the received power which is a function of the transmitter-receiver distance d and the radio wavelength λ, P_{Tx} is the transmitted power, A is the characteristic of the transmitting and receiving antennas, and $PL(d)$ is the path loss function. The path loss function is dependent on the communication medium. When the communication medium is air, the path loss function can be expressed as follows: $PL(d) = d^L$, where L is the path loss exponent that indicates the rate at which the path loss increases with the distance. When the communication medium is soil, the path loss function can be expressed as follows: $PL(d) = d^2 e^{2\alpha d}$ where α is the attenuation constant of the soil [33]. Based on the channel model, one can conclude that lower-frequency, i.e. longer-wavelength, radio signals may propagate further distances than higher-frequency radio signals with slower decay in signal strength.

6.3.3 Power Consumption Model

The power consumption of wireless sensor networks can be characterized in the following four categories: to keep the communication radio on, to transmit and receive control packets, to keep sensors on, and to transmit and receive data [84]. In the monitoring applications of wireless sensor networks, the energy will be consumed by environmental sensing, data processing, and packet delivery. The energy dissipation is mainly caused by communication, which includes transmit, receive, and idle operations. The power consumption of the sleep mode is negligible compared with the power consumptions of the radio modes, such as Tx/Rx/Idle modes [88]. The simple power and energy consumption model developed in [89, 90] is used to model power dissipation for the communication of wireless sensor nodes assuming that all nodes have power control functionality. The simple models do not consider the power consumption of the idle period on the network operation. More realistic power consumption models proposed in [91, 92] incorporate the characteristics of a typical low power transceiver and include the power consumption of the idle listening. The existing models ignore the interference and transmissions collisions by assuming the link capacity is high enough or the network traffic is light enough. To transmit and receive a bit at a distance d with an operating frequency f, the average power consumptions for transmitting and receiving the data are given by:

$$P^{T_f} = [P_{elec} + \varepsilon_{amp} \times PL(d)/\lambda^2] \tag{6.2}$$

$$P^{R_f} = [P_{elec}], \tag{6.3}$$

where P^{T_f} and P^{R_f} are the power consumption of transmitting and receiving the data, P_{elec} is the power dissipation of the circuitry in joules/bit, ε_{amp} is the power dissipation of the transmitting amplifier in joules/bit.

6.4 Network Lifetime Maximization Problem

In the proposed wireless sensor networks, sensor nodes are periodically sensing and processing the data. The power dissipation of these actions is constant and negligible for passive sensing. Most of the power dissipations are caused by the radio operations such

as transmitting and receiving data or idle listening. In the proposed network, each node i generates a data packet with the size of D bits at each periodic sensing action. For a sensor node i, the power dissipation for transmission from node i to node j on an operating frequency f can be expressed in joules/second as follows:

$$E_{ij}^{T} = E_{ij}^{T_f} = P_{ij}^{T_f} \times r_{ij}^{f}, \tag{6.4}$$

where $P_{ij}^{T_f}$ is the power consumption of transmitting the data when it is transmitting data from node i to j in joules/bit and r_{ij}^{f} is the transmitted data rate in packets/second using frequency f. The power dissipation at the receiver i can be expressed as follows:

$$E_{ji}^{R} = E_{1i}^{R_{f_1}} + \cdots + E_{Ni}^{R_{f_M}} = \sum_{k=1}^{M} [P^{R_{f_k}} \times \sum_{j \neq i} r_{ji}^{f_k}], \tag{6.5}$$

where $P^{R_{f_k}}$ is the power consumption of receiving the data using the frequency band k and $\sum_{j \neq i} r_{ji}^{f_k}$ is the rate of received data at node i. The total power dissipation at node i on the active period in joules/second can be expressed by:

$$E_i = \sum_{j \in N_{out}(i)} E_{ij}^{T} + \sum_{j \in N_{in}(i)} E_{ji}^{R} + E_i^{I}, \tag{6.6}$$

where $N_{out}(i)$ is the set of nodes which are the destination of all outgoing links form node i, $N_{in}(i)$ is the set of nodes, which are the source of all incoming links to node i, and E_i^I is the power dissipation in joules/second due to idle listening during no packet transmission and reception. If the sensors switch their power mode to the sleep mode right after transmitting data and receiving an ACK, the power consumption of E_i^I can be minimized. If each node has an initial energy budget of the battery, B_i, the lifetime (T_i) of sensor node i can be expressed as follows:

$$T_i = \frac{B_i}{E_i \times \rho_A}, \tag{6.7}$$

where $\rho_A = T_A/(T_A + T_S)$, T_A is the active period from when a node i wakes up to when it goes to sleep again, and T_S is the sleep period in the periodic cycles. Assuming all sensor nodes are equally important, the network life of the battery operated wireless

sensor networks in seconds can be defined as the time until the first sensor node exhausts its initial energy budget as follows:

$$T_{net} = \min_{i \in S} T_i, \tag{6.8}$$

where S is the set of all sensor nodes. Then, the problem of maximizing the network lifetime of wireless sensor networks can be expressed as follows:

$$\begin{aligned} \max \quad & T_{net} \\ \text{subject to} \quad & 0 < (\sum_{j \in N_{out}(i)} E_{ij}^T + \sum_{j \in N_{in}(i)} E_{ji}^R + E_i^I) T_i \leq B_i, \\ & \sum_{j \in N_{out}(i)} r_{ij}^f = \sum_{k=1}^{M} \sum_{j \in N_{in}(i)} r_{ji}^{f_k} + r_i, \\ & \sum_{j=1}^{N} r_{j0} = \sum_{i=1}^{N} r_i, \quad r_i, r_{j0} > 0, \ i, j \in [1, N]. \end{aligned} \tag{6.9}$$

In Equation 6.9, the first constraint guarantees that the power level of each node is non-negative and no greater than the initial power. The second constraint guarantees that the amount of data transmitted from node i is equal to the summation of the total incoming data and the data generated by node i. The third constraint ensures the requirement of successful data relay to the sink node (node 0). Due to its frequency/relay selection and combinatorial nature, the formulated problem is NP hard [86].

6.5 Topology Controls with Reconfigurable Radio

The solution of the network lifetime maximization is not currently practical in real wireless sensor networks due to its complexity and centralized nature. When the communication and operating environments are changing, finding the optimal solution is not capable using current wireless sensor nodes due to computational capabilities and time constraints. Thus, the dissertation presents two possible solutions which are the RTC (Reconfigurable Radio Topology Control) algorithm and the RDTC (Reconfigurable Radio Dynamic Topology Control) algorithm. The reconfigurable radio sensor networks is

represented by a graph $G = (V, E)$, where V is the set of sensor nodes and $E = (u, v, k)$ is the set of all bidirectional links between nodes u and v using frequency f_k in M frequency bands. Each node v has a unique ID $id(v)$ and records its hop distance to the sink node $d(v)$. For every node v except the sink node, its neighbor, precedent, and successor sets are expressed by $N^k(v) = \{u|(u, v) \in E\}$, $P^k(v) = \{u \in N^k(v)$ and $d(u) = d(v) - 1\}$, and $S^k(v) = \{u \in N^k(v)$ and $d(u) = d(v) + 1\}$. The relay node is expressed by $R^k(v) = \{u|u$ has the highest priority among $P^k(v)\}$, and the leaf node set is expressed by $L^k(v) = \{u|R^k(u) = v\}$. Initial hop counts are infinite which does not represent any paths to the sink node. In the network setup phase, every node broadcasts its routing information RI_v including its node ID $id(v)$, hop distance to the sink node $d(v)$, outgoing frequency f_k, selected relay node $R^k(v)$, neighbor nodes $N^k(v)$, successor nodes $S^k(v)$, and leaf nodes $L^k(v)$ on M frequency bands.

6.5.1 RTC: Reconfigurable Radio Topology Control

The wireless sensor networks periodically monitor the environment and report the data to the sink node. The relay nodes on the way to the sink node always need to forward the traffic from the neighbor senor nodes far from the sink node. Each node determines its shortest path to the sink node and shares its routing information RI_v. The aggregated data rate can be estimated from the number of leaf nodes. Each node v independently selects a relay node, among precedent set $P^k(v)$, based on the priority.

Priority for Relay Selection

For the energy efficient topology control, we define the priority rule in order to select a relay node including operating frequency selection as follows:

1. Hop counts: the smaller hop counts $d(v)$ to the sink node is the highest priority.

2. Interference: the node selects higher (default) frequency to connect the sink node or selects a relay node which uses higher outgoing frequency (f_k) among precedent set $P^k(v)$ to reduce interference.

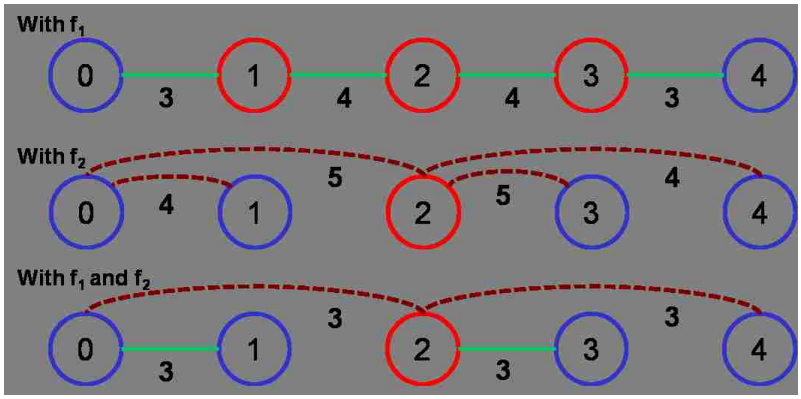

Figure 6.3: An example for the comparison of the link coverage which is marked on each link. The link with a solid line (green) is established using f_1 and the dashed line (brown) represents the link with f_2 which is the lower frequency. The red circle represents a relay node.

3. Load balancing: i) the higher value of $|N^k(v) - S^k(v)|$ which is the number of the difference between neighbor and successor sets, ii) the lower value of $|N^k(v)|$ which is the number of neighbor sets for the load balancing of the data relay.

4. Received power: the received power is the last priority.

The first priority guarantees the minimum hop counts to the sink node in order to reduce the power consumption and prolong the network lifetime as shown in Figure 6.2. The second priority reduces the interference from the adjacent link, which will incur longer transmission time and more power consumption. The interference can be analyzed by the coverage of link $E = (u, v, k)$ which represents the number of nodes affected by nodes u and v when u and v are communicating with their transmission power that are chosen such that they exactly communicate each other [93]. The link is affected by the Euclidean distance $|u, v|$, and the coverage of the link E is expressed as follows:

$$\begin{aligned} Cov(E) := |\{w \in V | w \; is \; covered \; by \; D(u, |u, v|, k)\} \cup \\ \{w \in V | w \; is \; covered \; by \; D(v, |v, u|, k)\}|, \end{aligned} \tag{6.10}$$

where $D(u, r, k)$ denotes the disk centered at node u with radius r using frequency f_k. The network lifetime can be extended by reducing the interference on the communication link, if $\sum_{k=1}^{M} \sum_{v=1}^{N-1} Cov(E(v, R^k(v), k)) \leq \sum_{v=1}^{N-1} Cov(E(v, R^k(v), k))$, where $E(v, R^k(v), k)$ is the link between node v and $R^k(v)$ using frequency f_k of the tree with N nodes and M frequency bands. An example of the link coverage is shown in Figure 6.3 where reconfigurable radio topology control uses two frequency bands (f_1 and f_2), and the communication distance of f_2 is $d_{f_2} = 2 \times d_{f_1}$. The topology with a frequency f_1 requires the maximum hop counts as 4 with 3 relay nodes and the average coverage of the links is $14/4$. The topology with a frequency f_2 requires the maximum hop counts as 2 with 1 relay node and the average coverage of the links is $18/4$. In case of using a lower frequency, which has longer communication distance, the topology can reduce the number of hop counts and relay nodes, however the interference increases due to the longer communication radius. The reconfigurable topology control can reduce the number of hop counts and relay nodes as well as the average coverage of the links which is $12/4$ in the example. The third priority distributes the load of the relay nodes. In general, the precedent with more successors has a greater chance to be a relay. To balance the relay load, the sensors first choose the higher value of $|N^k(v) - S^k(v)|$, which represents the lower chance to be a relay because the chance is proportional to the cardinality of $S^k(v)$. If all precedents have the same value of $|N^k(v) - S^k(v)|$, the sensors choose the lower value of $|N^k(v)|$, which represents less neighbors. Based on these two conditions on the third priority, the relay nodes can be distributed. In the case that all conditions are the same, which is the condition for the last priority, the higher received power represents the closer distance which is beneficial to prolong network lifetime.

Route Construction

The sink node constructs a routing tree which is rooted at the sink node in the setup phase considering M frequency bands so that each node determines the minimum hop distance to the sink node and selects a relay node with reduced interference. On the route construction in the setup phase, the control messages are transmitted with the maximum power. The routes are constructed as follows:

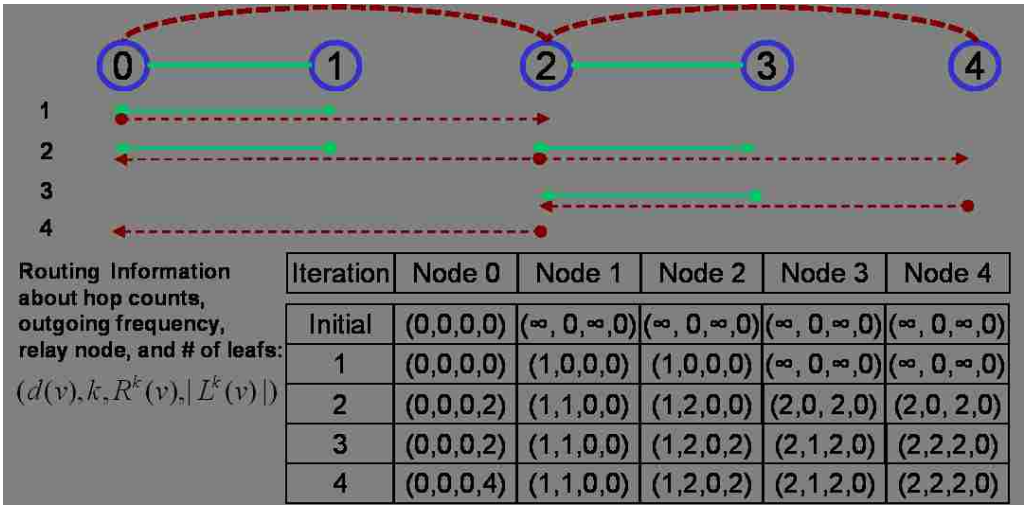

Iteration	Node 0	Node 1	Node 2	Node 3	Node 4
Initial	(0,0,0,0)	(∞, 0,∞,0)	(∞, 0,∞,0)	(∞, 0,∞,0)	(∞, 0,∞,0)
1	(0,0,0,0)	(1,0,0,0)	(1,0,0,0)	(∞, 0,∞,0)	(∞, 0,∞,0)
2	(0,0,0,2)	(1,1,0,0)	(1,2,0,0)	(2,0, 2,0)	(2,0, 2,0)
3	(0,0,0,2)	(1,1,0,0)	(1,2,0,2)	(2,1,2,0)	(2,2,2,0)
4	(0,0,0,4)	(1,1,0,0)	(1,2,0,2)	(2,1,2,0)	(2,2,2,0)

Figure 6.4: Sample processing of the route construction with control packets and the routing information table. Each entry for node i shows the hop counts to the sink node (node 0), the selected outgoing frequency, the selected relay node, and the number of leaf nodes. The effective broadcasting control messages at each iteration are shown by solid (f_1) and dashed (f_2) arrows.

1. Every node is ON in the setup phase and periodically broadcasting its routing information (RI_v).

2. The sink node (node ID=0) periodically broadcasts control packets (route request, RREQ) on M frequency bands to the network to trigger the route construction.

3. Each node selects a route/relay, which contains the highest priority based on RTC priority and updates the routing information with the relay node ID on a selected frequency f_k. The selected relay node updates its routing information with an increased number of leaf nodes, which will be relayed to the sink node via control packets (route reply, RREP).

4. The route construction is terminated, when the total number of leaf nodes on the sink node is N. In the last step, the sink node broadcasts a control message (ESTABLISH) to its leaf nodes, which relay the packet to their leaf nodes until it

reaches to the device node. In the case that the total number of nodes is not known, the route construction is terminated when the total number of leaf nodes on the sink node is constant and not changed for a specific amount of time ($T_{timeout}$).

An example of the routing algorithm is shown in Figure 6.4 with the routing information table showing hop counts, the selected relay node, and the number of leaf nodes. At initial time, all nodes cannot reach to the sink node (node 0) and the hop counts and relay node are infinite. At the first iteration, the node 1 and 2 receive a broadcasted control message (RREQ with $d(v) = 0$) from the sink node, will update hop counts, and then broadcast a control message (RREQ with $d(v) = 1$). If $d(N^k(v)) \geq d(v)$, the control packets (RREQ) are discarded. At the next iteration, the nodes 3 and 4 select the node 2 as a relay node based on the RTC priority, update the routing information, and send RREP control packets. When the node 2 receives the RREP packets, it will update the number of leaf nodes and send a updated RREP to the sink node. At the final iteration, the sink node receives a control message from node 2 and then the total number of leaf nodes is 4, which is the condition of the termination of the route construction.

6.5.2 RDTC: Reconfigurable Radio Dynamic Topology Control

During the network operation, a sensor node can be faulty or malfunctioned due to its battery exhaustion or low power level. If the sensor network have a distributed dynamic topology control algorithm, the network lifetime can be further extended. In the proposed distributed topology control, the local topologies are only updated by pruning and grafting the leaf branches of the low power relay, because the whole network topology update will cause more energy consumption and decrease the network lifetime. The reconfigurable radio dynamic topology control is as follows:

1. When the power level of a relay node is lower than the threshold level B_{th}, the low power relay node broadcasts control packets (topology change, TC) to its leaf nodes $L^k(v)$ and neighbor nodes $N^k(v)$ on M frequency bands. Then the neighbor nodes that received the control packet change its state to the dynamic phase.

2. The leaf nodes select new relay nodes based on the RTC priority except the low

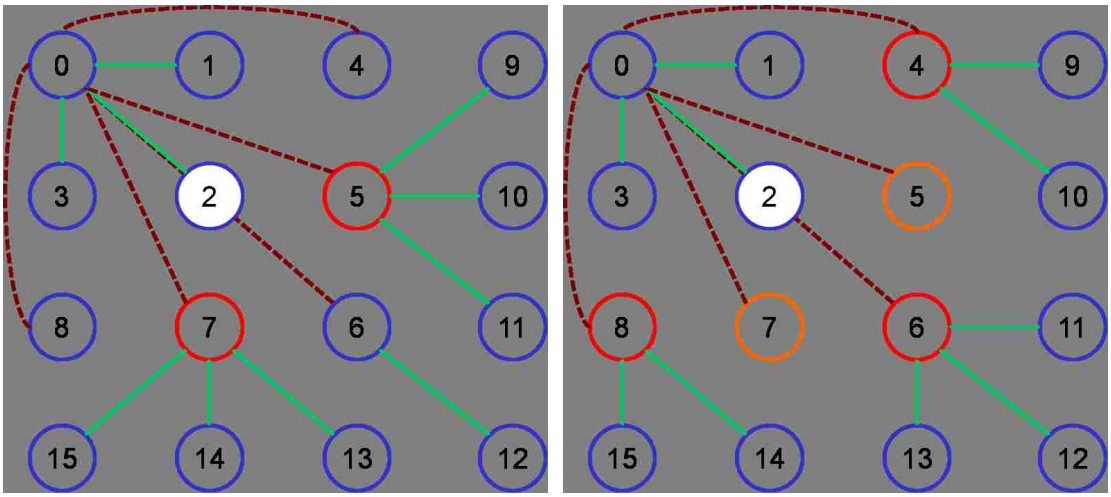

(a) The network topology based on RTC algorithm

(b) The network topology after applying RDTC algorithm

Figure 6.5: Examples of network topologies of RTC and RDTC algorithms. The red circle represents a relay node and the orange circle represents the node exempted from the duty of data relaying after the topology update.

power relay node and send control packets (topology update, TU) to their old and new relay nodes.

3. The topology reconfiguration is terminated, when all leaf nodes of the low power relay node find alternate relay nodes. The low power relay node determines the successful topology reconfiguration based on the topology update control packets from its leaf nodes, and broadcasts the control packets (topology update finish, TUF) to $L^k(v)$ and $N^k(v)$. On the new relay node selection, the low power relay remains a relay node with the reduced number of leaf nodes, but only if its leaf nodes cannot find alternate relays.

The constructed topologies of RTC and RDTC algorithms are demonstrated in the examples of Figure 6.5 where the communication distance of a solid line (green) using

f_1 is one hop and the communication distance of the dashed line (brown) using f_2 is two hops of the grid. Based on the RTC algorithm, the nodes 5 and 7 are selected as relay nodes and will use more power due to the relay traffic. When the power levels of nodes 5 and 7 are lower than the threshold, the nodes 4, 6, and 8 are selected as relay nodes after the topology update based on the RDTC algorithm. In the example, the node 5 and 7 are exempted from the duty of data relaying after the topology update, which leads the extended network lifetime.

6.6 Performance Evaluation

6.6.1 Comparisons for Aboveground Communications

On the performance evaluations, the system parameters are used as follows:

- The operating frequencies for aboveground communications are chosen as 2.4GHz for a higher frequency (f_1) and 433MHz for lower frequency (f_2) in ISM bands.
- The attenuation constant for aboveground communications L is set to 4.
- The gain of transmitting and receiving antennas is 1.76dBi, the maximum transmission power is 0dBm, and the minimum sensible power is -94dBm.
- The initial energy of the battery (B_i) is 10KJ, P_{elec}=50nJ/bit, and ε_{amp}=100$pJ/bit/m^2$.
- The data and control packets are 50 bytes in length.

In the evaluations, sensors are distributed in a square terrain of 200×200 square meters and the number of deployed sensor nodes is gradually changed from 150 to 400 to consider different density. The communication distance of 2.4GHz is 27m and the communication distance of 433MHz is 64m with the path loss exponent $L = 4$. Two popular node placements used in [88] are investigated in the comparisons. In the first (grid and random) placement, the first 144 nodes are located a 12×12 grid to guarantee connectivity in case of L=4, other nodes are randomly deployed inside the terrain, and the sink node is located

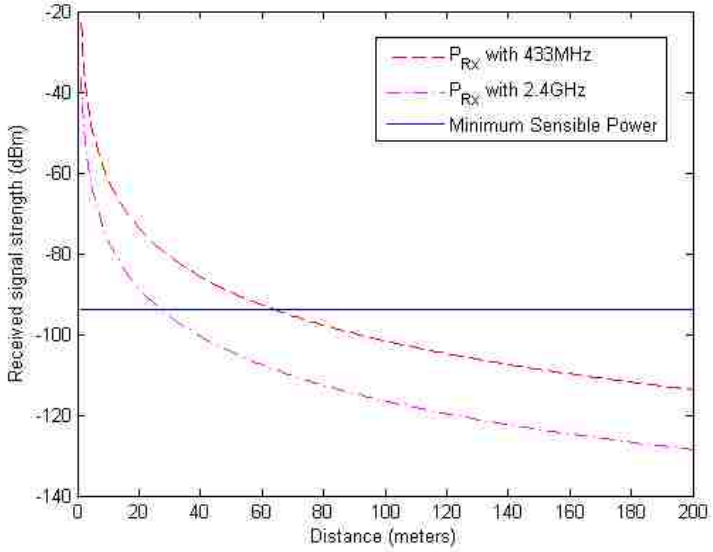

Figure 6.6: Received signal strengths of 433MHz and 2.4GHz with distance in case of the loss exponent L=4.

at the center or a corner. In the second (random) placement, all nodes are randomly distributed throughout the terrain. For each density and sink location, the experiments are repeated 50 times and the average values are taken. In the experiments, each sensor node is periodically performing sensing and generating the data packet every 1 hour, and it is in the sleep mode after transmitting the data successfully. Because the radio reconfiguration is not frequently performed and the number of reconfiguration is negligible comparing with the data transmissions, the power consumption of control overhead is ignored. In RDTC, B_{th} is set to $0.2 \times B_i$ because the performance of RDTC improves as the threshold value increases until $0.2 \times B_i$, after which value the performance improvement is saturated in the preliminary evaluations as shown in Figure 6.6.

To evaluate the proposed topology control with the frequency control using f_1 and f_2, we design two comparison models based on [80, 81, 84, 85], topology controls with the power control and time control using f_1, as follows:

- Topology Control with Power Control (TCPC): the topology control generates minimum hop routes where a sensor node selects a relay node among a precedent set $P^k(v)$ minimizing the power consumption of the data transmission.
- Topology Control with Time Control (TCTC): the topology control generates minimum hop routes where the sensor nodes select a relay node in turn among precedent set $P^k(v)$ for the load balancing of the power consumption.

Sink node at the center of the grid

The network lifetimes of the grid and random node placement are compared with the number of nodes, where the sink node is located at the center of the terrain. In Figure 6.7(a), the network lifetime decreases as the number of nodes increases because the relay nodes near the sink node have more data to relay as the number of node increases. The estimated network lifetimes on the simulations are reasonable comparing with real sensor node operations. In the comparisons, the network lifetime is ordered as RDTC>RTC>TCTC>TCPC. RTC has 1.55 times and 1.36 times longer network lifetime comparing with TCPC and TCTC on average. RDTC has 1.83 times and 1.62 times longer network lifetime comparing with TCPC and TCTC on average. With 3.02 topology updates on average, RDTC extends the network lifetime 18.5% more than RTC.

Sink node at a corner of the grid

In the case of the sink node being located at a corner of the terrain with the grid and random placement, the network lifetimes are compared. The relay nodes near the sink node have more leaf nodes due to the node placement and the location of the sink node. When the sink node is at the corner, the network lifetime is shorter than the placement of sink node at the center, but the network lifetime order is same as shown in Figure 6.7(b). The performance gains of RTC and RDTC over TCPC and TCTC in a sparse population are greater than a dense population, and there is not a significant difference between TCPC and TCTC because the number of relay candidates in turn for the load balancing is small. In the comparisons, RTC has 2.06 times and 1.95 times longer network lifetime

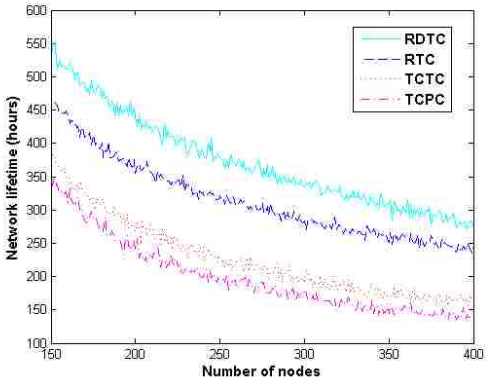

(a) The sink node is located at the center of the grid and random placement.

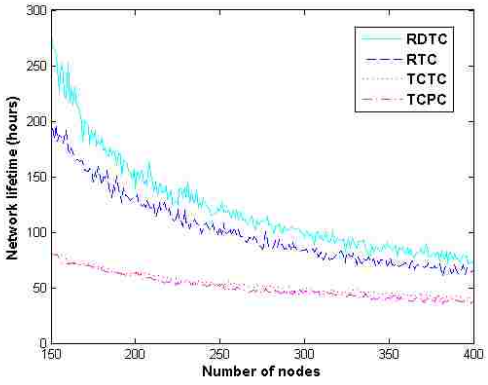

(b) The sink node is located at the corner of the grid and random placement.

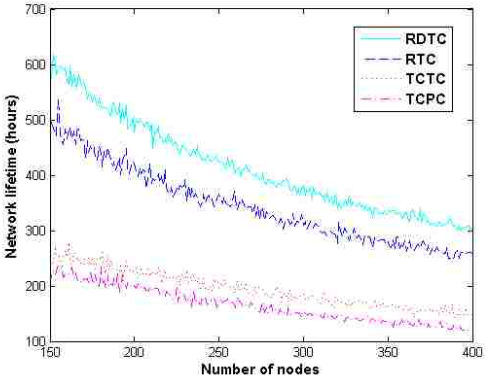

(c) The sink node is located at the center of the random placement.

Figure 6.7: The comparisons of network lifetime for aboveground communications.

and RDTC has 2.49 times and 2.36 times longer network lifetime comparing with TCPC and TCTC on average. With 1.81 topology updates, RDTC extends the network lifetime 21.3% more than RTC on average.

Sink node at the center of random placement

In the random placement where the sink node is located at the center of the terrain, the node that is not connected to the sink node at the route construction is not considered in the network lifetime calculation. In the comparisons of the random placement shown in Figure 6.7(c) RDTC and RTC provide longer network lifetime which is significant in a sparse population. In the comparisons, RTC has 2.08 times and 1.77 times longer network lifetime, and RDTC has 2.50 times and 2.14 times longer network lifetime comparing with TCPC and TCTC on average. With 3.11 topology updates, RDTC extends the network lifetime 20.3% more than RTC on average.

6.6.2 Comparisons for Underground Communications

On the performance evaluations of underground communications, the system parameters are the same as aboveground communications excepts some parameters as follows:

- The operating frequencies for underground communications are chosen as 433MHz for a higher frequency (f_1) and 13.5MHz for lower frequency (f_2) in ISM bands.
- Soil properties are from the wet clay type soil (measured electrical conductivity = 780 mS/m, estimated relative permittivity = 30) sampled in Lehigh University Goodman Campus.
- The attenuation constants (α) of the underground medium are calculated as 24.14 N/m for 433MHz and 6.37 N/m for 13.5MHz using Equation 3.15.
- The communication distances are shown in Figure 5.2(a) and Figure 5.2(b). The communication distance of 433MHz is 30cm and the communication distance of 13.5MHz is 135cm in clay type underground medium.

In the evaluations, sensors are distributed in a square terrain of 300$\times$300 square centimeters and the number of deployed sensor nodes is gradually changed from 257 to 300 to consider different density. Two node placements used in the comparisons of aboveground communications are investigated. In the first (grid and random) placement, the first 256

nodes generate a grid network which guarantee connectivity , other nodes are randomly deployed inside the terrain, and the sink node is located at the center or a corner In the second (random) placement, all nodes are randomly distributed throughout the terrain. For each density and sink location, the experiments are repeated 50 times and the average values are taken. In the evaluation of the proposed topology control for underground communications, two comparison models (TCPC and TCTC) are used.

Sink node at the center of the grid

The network lifetimes of the underground grid and random node placement are compared with the number of nodes, where the sink node is located at the center of the terrain. In Figure 6.8(a), the network lifetime decreases as the number of nodes increases because the relay nodes near the sink node have more data to relay as the number of node increases. In the comparisons, the network lifetime is ordered as RDTC>RTC>TCTC>TCPC. RTC has 3.34 times and 3.12 times longer network lifetime comparing with TCPC and TCTC on average. RDTC has 3.76 times and 3.51 times longer network lifetime comparing with TCPC and TCTC on average. With topology updates, RDTC extends the network lifetime 12.5% more than RTC on average.

Sink node at a corner of the grid

In the case of the sink node being located at a corner of the underground terrain, the network lifetimes are compared. The relay nodes near the sink node have more leaf nodes which are the same as aboveground communications. When the sink node is at the corner, the network lifetime is shorter than the placement of sink node at the center as shown in Figure 6.8(b). In the comparisons, RTC has 1.24 times and 1.22 times longer network lifetime and RDTC has 1.65 times and 1.63 times longer network lifetime comparing with TCPC and TCTC on average. With topology updates, RDTC extends the network lifetime 33.3% more than RTC on average. Between TCPC and TCTC, there is no significant difference.

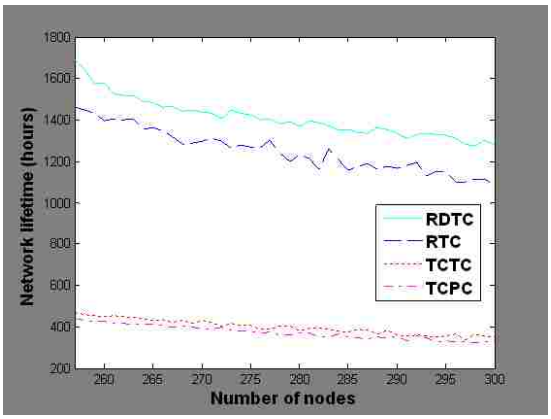

(a) The sink node is located at the center of the grid and random placement.

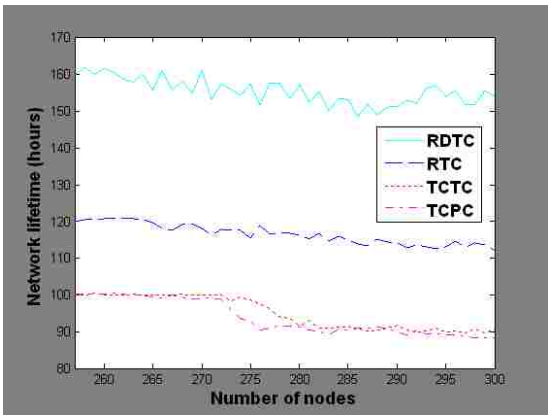

(b) The sink node is located at the corner of the grid and random placement.

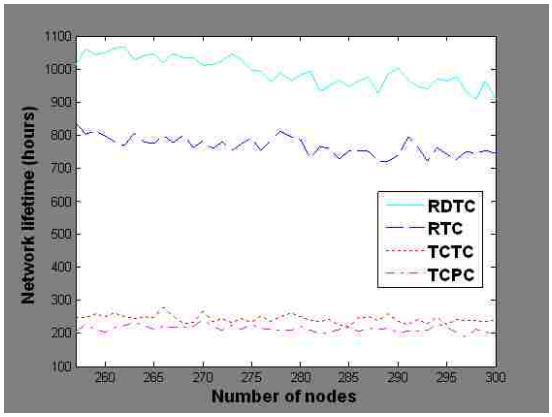

(c) The sink node is located at the center of the random placement.

Figure 6.8: The comparisons of network lifetime for underground communications.

Sink node at the center of random placement

In the random placement where the sink node is located at the center of the underground terrain, the node that is not connected to the sink node at the route construction is not considered in the network lifetime calculation. In the comparisons of the random placement

shown in Figure 6.8(c), RTC has 3.58 times and 3.14 times longer network lifetime, and RDTC has 4.63 times and 4.06 times longer network lifetime comparing with TCPC and TCTC on average. With topology updates, RDTC extends the network lifetime 29.3% more than RTC on average.

6.7 Summary

This chapter introduces a novel topology control with the reconfigurable radio to maximize network lifetime while maintaining successful data relay. To formulate the maximization problem, the chapter presents the system model of reconfigurable radio sensor networks that includes network, channel, power consumption models. To extend the network lifetime, the dissertation proposes two algorithms (RTC and RDTC) and evaluates their performance gains. In the comparisons of the topology control algorithms, the proposed RTC and RDTC have longer network lifetime than TCPC and TCTC in all ranges and conditions.

Chapter 7

Conclusions and Future Works

The dissertation introduces a novel concept of Wireless Signal Networks (WSiNs) which can provide real-time monitoring and global measurements based on the link quality (i.e., received signal strength) between wireless sensor nodes. The received signal strength information of underground sensors is used to characterize the geo-event in the proposed underground wireless signal network. For the subsurface characterization, the parameters and soil properties affecting the signal attenuations for underground communications are investigated with actual sensor network measurements. To evaluate the concept of WSiNs for subsurface event detection, three event detection simulations (water intrusion, relative density change, and relative motion) were conducted using MICAz. In the dissertation, the window-based minimum distance classifier is proposed to detect and classify geo-events of wireless underground sensor networks. The window-based minimum distance classifier accurately detects geo-events and classifies the water leakage event into different water contents. From the theoretical analysis and simulation, the proposed window-based minimum distance classifier has higher accuracy and less computation than whole range minimum distance classifier.

For the analysis of the proposed wireless signal networks, the dissertation provides theories and measured results to improve the understanding of underground radio signal propagation of wireless sensor networks. Based on the theories, we developed the received signal strength expression as well as the logarithmic scale expression of the underground radio propagation with respect to the distance between the sender and the receiver.

The proposed underground radio propagation model is accurate due to its derivation based on theoretical studies of how radio propagate in subsurface environments. The proposed model was validated using laboratory and field measurements. The estimated received signal strength from the underground radio propagation model provides a very good fit to the measured data of the wireless underground sensor networks.

To extend underground communication distance, prolong network lifetime, and provide adaptive topology construction, the dissertation presents the design of reconfigurable radio sensor networks in progress for low frequency wireless sensor networks. The proposed underground radio propagation model is used to investigate the underground communication distance and estimates that low frequency bands are suitable for subsurface monitoring applications. To extend the network lifetime and provide adaptive topology construction, the dissertation introduces a novel topology control with the reconfigurable radio while maintaining successful data relay. To formulate the maximization problem, the dissertation presents the system model of reconfigurable radio sensor networks that includes network, channel, power consumption models. To extend the network lifetime, the dissertation proposes two algorithms (RTC and RDTC) and evaluates their performance gains. In the comparisons of the topology control algorithms, the proposed RTC and RDTC have longer network lifetime than TCPC and TCTC in all ranges and conditions.

In future work, we would like to implement reconfigurable radio sensor nodes for wireless signal networks and subsurface characterization. The reconfigurable radio sensor nodes with lower frequency bands such as 125KHz and 6.78MHz ISM bands can provide longer underground communication distance (approximately 25m with 125KHz and 2m with 6.78MHz even in wet clay type soil based on the proposed propagation model assuming the same antenna gains of MICAz and 1W Tx power [53]). With the new system, we would like to conduct experiments for geo-event detection and classification of heterogeneous conditions, and to evaluate the proposed underground propagation model in low frequency bands for a practical system.

Bibliography

[1] Reedy, R. C. & R.Scanlon, B. Soil water content monitoring using electromagnetic induction. *Journal of Geotechnical and Geoenvironmental Engineering* **129** (2003).

[2] Sudduth, K. A., Drummond, S. T. & Kitchen, N. R. Accuracy issues in electromagnetic induction sensing of soil electrical conductivity for precision agriculture. *Journal of computers and electronics in agriculture* **31**, 239–264 (2001).

[3] Robinson, D. A., Jones, S. B., Wraith, J. M., Or, D. & Friedman, S. P. A review of advances in dielectric and electrical conductivity measurement in soils using time domain reflectometry. *Journal of vadose zone* **2** (2003).

[4] der Velde, R. V. *Soil moisture remote sensing using active microwaves and land surface modeling* (Ph.D. dissertation (ITC dissertation number: 176), University of Twente, The Netherlands, 2010).

[5] Lunt, I. A., Hubbard, S. S. & Rubin, Y. Soil moisture content estimation using ground-penetrating radar reflection data. *Journal of Hydrology* **307**, 254–269 (2005).

[6] Furlani, K. M., Miller, P. K. & Mooney, M. A. Evaluation of wireless sensor node for measuring slope inclination in geotechnical applications. In *Proc. of the 22nd International Symposium on Automation and Robotics in Construction* (2005).

[7] Terzis, A., Anandarajah, A., Moore, K. & Wang, I. J. Slip surface localization in wireless sensor networks for landslide prediction. In *Proc. of IPSN 2006*, 109–116 (ACM Press, 2006).

[8] Glaser, S. D., Shoureshi, R. & Pescovitz, D. Future sensing systems. *Smart Structures and Systems* **1**, 103–120 (2005).

[9] Chen, M., Glaser, S. D. & Oberheim, T. Terra-scope - a mems-based vertical seismic array. *Smart Structures and Systems* **2**, 115–126 (2006).

[10] Abdoun, T. *et al.* Wireless real time monitoring of soil and soil-structure systems. *Geotechnical Special Publication* **161** (2007).

[11] Instruments, D. Wireless vantage pro2 URL `http://www.davisnet.com/`.

[12] Akyildiz, I. F. & Stuntebeck, E. P. Wireless underground sensor networks: Research challenges. *Ad Hoc Networks Journal (Elsevier)* **4**, 669–686 (2006).

[13] Hu, W., Le, T. D., Corke, P. & Jha, S. Design and deployment of long-term outdoor sensornets: Experiences from a sugar farm. In *Proc. of EEE Pervasive Computing* (2010).

[14] Park, C., Xie, Q., Chou, P. & Shinozuka, M. Duranode: wireless networked sensor for structural health monitoring. In *Proc. of IEEE Sensors 2005*, 277–280 (2005).

[15] Cho, S. *et al.* Smart wireless sensor technology for structural health monitoring of civil structures. *Steel Structures* **8**, 267–275 (2008).

[16] Misra, P., Kanhere, S., Ostry, D. & Jha, S. Safety assurance and rescue communication systems in high-stress environments: A mining case study. *IEEE Communications Magazine* (2010).

[17] Liu, Z., Li, C., Ding, Q. & Wu, D. A coal mine personnel global positioning system based on wireless sensor networks. In *Proc. of the 8th World Congress on Intelligent Control and Automation* (2010).

[18] Trinchero, D., Stefanelli, R., Ricardo, M. & Cerquera, P. Design and optimization of the electromagnetic front-end for wireless sensors floating in dissipative media. In *Proc. of IEEE RWS 2010* (2010).

[19] Trinchero, D., Galardini, A., Stefanelli, R. & Fiorelli, B. Microwave acoustic sensors as an efficient means to monitor water infrastructures. In *Proc. of IEEE IMS 2009* (2009).

[20] Trinchero, D. & Stefanelli, R. Microwave architectures for wireless mobile monitoring networks inside water distribution conduits. *IEEE TRANSACTIONS ON MICROWAVE THEORY AND TECHNIQUES* **57** (2009).

[21] Trinchero, D., Stefanelli, R., Galardini, A. & Fiorelli, B. Wireless sensors for a wire-independent analysis of fluid networks. In *Proc. of IEEE Sensors Applications Symposium* (2009).

[22] Lin, M., Wu, Y. & Wassell, I. Wireless sensor network: Water distribution monitoring system. In *Proc. of IEEE RWS 2008* (2008).

[23] Sabin, D. D., Dimitriu, C., Santiago, D. & Baroudi, G. Overview of an automatic underground distribution fault location system. In *Proc. of IEEE Power and Energy Society General Meeting* (2009).

[24] Fujita, S., Fujiwara, K., Sumita, J., Konya, Y. & Muroyama, S. Automatic oil leak detection system for an underground tank. In *Proc. of IEEE Telecommunication Energy Conference* (1999).

[25] Sheth, A. *et al.* Senslide: a sensor network based landslide prediction system. In *Proc. of SenSys'05*, 280–281 (2005).

[26] de Dios, R. J., Enriquez, J., Mendoza, F. G. V. E. A., Talampas, M. C. & Marciano, J. J. Design, development, and evaluation of a tilt and soil moisture sensor network for slope monitoring applications. In *Proc. of IEEE TENCON 2009* (2009).

[27] Werner-Allen, G. *et al.* Deploying a wireless sensor network on an active volcano. *IEEE Internet ComputingS* **10**, 18–25 (2006).

[28] Dinh, T. L. *et al.* Design and deployment of a remote robust sensor network: Experiences from an outdoor water quality monitoring network. In *Proc. of 32nd IEEE Conference on Local Computer Networks* (2007).

[29] Bocchetti, G., Flammini, F., Pragliola, C. & Pappalardo, A. Dependable integrated surveillance systems for the physical security of metro railways. In *Proc. of IEEE International Conference on Distributed Smart Cameras* (2009).

[30] Technology, C. Guidelines for wsn design and deployment URL `http://www.xbow.com`.

[31] Technology, C. URL `http://www.xbow.com/support/Support_pdf_files/XMesh_Avg_Current.xls`.

[32] Technology, C. Mica2 aa battery pack service life test URL `http://www.xbow.com`.

[33] Yoon, S.-U., Cheng, L., Ghazanfari, E., Pamukcu, S. & Suleiman, M. T. A radio propagation model for wireless underground sensor networks. In *Proc. of the IEEE Globecom 2011* (2011).

[34] Ritsema, C. J. *et al.* A new wireless underground network system for continuous monitoring of soil water contents. *Water Resour. Res. 45:W00D36* (2009).

[35] Bogena, H. R. *et al.* Potential of wireless sensor networks for measuring soil water content variability. *Vadose Zone J.* **9**, 1002–1013 (2010).

[36] Friis, H. T. A note on a simple transmission formula. In *Proceedings of the IRE*, vol. 34, 254–256 (1946).

[37] Rappaport, T. S. *Wireless communications Principles and Practice* (Prentice Hall, 1996).

[38] Orfanidis, S. J. Electromagnetic waves and antennas. *Online Book* URL `http://www.ece.rutgers.edu/~orfanidi/ewa`.

[39] Feng, W., Lin, C. P., Deschamps, R. J. & Drnevich, V. P. Theoretical model of a multisection time domain reflectometry measurement system. *Water Resources Research* **35**, 2321–2331 (1999).

[40] Li, L., Vuran, M. C. & Akyildiz, I. F. Characteristics of underground channel for wireless underground sensor networks. In *Proc. IFIP Mediterranean Ad Hoc Networking Workshop (Med-Hoc-Net'07)* (2007).

[41] Vuran, M. C. & Akyildiz, I. F. Channel model and analysis for wireless underground sensor networks in soil medium. *Physical Communication Journal (Elsevier)* (2010).

[42] Akyildiz, I. F., Sun, Z. & Vuran, M. C. Signal propagation techniques for wireless underground communication networks. *Physical Communication Journal (Elsevier)* **2**, 167–183 (2009).

[43] Peplinski, N. R., Ulaby, F. T. & Dobson, M. C. Dielectric properties of soils in the 0.3-1.3-ghz range. *IEEE Transactions On Geoscience and Remote Sensing* **33** (1995).

[44] Silva, A. & Vuran, M. C. Development of a testbed for wireless underground sensor networks. *EURASIP Journal on Wireless Communications and Networking* **2010** (2010).

[45] Silva, A. R. & Vuran, M. C. Empirical evaluation of wireless underground-to-underground communication in wireless underground sensor networks. In *Proc. IEEE DCOSS '09* (2009).

[46] Dong, X. & Vuran, M. C. A channel model for wireless underground sensor networks using lateral waves. In *Proc. IEEE Globecom '11* (2011).

[47] Bogena, H. R., Huisman, J. A., Meier, H., Rosenbaum, U. & Weuthen, A. Hybrid wireless underground sensor networks: Qualification of signal attenuation in soil. *Vadose Zone Journal* **8**, 755–761 (2009).

[48] Dane, J. H. & Topp, G. C. Methods of soil analysis: Part 4. *Physical methods. SSSA Book Ser. 5. SSSA* (2002).

[49] Chaamwe, N., Liu, W. & Jiang, H. Wave propagation communication models for wireless underground sensor networks. In *Proc. IEEE International Conference on Communication Technology (ICCT)* (2010).

[50] WAIT, J. R. & FULLER, J. A. On radio propagation through earth. *IEEE Transactions On Antennas and Propagation* (1971).

[51] Sommerfeld, A. Uber die ausbreitung der wellen in der drahtlosen telegraphie. *Ann. Phys. Lpz.* 665–736 (1909).

[52] Cheng, D. K. Field and wave electromagnetics 2nd edition. *Addison-Wesley* .

[53] Yoon, S.-U. *et al.* Subsurface monitoring using low frequency wireless signal networks. In *Proc. of IEEE PerCom 2012 (WiP session)* (2012).

[54] Hubbard, S. S. *et al.* Estimation of permeable pathways and water content using tomographic radar data. *The Leading Edge* **16**, 1623–1628 (1997).

[55] Stuntebeck, E., Pompili, D. & Melodia, T. Underground wireless sensor networks using commodity terrestrial motes. In *Poster presentation at IEEE SECON 2006* (2006).

[56] Ahmed, A. A. & Fisal, N. Experiment measurements for packet reception rate in wireless underground sensor networks. *International Journal of Recent Trends in Engineering* **2** (2009).

[57] Rohini, K. & Singh, D. N. Methodology for determination of electrical properties of soils. *Journal of Testing and Evaluation* **32** (2004).

[58] Swanson, D. A., Tayman, J. & Bryan, T. M. Mape-r: a rescaled measure of accuracy for cross-sectional subnational population forecasts. *Journal of Population Research* **28**, 225–243 (2011).

[59] The physics hypertextbook URL `http://physics.info/dielectrics/`.

[60] Technology, C. Products of micaz, mica2, and mts sensor boards URL `http://www.xbow.com`.

[61] Li, X., sup Yun, T., Cheng, L., Pamukcu, S. & Dong, Y. In-situ geo-characterization using wireless functional signals. In *Proc. SPIE Smart Structures/NDE 2010* (2010).

[62] ASTM. Methodology for determination of electrical properties of soils. *Standard Test Method for Measurement of Soil Resistivity Using the Two-Electrode Soil Box Method, Designation: G187-05* .

[63] Griss, R., Alley, M., Holshouser, D. & Thomason, W. Precision farming tools: Soil electrical conductivity. *Virginia Cooperative Extention* 442–508 (2009).

[64] Zhurbenko, V. Electromagnetic waves. *InTech, ISBN 978-953-307-304-0* (2011).

[65] Jaganathan, A. P. & Allouche, E. N. Temperature dependence of dielectric properties of moist soils. *Canadian Geotechnical Journal* **45**, 888–894 (2008).

[66] Duda, R. O., Hart, P. E. & Stork, D. G. *Pattern Classification* (Wiley-Interscience (2nd Edition), 2000).

[67] Locher, T., Wattenhofer, R. & Zollinger, A. Received-signal-strength-based logical positioning resilient to signal fluctuation. In *Proc. of SNPD/SAWN*, 396–402 (2005).

[68] Milioris, D., Kriara, L., Papakonstantinou, A. & Tzagkarakis, G. Empirical evaluation of signal-strength fingerprint positioning in wireless lans. In *Proc. of ACM MSWiM 10* (2010).

[69] Sheng, Y., Tan, K., Chen, G., Kotz, D. & Campbell, A. Detecting 802.11 mac layer spoofing using received signal strength. In *Proc. of IEEE INFOCOM 2008* (2008).

[70] Chen, Y., Trappe, W. & Martin, R. P. Detecting and localizing wireless spoofing attacks. In *Proc. of SECON 07* (2007).

[71] Elnahrawy, E., Li, X. & Martin, R. P. The limits of localization using signal strength: A comparative study. In *Proc. of SECON 04*, 406–414 (2004).

[72] Ash, J. N. & Potter, L. C. Sensor network localization via received signal strength measurements with directional antennas. In *Proc. of 2004 Allerton Conference on Communication, Control, and Computing*, 1861–1870 (2004).

[73] URL `http://www.etsi.org/website/technologies/RRS.aspx`.

[74] Yoon, S.-U. & Ekici, E. Voluntary spectrum handoff: A novel approach to spectrum management in cognitive radio networks. In *Proc. of IEEE International Conference on Communications (ICC) 2010* (2010).

[75] Markus Dillinger, N. A., Kambiz Madani. *Software Defined Radio: Architectures, Systems and Functions* (Wiley & Sons, 2003).

[76] Universal software radio peripheral URL `http://www.ettus.com/`.

[77] URL `http://www.ettus.com`.

[78] Aziz, A. A., Sekercioglu, Y. A., Fitzpatrick, P. & Ivanovich, M. A survey on distributed topology control techniques for extending the lifetime of battery powered wireless sensor networks. *IEEE Communications Surveys and Tutorials* (2012).

[79] Chang, J.-H. & Tassiulas, L. Maximum lifetime routing in wireless sensor networks. *IEEE/ACM TRANSACTIONS ON NETWORKING* **12** (2004).

[80] Rodoplu, V. & Meng, T. H. Minimum energy mobile wireless networks. *IEEE JOURNAL ON SELECTED AREAS IN COMMUNICATIONS* **17** (1999).

[81] Xu, Y., Heidemann, J. & Estrin, D. Geography-informed energy conservation for ad hoc routing. In *Annual International Conference on Mobile Computing and Networking (MOBICOM)*, 70–84 (2001).

[82] Hou, Y. T., Shi, Y. & Sherali, H. D. Rate allocation in wireless sensor networks with network lifetime requirement. In *ACM MobiHoc04* (2004).

[83] Melodia, T., Pompili, D. & Akyildiz, I. F. Optimal local topology knowledge for energy efficient geographical routing in sensor networks. In *IEEE INFOCOM 2004* (2004).

[84] Kim, J., Lin, X., Shroff, N. B. & Sinha, P. Minimizing delay and maximizing lifetime for wireless sensor networks with anycast. *IEEE/ACM Transactions on Networking* **18**, 515–528 (2010).

[85] Song, C. *et al.* Maximizing network lifetime based on transmission range adjustment in wireless sensor networks. *Computer Communications* **32**, 1316–1325 (2009).

[86] Himsoon, T., Siriwongpairat, W. P., Han, Z. & Liu, K. J. R. Lifetime maximization via cooperative nodes and relay deployment in wireless networks. *IEEE Journal on Selected Areas in Communications* **25**, 306–317 (2007).

[87] Marina, M. K., Das, S. R. & Subramanian, A. P. A topology control approach for utilizing multiple channels in multi-radio wireless mesh networks. *Computer Networks* **54**, 241–256 (2010).

[88] Ma, J., Gao, M., Zhang, Q. & Ni, L. M. Energy-efficient localized topology control algorithms in ieee 802.15.4-based sensor networks. *IEEE TRANSACTIONS ON PARALLEL AND DISTRIBUTED SYSTEMS* **18** (2007).

[89] Heinzelman, W., Chandrakasan, A. & Balakrishnan, H. Energy-efficient routing protocols for wireless microsensor networks. In *Proc. of 33rd Hawaii Int. Conf. System Sciences (HICSS)* (2000).

[90] Heinzelman, W. B., Chandrakasan, A. P. & Balakrishnan, H. An application-specific protocol architecture for wireless microsensor networks. *IEEE TRANSACTIONS ON WIRELESS COMMUNICATIONS* **1** (2002).

[91] Wang, Q., Hempstead, M. & Yang, W. A realistic power consumption model for wireless sensor network devices. In *IEEE SECON 2006* (2006).

[92] Liu, F., Tsui, C.-Y. & Zhang, Y. J. Joint routing and sleep scheduling for lifetime maximization of wireless sensor networks. *IEEE TRANSACTIONS ON WIRELESS COMMUNICATIONS* **9** (2010).

[93] Burkhart, M., von Rickenbach, P., Wattenhofer, R. & Zollinger, A. Does topology control reduce interference. In *ACM MobiHoc04* (2004).

Vita

Suk-Un Yoon is a Ph.D. candidate in the Department of Computer Science and Engineering at Lehigh University. His research interests cover wireless sensor network, cognitive radio networks, underground communications, embedded system, and IP networking. He was a senior engineer at Samsung Electronics from 2001 to 2007. He received the BS degree in Electronics Engineering from Soongsil University, Seoul, Korea in 1998, the MS degree in Electronics Engineering from Korea University, Seoul, Korea in 2001, and the MS degree in Electrical and Computer Engineering from the Ohio State University, Columbus, Ohio, USA in 2010.

E-mail Address: suy309@lehigh.edu, sukunyoon@gmail.com